

Protein Misfolding Studies on Human Semenogelin-1 and Serum Albumin Proteins

By

Neetu Sharma

A Dissertation Submitted to
Indian Institute of Technology Hyderabad
In Partial Fulfilment of the Requirements for
The Degree of Doctor of Philosophy



भारतीय प्रौद्योगिकी संस्थान हैदराबाद
Indian Institute of Technology Hyderabad

Department of Biotechnology

February, 2016

Declaration

I declare that this written submission represents my ideas in my own words, and where others' ideas or words have been included, I have adequately cited and referenced the original sources. I also declare that I have adhered to all principles of academic honesty and integrity and have not misrepresented or fabricated or falsified any idea/data/fact/source in my submission. I understand that any violation of the above will be a cause for disciplinary action by the Institute and can also evoke penal action from the sources that have thus not been properly cited, or from whom proper permission has not been taken when needed.



(Signature)

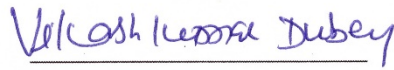
NEETU SHARMA

BO11P1003

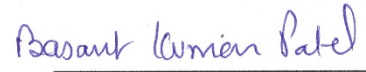
(Reg. No)

Approval Sheet

This thesis entitled "Protein misfolding studies on human Semenogelin-1 and Serum Albumin proteins" by Neetu Sharma, Reg. No. BO11P1003, is approved for the degree of Doctor of Philosophy from IIT Hyderabad.



Prof. Vikash Kumar Dubey
Dept. of Biosciences & Bioengineering
IIT Guwahati
(External Examiner)



Dr. Basant K. Patel
Associate Professor
Dept. of Biotechnology
IIT Hyderabad
(Thesis Advisor)



Dr. Anindya Roy
Associate Professor
Dept. of Biotechnology
IIT Hyderabad
(Internal Examiner)



Dr. Parag Pawar
Assistant Professor
Dept. of Chemical Engineering
IIT Hyderabad
(Chairman)

Acknowledgements

I would like to offer my sincere thanks to several people who have made this journey possible, by helping and encouraging me during all these years. First of all I would like to express my deepest gratitude to my advisor and mentor, Dr. Basant K. Patel for providing me an opportunity to work under his esteemed guidance. I have learned so much from him both as a scientist and as a person. I am thankful to Dr. Basant K. Patel for his patience, generosity, guidance and continuous support. I would like to thank him for helping me develop self-learning ability and for the excellent scientific discussions.

I would especially like to sincerely thank my doctoral committee members, Dr. Anindya Roy from Department of Biotechnology and Dr. Parag D. Pawar from Department of Chemical Engineering, IIT-Hyderabad for their valuable suggestions and expertise. I am grateful to Dr. Pankaj Poddar and Puneet Khandelwal from Physical and Materials Chemistry Division CSIR-National Chemical Laboratory for providing necessary help with the AFM facility. I would like to acknowledge Dr. Subhash Chandra Yadav from Department of Anatomy, All India Institute of Medical Sciences, New Delhi for helping with TEM characterization. I would like to extend my thanks to Dr. Saptarshi Majumdar and Utkarsh Bhutani of Dept. of Chemical Engineering, IIT-Hyderabad for help with DLS facility. Thanks to all the faculty members of Department of Biotechnology, IIT Hyderabad.

I gratefully acknowledge the Ministry of Human Resource and Development (MHRD), Government of India for awarding me scholarship to carry out the research work and also I acknowledge IIT-Hyderabad funded by MHRD, Government of India for providing infrastructure and research support.

I warmly thank my parents, my brother and sister for always believing in me, particularly my father for motivating me to pursue a career in research, encouraging me and keeping hopes alive. You made this possible. I truly appreciate my husband Anubhav for his constant support and for making me a happier and better person. Their unconditional love and support throughout this journey helped me in completing my PhD work

successfully. I would also like to thank my mother and father-in-law for always being supportive of my goals.

I would like to thank my group colleagues Vishwanath, Archana, Aman, Sonalika, Vidhya Prassana and other friends for their help and kind cooperation during my time here. I appreciate the friendly environment of our group. Finally, I am thankful to God, the almighty for providing me this opportunity and granting me the capability to proceed successfully. Overall it has been an excellent experience and would not have been the same without all of these people.

Neetu Sharma

*Dedicated to
my beloved family*

Abstract

Proper folding of proteins into native structure is essential for their biological activity. Proteins achieve native state with the help of several cellular regulatory mechanisms assisted by molecular chaperones. Alteration in these regulatory mechanisms can lead to protein misfolding. Also failure to dispose of the misfolded protein load causes accumulation of misfolded proteins and toxicity. The accumulated protein in some cases may self-assemble into stable, β -sheet rich oligomers and aggregates known as amyloid fibrils. Amyloid aggregation has been implicated to cause several diseases such as Alzheimer's, Parkinson's and renal amyloidosis etc.

In this study, amyloid-like aggregation of human proteins Semenogelin-1 (Sg1), and Serum albumin (HSA) have been investigated. Aggregation of human Sg1 protein is observed in Senile seminal vesicle amyloidosis (SSVA) disorder. HSA is the most abundant protein in blood plasma and has been shown to aggregate *in vitro* similar to amyloid proteins. Key unanswered questions that have been investigated here are, whether Sg1 full length protein can form amyloid aggregates *in vitro* and whether HSA aggregates exhibit true amyloid properties. We succeeded in obtaining aggregates of Sg1 and Sg1 (1-159), which manifested amyloid-like binding to Thioflavin-T and Congo red dyes and also followed lag-dependent sigmoidal growth pattern and beta-sheet rich conformation, as established previously for several amyloids. Furthermore, these aggregates also exhibited amyloid-like stabilities to ionic detergents: SDS and Sarkosyl. In addition, dynamic light scattering (DLS) results estimated presence of > 400 nm size particles in both Sg1 and Sg1(1-159) aggregates and exhibited amyloid-like fibrillary morphology in TEM. Notably, Zn^{2+} which is known to bind to Sg1 *in vivo* was found to partially inhibit amyloid aggregation of Sg1 and Sg1 (1-159) *in vitro*.

Here, it is also observed that HSA aggregates display true amyloid characteristics of self-seeding and detergent stability. This was further supported by fibrillar morphologies as observed by TEM and AFM. Furthermore, HSA homodimer has been obtained without the use of a chemical cross-linker, which being non-immunogenic, can find potential therapeutic preference over conventional HSA dimers obtained *via* chemical cross-linking. Notably, HSA dimers retain the amyloidogenic properties similar to that of the HSA monomers, thus suggesting need for therapeutic precautions. In conclusion, this thesis explores the amyloidogenic properties of full length Sg1 and also provides new insights into amyloid-like aggregation of HSA monomer and dimer.

Abbreviations

3AP	-	3-aminophenol
AFM	-	Atomic force microscopy
BSA	-	Bovine serum albumin
CD	-	Circular dichroism
DTNB	-	5,5'-dithiobis-(2-nitrobenzoic acid)
DLS	-	Dynamic light scattering
EDTA	-	Ethylene diamine tetraacetic acid
GuHCl	-	Guanidine hydrochloride
HSA	-	Human serum albumin
IPTG	-	Isopropyl β -D-thiogalactopyranoside
PMSF	-	Phenylmethylsulfonyl fluoride
PSA	-	Prostate specific antigen
PTA	-	Phosphotungstic acid
PVDF	-	Polyvinylidene fluoride
Sg1	-	Semenogelin-1
SSVA	-	Senile seminal vesicle amyloidosis
SDD-AGE	-	Semi-denaturing detergent agarose gel electrophoresis
SDS	-	Sodium dodecyl sulfate
ThT	-	Thioflavin-T
TEM	-	Transmission electron microscopy
TAE	-	Tris acetate EDTA
Trp	-	Tryptophan
Tyr	-	Tyrosine

Contents

Declaration	ii
Approval Sheet	iii
Acknowledgements.....	iv
Abstract	vii
Abbreviations	viii
Chapter I.....	1
Introduction to protein misfolding, amyloid aggregation and amyloidoses	1
1.1 Protein folding and misfolding.....	1
1.2 Amyloid aggregation	2
1.3 Pathology of amyloidoses	4
1.4 Naturally occurring amyloids.....	7
1.5 Amyloid forming protein: Semenogelin-1	8
1.6 Human serum albumin: amyloidogenic protein	15
Chapter II.....	19
Recombinant expression, purification & characterization of human Semenogelin-1 (Sg1) and Sg1 (1-159) proteins.....	19
2.1 Abstract	19
2.2 Introduction	20
2.3 Results and Discussion	21
2.3.1 Cloning of Sg1 (1-159) in a recombinant expression vector and expression of recombinant Sg1 and Sg1 (1-159) proteins.....	22
2.3.2 Purification of recombinant Sg1 and Sg1 (1-159) by Ni-NTA affinity chromatography.....	24
2.3.3 Assessment of homogeneity and molecular weight of recombinant Sg1 and Sg1 (1-159) proteins.....	24
2.3.4 Identification of His-tag in purified Sg1 by western blotting	26
2.3.5 Characterization of the recombinant Sg1 and Sg1 (1-159) proteins	27
2.3.6 Aggregation of Sg1 and Sg1 (1-159) fractions during dialysis.....	34
2.4 Materials and Method	35
2.4.1 Materials.....	35

2.4.2	Cloning of Sg1 (1-159) and expression of recombinant Sg1 and Sg1 (1-159) proteins.....	36
2.4.3	Ni-NTA affinity purification of recombinant Sg1 and Sg1 (1-159) proteins	39
2.4.4	Western blotting	40
2.4.5	Intrinsic fluorescence.....	40
2.4.6	Refolding of Sg1 assessed by Circular dichroism.....	40
2.4.7	Dialysis of Sg1 and Sg1 (1-159) purified in 8 M urea.....	41
Chapter III 42
Amyloid-like <i>in vitro</i> aggregation of Sg1 and Sg1 (1-159) proteins.....		. 42
3.1	Abstract	42
3.2	Introduction	42
3.3	Results and Discussion	43
3.3.1	Sg1 aggregation and amyloid formation.....	43
3.3.2	Stability assessment of Sg1 aggregates	46
3.3.3	Kinetics of <i>in vitro</i> amyloid aggregation of Sg1	49
3.3.4	Secondary structure estimation by Circular dichroism.....	51
3.3.5	Transmission electron microscopy of Sg1 and Sg1 (1-159) aggregates...	52
3.3.6	Estimation of Sg1 aggregate sizes by Dynamic light scattering (DLS) ...	52
3.3.7	Inhibition of Sg1 aggregation by Zn ²⁺	54
3.4	Materials and Methods.....	56
3.4.1	Materials.....	56
3.4.2	Sg1 aggregation and amyloid formation.....	56
3.4.3	Kinetics of <i>in vitro</i> amyloid aggregation of Sg1	57
3.4.4	Stability assay of Sg1 aggregates	58
3.4.5	Secondary structure estimation by CD	61
3.4.6	Transmission electron microscopy (TEM) of Sg1 and Sg1 (1-159) aggregates.....	61
3.4.7	Estimation of Sg1 aggregate sizes by DLS	62
3.4.8	Inhibition of Sg1 aggregation by Zn ²⁺	62
Chapter IV 63

New insights into amyloid-like <i>in vitro</i> aggregation of human serum albumin protein	63
4.1 Abstract	63
4.2 Introduction	63
4.3 Results and Discussion	65
4.3.1 <i>In vitro</i> formation of HSA aggregates	65
4.3.2 Intrinsic tryptophan fluorescence of HSA aggregates	67
4.3.3 Estimation of molecular sizes of HSA aggregates by DLS	68
4.3.4 Transmission electron microscopy of HSA aggregates	69
4.3.5 Evaluation of HSA aggregates as true amyloid.....	69
4.3.6 HSA homo-dimerization and purification.....	74
4.3.7 <i>In vitro</i> amyloid-like aggregation of HSA homodimer	78
4.4 Materials and Methods.....	80
4.4.1 Materials.....	80
4.4.2 Amyloid aggregation and detection.....	81
4.4.3 Semi-denaturing detergent agarose gel electrophoresis (SDD-AGE)	81
4.4.4 Amyloid seeding assay	82
4.4.5 Transmission Electron Microscopy	83
4.4.6 Atomic Force Microscopy	83
4.4.7 Dynamic Light Scattering	84
4.4.8 HSA homo-dimerization and purification.....	84
Chapter V	86
Conclusions	86
Chapter VI	89
Bibliography.....	89
Publications.....	100

List of Figures

Figure 1. Protein misfolding: the various states accessible to a protein molecule	2
Figure 2. Cross β structure of peptide from the amyloid domain of the yeast prion Sup35p	3
Figure 3. Characteristic increase in Thioflavin-T fluorescence upon binding to amyloid fibrils	3
Figure 4. Nucleation dependent amyloid growth	4
Figure 5. Amyloid aggregates in neurodegenerative diseases	5
Figure 6. Congo red stained sections of seminal vesicle showing Sg1 aggregates deposits.....	8
Figure 7. Schematics of Isoform 1 and Isoform 2 of semenogelin-1 protein	9
Figure 8. Electron micrographs of fibrillar structures from Semenogelin-1 peptides	12
Figure 9. Sg1 peptide amyloid facilitates HIV virion attachment and entry to cultured cells	13
Figure 10. Congo red staining of seminal vesicle sections	14
Figure 11. Secondary structure of HSA molecule	15
Figure 12. Proposed model for amyloid aggregation pathway of HSA.....	17
Figure 13. Schematics of recombinant proteins, his-tagged Sg1 full length and a cloned out fragment Sg1 (1-159) encompassing the previously reported amyloidogenic peptide region of 45-107 amino acids.	21
Figure 14. Plasmid maps of pRB01-Sg1 and pBKP-Sg1(1-159).....	22
Figure 15. Plasmid construction of pBKP-Sg1(1-159).....	23
Figure 16. Ni-NTA affinity purification profile of recombinant proteins	24
Figure 17. Homogeneities of the recombinant proteins assessed by SDS-PAGE.....	25
Figure 18. Estimation of mol. wt. of recombinant Sg1 and Sg1 (1-159) using relative mobility plot of mol. wt. standards from figures 17B & 17D.....	26
Figure 19. Identification of his ₆ -tag in the recombinantly purified full length Sg1 protein by anti-his antibody using western blotting	27
Figure 20. Absorbance spectra of purified recombinant proteins (A) Sg1 and (B) Sg1 (1- 159) by UV-visible spectroscopy	28
Figure 21. Intrinsic fluorescence emission spectra of Sg1 dialyzed at pH 7.4.....	30

Figure 22. Assessment of refolding of Sg1 by intrinsic Tryptophan fluorescence	31
Figure 23. Refolding of Sg1 as assessed by far-UV CD spectra.....	33
Figure 24. Protein precipitation during dialysis	34
Figure 25. Assessment of amyloid nature of aggregates of Sg1 and Sg1 (1-159)	44
Figure 26. Congo red birefringence of Sg1 and Sg1 (1-159) aggregates	45
Figure 27. Detergent stability of Sg1 and Sg1 (1-159) amyloid aggregates.....	47
Figure 28. Partial resistance of Sg1 amyloid aggregates to Proteinase-K digestion	48
Figure 29. Sg1 aggregation at different pH.....	49
Figure 30. Aggregation of Sg1 (1-159) compared with Sg1.....	50
Figure 31. Far-UV Circular dichroism spectra of Sg1 and Sg1 (1-159) aggregates	51
Figure 32. Transmission electron micrographs of Sg1 and Sg1 (1-159) aggregates.....	53
Figure 33. Estimation of Sg1 and Sg1 (1-159) aggregate sizes by DLS	54
Figure 34. Aggregation of Sg1 and Sg1 (1-159) fragment in presence of Zn ²⁺ or 3-aminophenol	55
Figure 35. Assessment of amyloid nature of HSA aggregates by ThT fluorescence	66
Figure 36. Congo red absorbance spectrum in presence of HSA aggregates	66
Figure 37. Tryptophan fluorescence emission spectra of HSA aggregates	67
Figure 38. Estimation of molecular sizes of HSA aggregates by DLS.....	68
Figure 39. Morphologies of HSA amyloid aggregates viewed in TEM.....	69
Figure 40. Amyloid-like detergent stability of HSA aggregates.....	70
Figure 41. Amyloid-like self-seeding of HSA aggregates.....	71
Figure 42. Morphologies of HSA amyloid aggregates obtained upon seeded aggregation	72
Figure 43. Cross-seeding kinetics of HSA and BSA aggregation.....	73
Figure 44. Hydrogen peroxide induced dimerization of HSA.	75
Figure 45. Purification of HSA dimer by size exclusion chromatography.....	76
Figure 46. Comparison of hydrodynamic radius of HSA monomer (A) and purified HSA dimer (B) using DLS.	77
Figure 47. Assessment of stability of HSA homodimer	78
Figure 48. Assessment of amyloid nature of HSA dimer aggregates.....	79
Figure 49. Assessment of Congo red binding of HSA dimer aggregates	79

Figure 50. AFM imaging of HSA dimer aggregates.	80
Figure 51. Steps for self-seeding aggregation assay of HSA.....	83

List of Tables

Table 1. Examples of amyloid diseases and associated aggregating protein in humans .	6
Table 2. Characteristics of semenogelin-1 gene and protein.....	10
Table 3. Secondary structure estimation of Sg1 under different urea concentrations	34
Table 4. Reagents for PCR amplification of Sg1 (1-159).....	37
Table 5. Estimation of free cysteine in HSA by Ellman’s reagent assay	74

Chapter I

Introduction to protein misfolding, amyloid aggregation and amyloidoses

1.1 Protein folding and misfolding

Proper folding of proteins into native structure is essential for their function and solubility [1]. The biological function of cells depends on the correct folding of several proteins. The information required to fold a protein into its functional conformation resides in its amino acid sequence. Transition between different folded states of protein is regulated by cellular environment and factors such as molecular chaperones. Generally proteins fold properly into their native conformation and, any misfolding during the process is corrected by chaperone proteins. But if this cellular quality control mechanism fails, it can result in aggregation and accumulation of misfolded protein deposits (Figure 1). This may lead to the development of protein misfolding disorders such as amyloid and prion diseases [1]. Also alterations in a protein's primary amino acid sequence due to mutations or changes in the cellular homeostasis, can lead to misfolding of proteins that compromises their function. Additionally, misfolded proteins can accumulate *in vivo* into ordered beta sheet-rich aggregates termed amyloid that cause toxicity and disease [1,2].

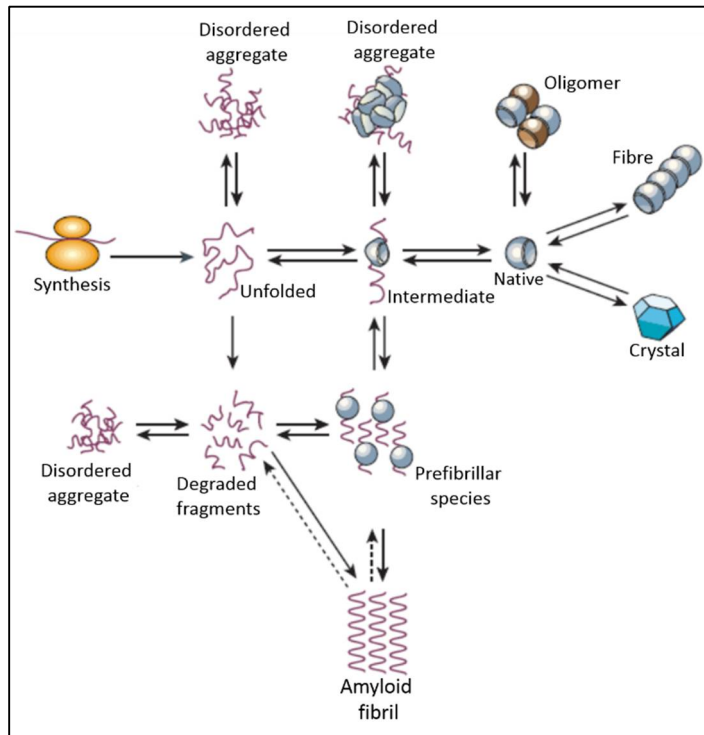


Figure 1. Protein misfolding: the various states accessible to a protein molecule
(adapted from Dobson, 2003, Nature) [1]

1.2 Amyloid aggregation

Amyloid fibrils are highly organized, insoluble, thread-like aggregates of misfolded protein and are associated with various diseases. These are approximately 75-100 Å in diameter. They have characteristic cross β -sheet structure, revealed by X-ray diffraction studies, where the β -sheets are parallel to the axis of the fibril with their strands perpendicular to this axis (Figure 2). Amyloid deposits exhibit characteristic apple green birefringence when stained with Congo red dye and viewed under polarized light, they also exhibit enhanced fluorescence on binding with Thioflavin-T [3,4]. Amyloid aggregates show unusual stabilities against denaturants (such as urea and ionic detergents) at room temperature, also partial resistance to proteinase-K digestion and can self-seed and coax the non-amyloid forms of their protein monomers, also into amyloid aggregated conformation [5,6].

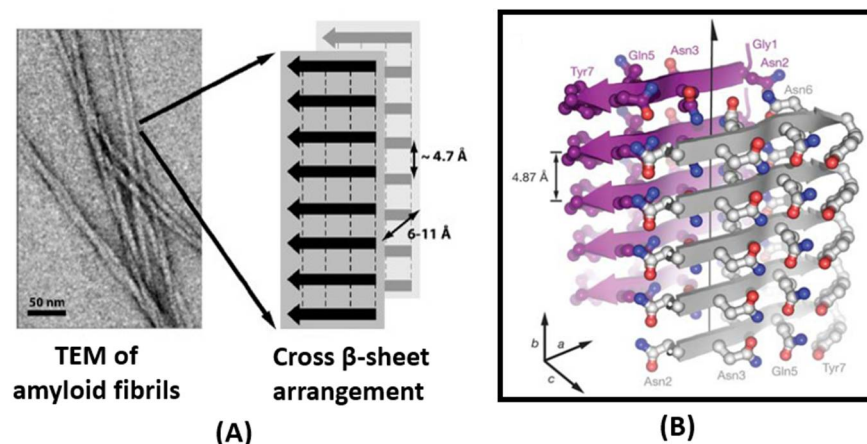


Figure 2. Cross β structure of peptide from the amyloid domain of the yeast prion Sup35p
(adapted from Nelson et al. 2005, Greenwald, 2010) [3,4]

Thioflavin-T (ThT), a cationic benzothiazole dye, is widely used for the detection of amyloid aggregates both in solution and in tissue. Upon binding to amyloid fibrils, this dye exhibits an enhanced fluorescence with an emission maximum around 482 nm and a new absorption peak at 450 nm (Figure 3) [7]. Although, the specificity of ThT and Congo red dyes for amyloid detection has been debated, these continue to be preliminary probes for amyloid aggregation [8,9].

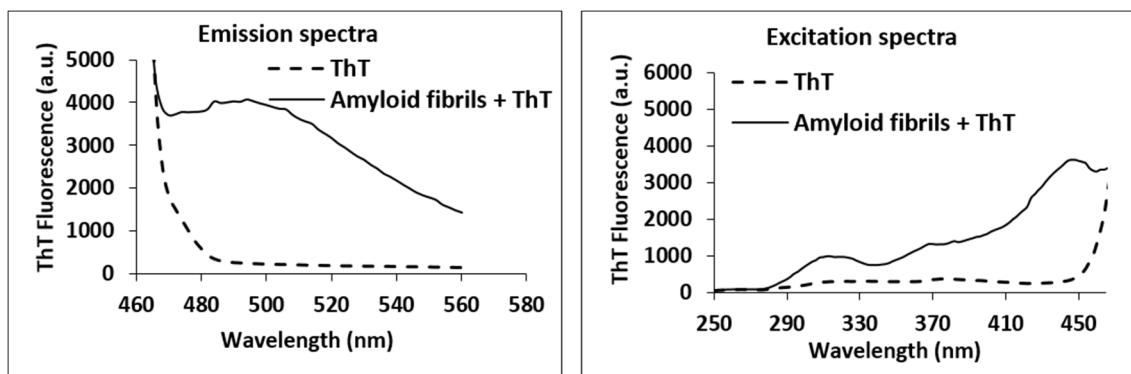


Figure 3. Characteristic increase in Thioflavin-T fluorescence upon binding to amyloid fibrils [7]

Amyloid aggregation follows lag dependent sigmoidal kinetics of formation [5]. Starting with a slow lag phase during which seed (or nucleus) is formed followed by elongation and then saturation phase therefore also referred to as nucleation dependent polymerization process (Figure 4). The rate of growth of amyloid fibres is increased by

the presence of pre-formed ordered aggregates which act as seed, in a process referred to as seeding [5]. Seeding ability of aggregates serve as a measure to distinguish ordered amyloid structures from randomly misfolded amorphous aggregates.

The seeds act as a starting material or template for the assembly and growth of amyloid fibers. This also acts as a basis for the spread of amyloid deposits in tissues and from one organ to another in case of systemic amyloidosis. Amyloid aggregation shows sigmoidal growth curve with three phases:

- a) Initial lag phase, during which oligomer protein “seed” or nucleus is formed
- b) Log phase also called as exponential phase or polymerization phase, wherein seeds recruit the monomeric protein molecules in exponential manner.
- c) Stationary phase, when amyloid is formed completely with no further increase in its fibrillization process.

Seeding affects the kinetics by decreasing the lag phase and thus over all time to form the amyloid.

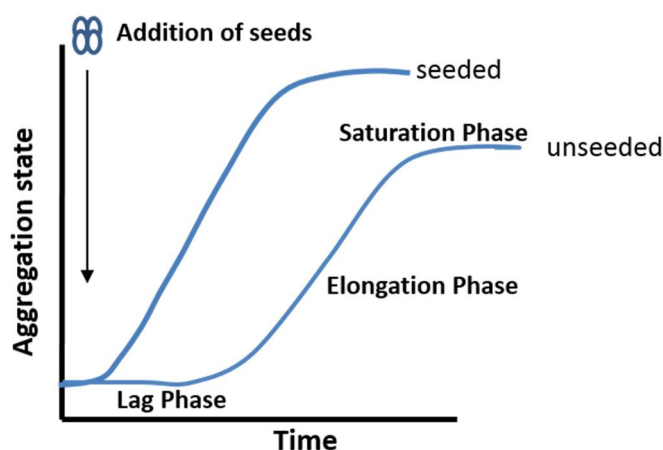


Figure 4. Nucleation dependent amyloid growth [5,10]

1.3 Pathology of amyloidoses

Amyloidosis is the pathological state which involves extracellular deposition of protease resistant protein fibrils in tissues and organs as a result of the transition of soluble protein to insoluble form with ordered structure [11]. A wide range of human pathologies are associated with aggregation of misfolded proteins. Although, they exhibit clinically

distinct conditions (Figure 5). At present, more than 30 different types of amyloidoses have been defined [12].

Several amyloid associated debilitating human diseases have been identified such as Alzheimer's disease, Prion disease, Huntington's disease & renal amyloidosis where the A β -42 peptide, PrP^C protein, mutant huntingtin protein & human lysozyme, are respectively found to be amyloid aggregated and deposited (Figure 5).

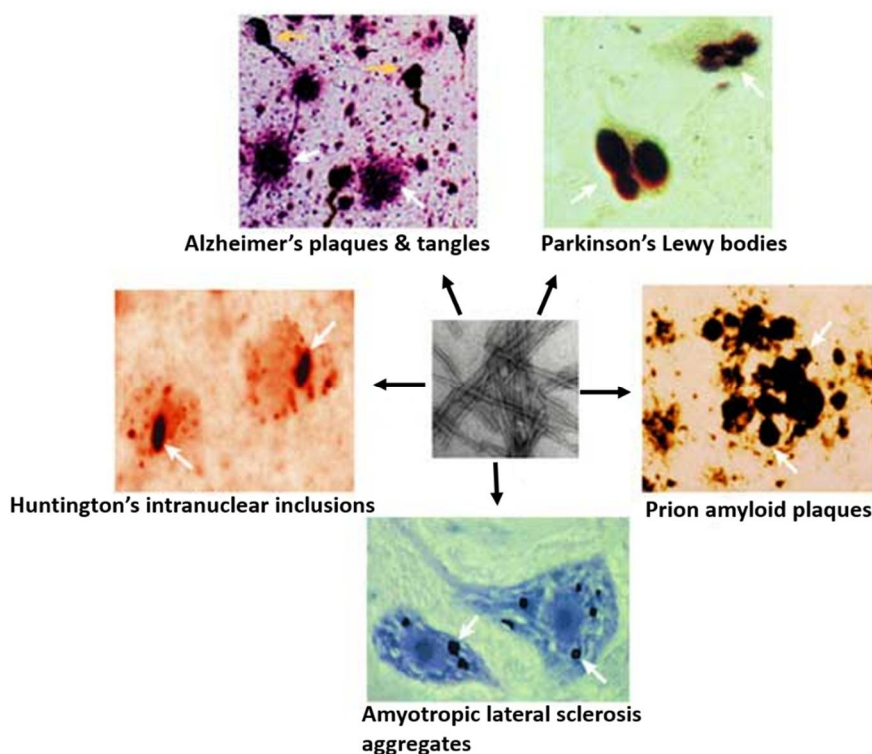


Figure 5. Amyloid aggregates in neurodegenerative diseases
(adapted from Soto.C et al, *Nat Rev Neurosci*, 2003) [13]

Amyloidoses can be systemic or localized (Table 1). Localized amyloidoses are thought to be amyloid deposits derived from the proteins synthesized at the cells located in the region of accumulation. Semenogelin-1 has been identified as the amyloid protein that accumulate in localized senile seminal vesicle amyloidosis (SSVA) [12,14]. SSVA is mostly asymptomatic while other amyloidoses can be neurodegenerative or non-neuropathic.

Table 1. Examples of amyloid diseases and associated aggregating protein in humans
(adapted and modified from Chiti & Dobson, 2006; Sipe et al 2010) [2,12]

Amyloid disease	Aggregating protein
a) Non-neuropathic amyloidosis	
Systemic	
Primary systemic amyloidosis	Immunoglobulin light chain
Ig-heavy chain associated amyloidosis	Immunoglobulin heavy chain
Hemodialysis-related amyloidosis	β 2-microglobulin
Senile systemic amyloidosis	Transthyretin
Secondary (reactive) systemic amyloidosis	Serum amyloid A protein
Hereditary systemic ApoAI amyloidosis	Apolipoprotein AI
Sporadic systemic ApoAIV amyloidosis	Apolipoprotein AIV
Familial hereditary amyloidosis	Gelsolin
Hereditary lysozyme amyloidosis	Lysozyme
Hereditary renal amyloidosis	Fibrinogen α chain
Localized	
Spongiform encephalopathies	A β precursor protein (PrP)
Medullary carcinoma of the thyroid	(Pro)calcitonin
Diabetes mellitus	Islet amyloid polypeptide
Atrial amyloidosis	Atrial natriuretic factor
Injection-localized amyloidosis	Insulin
Pulmonary alveolar proteinosis	Lung surfactant protein C
Odontogenic tumors	Odontogenic ameloblast-associated protein
Seminal vesicle amyloid	Semenogelin I
b) Neurodegenerative amyloidosis	
Alzheimer's disease	Amyloid β peptide
Spongiform encephalopathies	Prion protein (PrP)
Parkinson's disease	α -synuclein
Huntington's disease	Huntingtin with poly Q expansion
Amyotrophic lateral sclerosis	Superoxide dismutase 1

1.4 Naturally occurring amyloids

Besides pathological amyloid some functional amyloids have also been identified in both eukaryotes and prokaryotes where they can have beneficial roles [2].

Amyloid structures can sometimes have beneficial function rather than disease-associated properties in living systems under particular environmental conditions. For example *E. coli* have amyloid forming protein curlin helping it to colonize inert surfaces and mediate binding to host proteins. The filamentous bacterium *Streptomyces coelicolor* secrete amyloid forming protein chaplins that lower the water surface tension and allow the development of aerial hyphae [2]. Numerous other proteins, including some human proteins, which are not associated with any disease, can also form amyloid-like aggregates *in vivo* (e.g. mammalian Pmel17 protein; yeast Sup35 & Cyc8 proteins etc.) or even *in vitro* (e.g. human serum albumin, bovine serum albumin, hen egg white lysozyme, endocrine hormones such as ACTH & Oxytocin etc.) [2,15-17]. Non-disease associated amyloid forming proteins have been used as a model system to understand: a) General mechanism of amyloid formation [18]; b) Amyloid cross-seeding such as study of crossing of species barrier by prions [19]; c) Potential application as structural nano-materials [20]; d) The propagation of amyloid and prion e.g. sup 35 is used to study the infection mechanism of prion [21]; e) Potential application as drug delivery agent; e.g. Insulin amyloid aggregates as potential sustained insulin delivery tool for diabetes treatment [22].

Prions are infectious proteins capable of propagating protein misfolding and aggregation [23]. They cause fatal neurodegenerative diseases. Prion diseases are characterized by accumulation of the misfolded, protease-resistant prion protein termed PrP^{Sc}. When a prion enters a healthy organism, it induces existing, properly folded proteins to convert into the disease-associated, prion form; the prion acts as a seed to bind with normal, cellular prion protein of host denoted as PrP^C catalyzing its conversion into the misfolded, pathogenic form PrP^{Sc} thus mediate prion transmission [24]. The molecular mechanism underlying prion propagation is strikingly similar to the mechanism of amyloid formation. Prion proteins are also found in yeast, which has been useful to understand mammalian prions.

Yeast prions are infectious protein that behaves as a non-Mendelian genetic element and transmits biological information in the absence of nucleic acid [25]. The well-known prion proteins in yeast are Sup35, Rnq1, Ure2, Cyc8 and HET-S, which leads to the corresponding prion state [PSI+], [PIN+],[URE3], [OCT+] and [Het-s] respectively [26,27]. Most of the yeast prions are rich in glutamine/asparagine residues. Prion proteins can adopt different stably propagating conformations which gives rise to prion variants *in vivo* [28]. All known prion diseases, collectively called transmissible spongiform encephalopathies (TSEs). The human prion disease variant Creutzfeldt-Jakob disease, is believed to be caused by a prion which typically infects cattle, causing Bovine spongiform encephalopathy and is transmitted through infected meat [24].

1.5 Amyloid forming protein: Semenogelin-1

Senile seminal vesicle amyloidosis (SSVA) is a form of localized amyloidosis affecting male reproductive system. SSVA manifestation could remain asymptomatic or display as hematospermia and supra pubic pain which may be frequently mis-diagnosed as carcinoma [29,30].

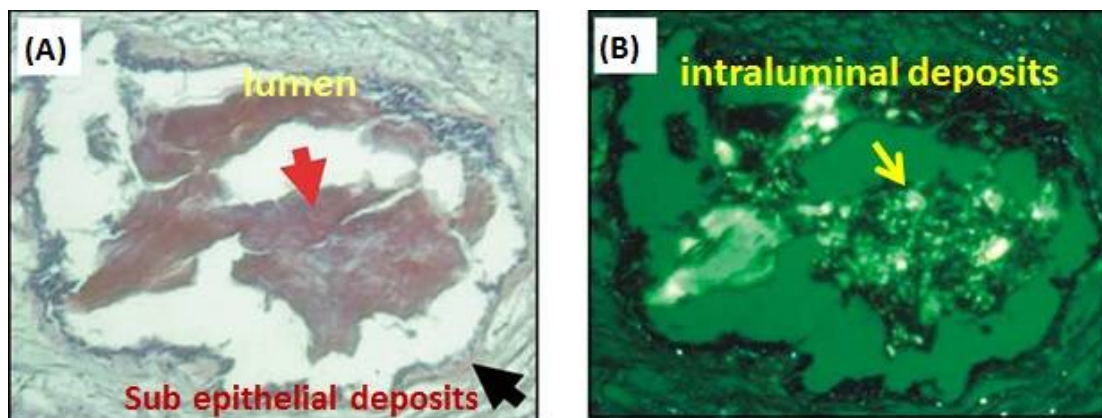


Figure 6. Congo red stained sections of seminal vesicle showing Sg1 aggregates deposits (A) under bright field (B) polarized light (adapted from Linke et al, 2005) [14]

The occurrence of SSVA increases with progressing age and it is found in over 20 % of men above 75 years of age [31]. The protein Semenogelin-1 (Sg1) has been identified to

be the major component of protein deposits in SSVA (Figure 6) [12,14]. Sg1 is also the predominant protein required for formation of human semen coagulum, the gel matrix that encases spermatozoa [32]. This form of amyloidosis is designated as ASemI [12,14]. Semenogelin-1 is the most abundant protein of human semen coagulum. It is synthesized and secreted by the seminal vesicle and are involved in formation of gel matrix that encases spermatozoa just after ejaculation [32].

Human semen coagulum contains semenogelin-1 (Sg1) and semenogelin-2 (Sg2), Sg1 is the predominant form with molecular mass of 52 kDa while less abundant protein Sg2 has two different forms of 70 kDa and 76 kDa. The precursor for semenogelin consists of 462 amino acid residues which after cleavage of 23 residue signal peptide yields mature functional protein of 439 amino acids [33]. Alternative splicing gives rise to two different isoforms of semenogelin-1 (Figure 7).

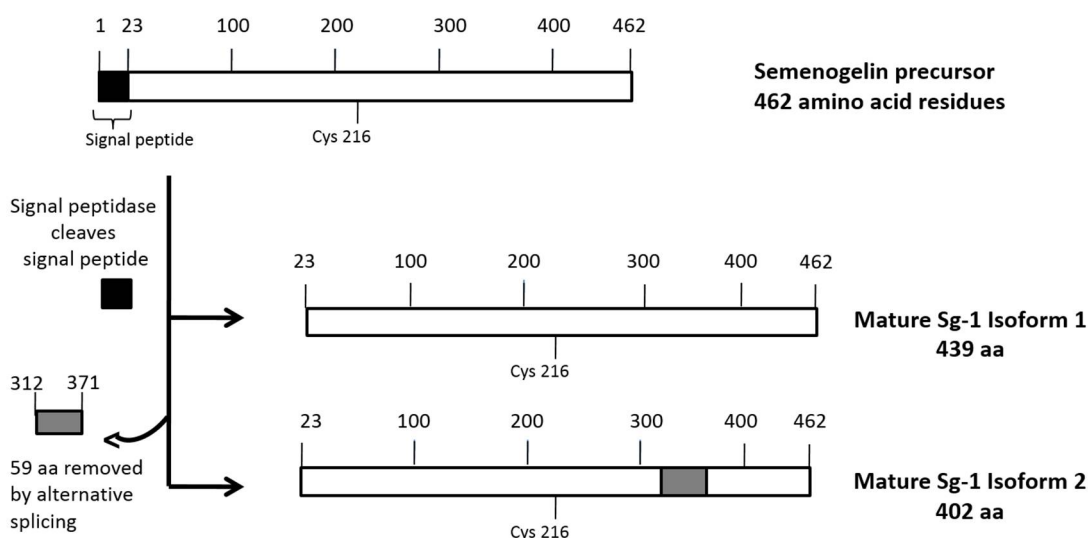


Figure 7. Schematics of Isoform 1 and Isoform 2 of semenogelin-1 protein

Semenogelin has abundance of glutamine, asparagine and lysine amino acid residues analogous to yeast prion proteins which can form amyloid aggregates. The semenogelins exhibit 78 % similarity in their primary structure, and are composed of repetitive units

[34]. The only post translational modification is the presence of a pyroglutamine residue at its N-terminus [32,35].

Table 2. Characteristics of Semenogelin-1 gene and protein [33]

	Characteristics	Properties
Gene	Open reading frame	1389 nucleotides
	Exon structure	exon I: signal peptide exon II: mature protein exon III: 3% non-translated region
	Chromosomal localization	20 q12–13.1
Protein	Molecular weight	49620–49958 Da
	Amino acid residues	signal peptide: 23 mature protein: 439 total: 462
	Cysteine residue	1 (at residue 216)
	Internal repeats	six repeats of 60 amino acid units
	Isoelectric point	9.5
	Similarity with Sg2	nucleic acid 89% (within exons) protein 78%
	Posttranslational modification	N-terminal pyroglutamination
	Sperm motility inhibitor (SPMI) domain	85-106

Semenogelin undergoes proteolytic processing by protease, prostate specific antigen (PSA) [36]. This mediates liquefaction of the gel aiding in progressive release of motile spermatozoa. Semen contains a high concentration of Zn^{2+} ions, which is known to inhibit the protease activity of PSA. Semenogelins bind Zn^{2+} ions with high affinity, thus regulate the enzymatic activity of PSA by bringing down the level of free Zn^{2+} ions low enough to block the inhibition and thereby enable activation of PSA [37]. Cleavage of the semenogelins by PSA during liquefaction is important for fertilization as semen with slow liquefaction rate leads to infertility. In addition to having coagulum forming functions the semenogelins have been reported to be involved in other functions like activation of

sperm hyaluronidase which facilitates fertilization, serve as substrates for transglutaminase [38], affect sperm motility [35], possess anti-microbial activity derived from peptides generated by fragmentation of the semenogelins which provides protection for the spermatozoa in the female reproductive tract [39,40], and exhibit amyloid properties [14].

Besides being expressed in seminal vesicle, studies have shown that semenogelin-1 and semenogelin-2 are also expressed in salivary glands, trachea, kidney, pancreas, prostate, but at much lower levels and retinal pigment epithelial cells (which is known to contain high levels of zinc) this indicates that these proteins are involved in functions beyond reproduction and fertility [41,42]. A wider role for semenogelin-1 may be suggested by observations that, it has been found to be expressed in leukaemia, small cell lung carcinoma, and prostate cancer. Recently Sg1 have been reported to be expressed in renal cell carcinoma, suggesting Sg1 expression as a marker for human malignancies [43-46].

It has been reported previously that naturally occurring fragments of prostatic acid phosphatase (PAP), an abundant protein secreted into semen from the prostate form amyloid fibrils consisting of amino acid residues 248–286. These fibrils, termed Semen-derived Enhancer of Virus Infection (SEVI), promote attachment of HIV virions to target cells, thereby enhancing HIV infectivity [47].

Like SEVI, certain peptide fragments of Sg1 [Sg1 (45-107), Sg1 (68-107), Sg1 (86-107) and Sg1 (38-48)] have been reported to form amyloid aggregates *in vitro* and have been shown to greatly enhance HIV infection in cell cultures (Figure 8). Data suggest that the enhancement of HIV infectivity may be due to the cationic surfaces which may facilitate HIV virion attachment and entry [48-50]. Very recently, the interaction of fibronectin with semen amyloids (such as Sg1 amyloid and SEVI) has also been reported to facilitate enhancement of HIV infection [51]. Therefore, Sg1 may be used as a model amyloid protein. Also a small peptide Sg1 (38-48) was reported to be capable of self-assembling into hydrogel at neutral pH mostly pH 7.0 and pH 9.0, containing β -sheet rich fibrillar aggregates. The size of the formed aggregates by this peptide were reported to be in

micrometres as measured by dynamic light scattering [52]. However, the amyloid forming ability of Sg1 full length protein has not been established *in vitro*.

Very recently, Hsp104 has been shown to be remodelled to antagonise against seminal amyloids like SEVI and Sg1. Thereby, acting as a strategy to reduce their ability to promote HIV infection [53].

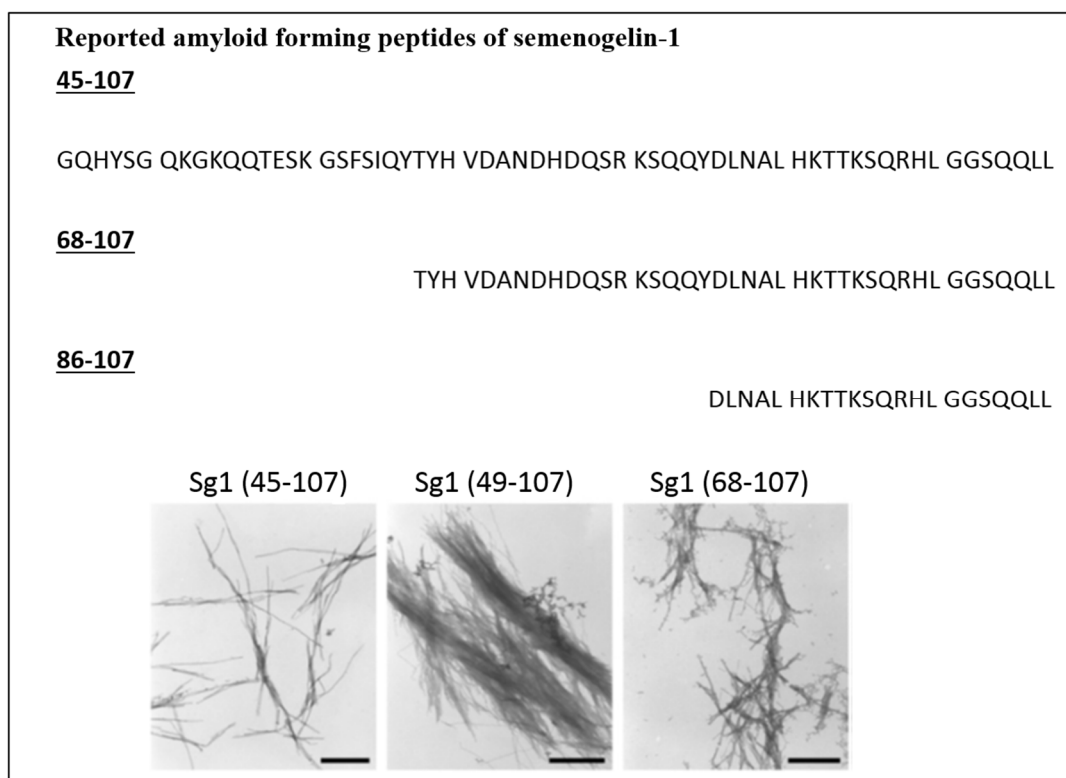


Figure 8. Electron micrographs of fibrillar structures from Semenogelin-1 peptides
Scale bars indicate 500 nm (*adapted from Roan et al, 2011*) [48,49]

Semenogelin aggregates enhance HIV infectivity. During semen liquefaction, fragments released from the semenogelin proteins form amyloid fibrils that electrostatically attach to HIV virions and direct them to target cells (Figure 9).

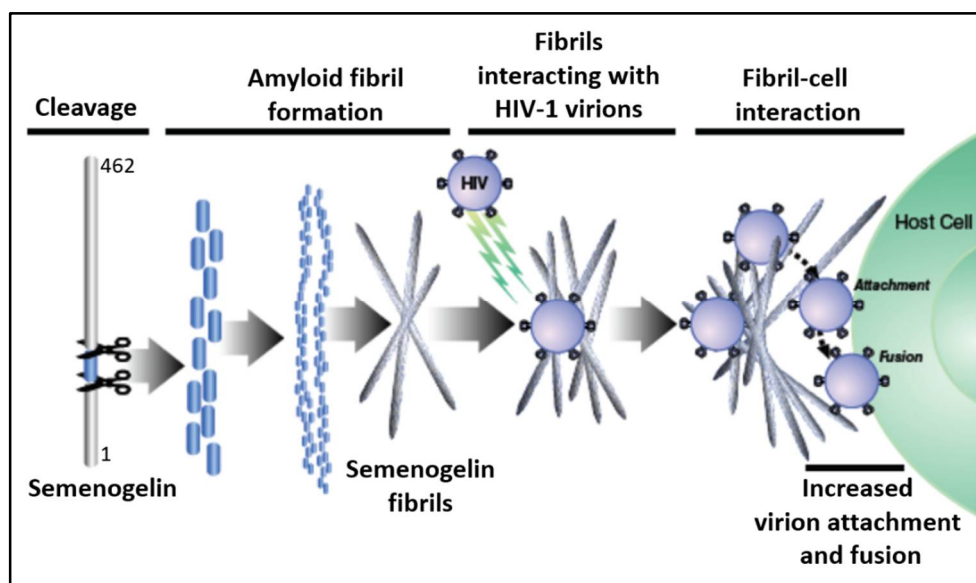


Figure 9. Sg1 peptide amyloid facilitates HIV virion attachment and entry to cultured cells (adapted from Roan, Warner C. Greene et al, 2011) [48]

In SSVA disorder, Sg1 amyloid deposits in the sub-epithelium and lumen of seminal vesicles (Figure 6 & Figure 10). Thus, we expect that it is the full length Sg1 which would form amyloid aggregates *in vivo*, as it would not have, thus far, encountered the protease PSA. The fragmentation of Sg1 by PSA occurs after it is released out of the vesicles and mixed with prostatic fluid. Thus, amyloidogenicity of full length Sg1 needs to be examined to get a mechanistic insight into the development of SSVA. Also, examination of HIV infectivity in presence of full length Sg1 amyloid aggregates may be physiologically more relevant compared with the thus far obtained amyloid aggregates of Sg1 peptides which are generated only downstream post-ejaculation. Further, the formed amyloid aggregates can act as a target for inhibitor analysis with relevance to SSVA disease.

Seminal vesicle amyloidosis incidence increases with age [31]. Seminal levels of certain constituents such as α -glucosidase, fructose, and zinc also decrease with age, however any correlation with SSVA is yet to be established [54,55]. The average reported seminal concentration of α -glucosidase is 2.74 mg/100mL, fructose is 272 mg/100mL and zinc is 16.5 mg/100mL in healthy adults [56,57].

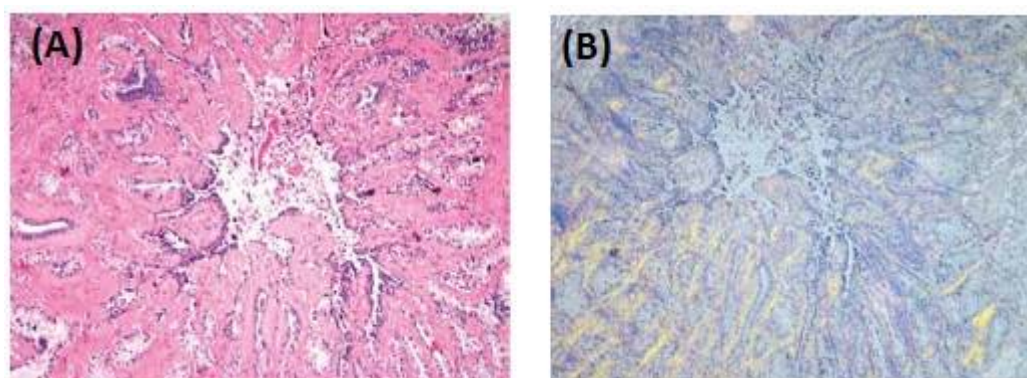


Figure 10. Congo red staining of seminal vesicle sections

(A) Nodular amyloid deposits with sub-epithelial location in seminal vesicle on light microscopy (x40). (B) Amyloid deposits with apple green reflection on polarized light microscopy (x40) [29]

These constituents play significant role in maintaining fertility. The level of α -glucosidase in seminal plasma reflects the functional state of the epididymis. The α -glucosidase levels are positively correlated with sperm count and motility. Fructose has been reported to be a source of energy for the motility of the gametes [58]. Zinc is secreted from prostate into seminal fluid and is required for the formation of semen coagulum by Sg1 thereby plays an important role in sperm release and motility [59]. Reducing levels of prostate zinc content with aging is associated with prostate diseases like prostate cancer and oxidative stress that can cause increased DNA damage [60]. By seeing the relationship among advanced age, decreased prostate zinc content and increased occurrence of associated diseases we hypothesize that it may affect Sg1 dependent senile seminal vesicle amyloidosis. Zinc as well as other cations like Copper have been shown to have a significant effect on amyloid aggregation. Zn^{2+} and Cu^{2+} have been shown to inhibit $A\beta_{42}$ amyloid formation which is implicated in development of Alzheimer's disease [61,62]. As semen contains high concentrations of Zn^{2+} ions in young individuals which decline with age and SSVA cases increase with age, we tested if Zn^{2+} affects the aggregation of Sg1. Thus, understanding the role of Zn^{2+} in relation to aging would help to understand SSVA amyloidosis. In addition to full length Sg1 a large Sg1 (1-159) fragment encompassing the reported amyloidogenic peptide regions of Sg1 was also recombinantly purified and tested for amyloid aggregation and effect of Zn^{2+} was assessed. The Sg1 (1-

159) fragment is still relevant to SSVA as it has all the available binding sites for cellular factors like Zinc. The amyloid formed by this fragment can act as a target for inhibitor analysis against SSVA disorder.

1.6 Human serum albumin: amyloidogenic protein

Human serum albumin (HSA) is the most abundant protein in human blood plasma. HSA is an all α -helix, globular protein made of a single peptide chain of 585 amino acid residues with one free sulfhydryl group (on Cysteine-34) and 17 intrachain disulfide bonds (Figure 11) [63]. HSA contains one tryptophan residue (Trp-214). The molecular weight of HSA is 67 kDa.

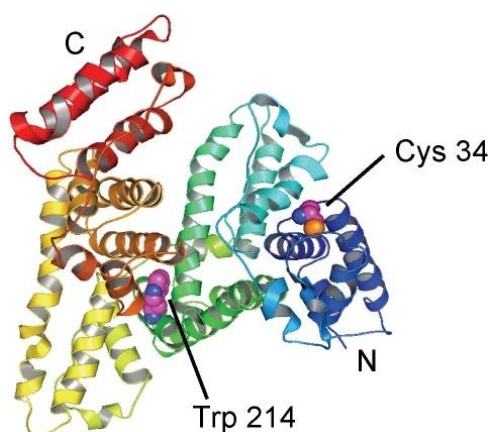


Figure 11. Secondary structure of HSA molecule
(adapted from Biswas.S. et al, 2015) [64]

HSA has multiple physiological roles like: as a regulator for blood pH & osmotic pressure and as a macromolecular carrier for transport of nutrients, hormones, & several compounds such as fatty acids, amino acids, bile salts & metals [65-67]. HSA is considered as a safe and non-immunogenic drug carrier and as a versatile plasma expander, as its administration is found to be helpful in the treatment of severe hypoalbuminemia during burns, nephritic syndrome, chronic liver cirrhosis and hemorrhagic shocks [68]. In fact, dimerized HSA molecules are preferred over monomeric HSA as plasma expander & drug carrier due to increased circulatory life and alleviating effect on the edema associated with unwanted extravasation of the monomeric HSA [68,69]. Nitric oxide (NO) is emerging as an anti-oncogenic agent. It has been

shown to have potential use in cancer therapy [70]. HSA can be a suitable candidate for NO transport because NO binds to Cys-34 of HSA to form S-nitrosylated HSA. HSA is an efficient carrier of NO and good candidate as antitumor drug due to its ability to promote the uptake of drugs with specificity to tumour tissue. Also, the HSA dimer is expected to have enhanced accumulation in tumors because of its large molecular weight [68].

So far, HSA dimers for clinical applications are obtained by cross-linking of its free cysteine residues using chemical cross-linkers that can be potentially immunogenic [68]. Thus the need is to obtain disulfide-linked HSA dimers without any chemical cross-linkers. Although, HSA monomer can misfold *in vitro* and aggregate with several properties expected of amyloid aggregates, however, key amyloid property of self-seeding remains to be demonstrated. Also, whether HSA dimer, which finds clinical applications, can also form amyloid is unexplored. For a protein as functionally versatile as HSA, both *in vivo* as well as in clinical applications, formation of self-seeding stable amyloid aggregates can be potentially hazardous.

HSA is found to form amyloid-like aggregates *in vitro* at physiological pH 7.4 and also at acidic pH but only at elevated temperatures (65°C), when present in aqueous solvents (Figure 12) [71]. HSA aggregation has been reported at physiological pH at lower temperatures also (25°C, 37°C) however in presence of organic solvent ethanol [72-74]. HSA aggregates display varying morphologies under different aggregation conditions, possibly due to formation of different structural intermediates during the aggregation pathway [71,72]. Unlike a typical amyloid aggregation trend, which follows a lag dependent sigmoidal kinetics, there is absence of any apparent lag period in HSA aggregation [5,72].

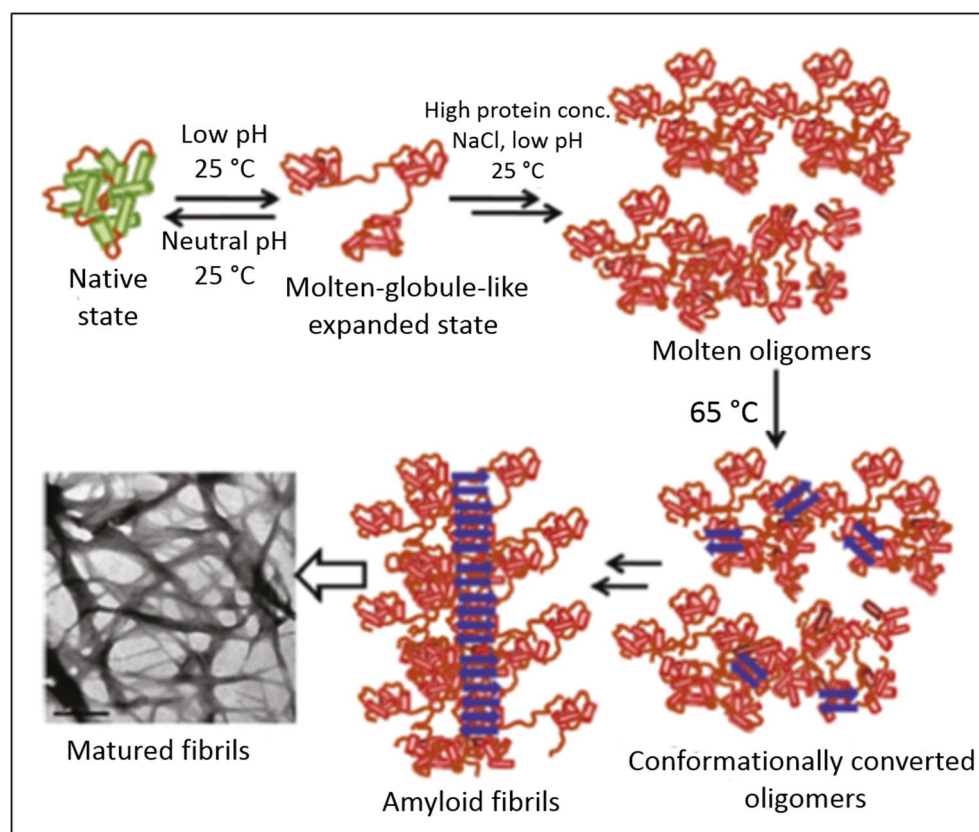


Figure 12. Proposed model for amyloid aggregation pathway of HSA
(adapted from Bhattacharya et al, 2011) [18]

Although, HSA aggregates have previously been shown to conform to several amyloid aggregate-associated properties such as thioflavin-T (ThT) dye binding, Congo red binding, electron microscopy and atomic force microscopy etc.[72] certain important properties such as the self-seeding ability and detergent stability have not been established yet. Amyloid self-seeding is usually assayed *in vitro* and monitored as decrease in lag period of aggregation, suggesting acceleration of conversion of monomers to aggregates [10]. If HSA aggregates exhibited self-seeding at physiological conditions, any unwanted HSA amyloid contamination in samples used for therapeutics, could potentially seed the *in vitro* circulating HSA monomers into amyloid form, which would be hazardous.

Here we first converted HSA into aggregates exhibiting amyloid-like ThT dye binding and then we examined if the aggregates display amyloid-like detergent stability. Furthermore, we examined self-seeding behaviour of HSA aggregates at sub-optimal aggregation temperature, in the view that few previous attempts at optimal aggregation

conditions were inconclusive, possibly due to lack of a discernible lag period in aggregation [72,75]. Due to buried nature of the free cysteine-34 in HSA structure, HSA dimers employed for clinical applications have often been obtained using chemical cross-linkers of cysteine, which may potentially be immunogenic [68]. Here we attempted homodimerizing HSA *via* disulfide linkage using denaturation in urea and hydrogen peroxide (H₂O₂) induced oxidation. We then examined if HSA homodimers retain the amyloidogenic properties similar to the HSA monomers.

We tried to explore further into some unanswered questions through this study. We hypothesize that full length Sg1 is expected to aggregate *in vivo* in the seminal vesicles as it has not encountered PSA which is secreted by prostate further downstream. Thus we investigated whether full length Sg1 show amyloid aggregation *in vitro* as it would be helpful to understand SSVA. Also, all the known amyloid forming fragments of Sg1 are generated by PSA digestion. Therefore, we examined whether any larger fragment of Sg1 [here: Sg1 (1-159)] containing amyloid core is able to show amyloid-like aggregation.

Next, we examined new aspects of HSA aggregation and investigated whether HSA aggregates exhibit true amyloid-like characteristics particularly exploring key amyloid properties of amyloid like self-seeding ability and detergent stability. HSA dimer is preferred for medical applications, therefore, we also assessed the amyloidogenic properties of HSA homodimer.

Chapter II

Recombinant expression, purification & characterization of human Semenogelin-1 (Sg1) and Sg1 (1-159) proteins

2.1 Abstract

In this chapter we successfully demonstrated cloning, expression and purification of recombinant Sg1 full length and Sg1 (1-159) using bacterial expression vector. A segment of Sg1 encoding 1-159 amino acid residues was PCR amplified from pReceiver-B01 expression vector containing ORF for full length Sg1, and cloned into the same recombinant expression vector to code for an N-terminal 6xHis-tagged fusion protein under the control of T7 promoter to obtain pBKP-Sg1 (1-159). The obtained clone was verified by DNA sequencing. The recombinant plasmids pReceiver-B01-Sg1 or pBKP-Sg1 (1-159) respectively encoding full length Sg1 or Sg1 (1-159) fragment, were transformed into *E. coli* BL21-AI cells. The proteins were expressed as N-terminal 6xHis-tagged fusion proteins by induction with 1mM IPTG and 0.15% L- arabinose, which were subsequently purified under denaturing conditions (8 M urea) using Ni-NTA agarose affinity column chromatography. Homogeneity of the purified proteins were assessed by SDS-PAGE and their molecular weights were estimated by relative mobility plots of protein molecular weight standards. Identity of the protein was further confirmed by western blotting using anti-His antibody. Then, refolding of the purified Sg1 was examined by intrinsic Tryptophan (Trp) fluorescence. Trp fluorescence spectrum of Sg1

showed a blue shift in λ_{\max} from ~ 350 nm to ~ 345 nm on decreasing urea concentration from 8 M to 0.5 M urea. Upon complete removal of the urea by dialysis, further blue shift in λ_{\max} at 336 nm was observed thereby indicating presence of tryptophan in a relatively hydrophobic environment and suggesting structure induction. However, as tryptophan λ_{\max} is expected to be ~ 320 nm if it is in a completely internalized hydrophobic micro-environment, the Sg1 even in absence of any denaturant, is largely unstructured as reported earlier. Notably, both Sg1 full length and Sg1 (1-159) proteins were found to precipitate upon dialysis when carried out above pH 7.0, even in the presence of over 100 mM NaCl, however, they remained soluble when dialyzed at pH 3.0 -4.0. This observed aggregation around and above physiological pH bears resemblance to aggregation of Sg1 in seminal vesicles in the SSVA disorder as the reported pH in seminal vesicles is ~ 8.5 . As Sg1 (1-159) contains the reported amyloid forming regions, it can be employed for studying aggregation behaviour. SSVA disorder involves aggregation and deposition of Sg1 amyloid aggregates. But so far it has not been established whether full length Sg1 can form amyloid aggregates. We further characterized the purified proteins Sg1 and Sg1 (1-159) and found that they are in their native conformation. These recombinant proteins were then utilized further for study of amyloid aggregation abilities as reported in next chapter.

2.2 Introduction

Originally, Linke & Westermarck et al in the year 2005, isolated samples from patients and upon proteomics studies utilizing mass spectroscopy identified peptides corresponding to Sg1 amino acid sequence thereby suggesting role of Sg1 aggregation in Senile Seminal Vesicle Amyloidosis (SSVA) [14]. It has been reported that Sg1 protein has a non-globular structure and an increasing tendency towards random coil formation [76]. Many recent studies have reported the probable role of Sg1 as a cancer marker [43-46]. Also certain peptide fragments of Sg1 [Sg1 (45-107), Sg1 (68-107), Sg1 (86-107) and Sg1 (38-48)] have been reported to form amyloid aggregates *in vitro* and have been shown to greatly enhance HIV infection to cell cultures [48-50]. So far amyloid aggregation of full length Sg1 has not been demonstrated *in vitro*. Recombinant full length Sg1 protein could be employed for examining amyloid aggregation properties to

get better insight into the development of SSVA disorder and further may also serve for amyloid inhibitor analysis. Therefore, with the objective to explore the amyloid forming ability of full length Sg1 and Sg1 (1-159), we attempted recombinant expression and purification of these proteins. This chapter presents the cloning, recombinant expression and purification of Sg1 full length and Sg1 (1-159) and describes the characterization of the purified proteins.



Figure 13. Schematics of recombinant proteins, his-tagged Sg1 full length and a cloned out fragment Sg1 (1-159) encompassing the previously reported amyloidogenic peptide region of 45-107 amino acids.

2.3 Results and Discussion

SSVA disorder is associated with deposition of Sg1 amyloid aggregates in seminal vesicle. Sg1 protein has previously been extracted from human semen however, the extraction procedure is complex [77]. Although, bacterial expression system is not considered very suitable for expression of human proteins primarily due to incapability of proper post-translational modification, as no major post translational modifications like glycosylation have been reported for Sg1 *in vivo* therefore, expression and purification from *E. coli* system would be expected to yield native like Sg1 protein [33]. Thus, we attempted recombinant expression of Sg1 protein and its fragment Sg1 (1-159) in *E. coli* and purification using Ni-NTA affinity chromatography under denaturing conditions. Furthermore, to assess amyloidogenicity, a larger fragment of Sg1 (amino acids 1-159) containing the previously reported small amyloidogenic peptide regions was also recombinantly expressed and purified like Sg1 [48]. Expectedly, additional amino acid sequences in this fragment compared with the small reported amyloidogenic peptides,

may interact with cellular factors (like Zn²⁺) and could be examined for any effect of cellular factors on Sg1 amyloid aggregation.

2.3.1 Cloning of Sg1 (1-159) in a recombinant expression vector and expression of recombinant Sg1 and Sg1 (1-159) proteins

A plasmid containing cDNA of SEMG1 ORF for encoding human semenogelin-1 cloned in pReceiver-B01 bacterial expression vector was procured from Gene Copoeia, USA (Cat. No.EX-Z2245-B01). A segment of Sg1 encoding 1-159 amino acid residues was PCR amplified from pReceiver-B01 using primers (Forward: 5'GCCAGCTTCGAATCGAAGGTCGAATGAAGCCCAACATCATC 3' and Reverse: 5'GGTGGCGATGCGGCCGCCTATTAATATTGACTGGATATTCCTTTC 3') and cloned into the same recombinant expression vector in frame with 6x histidine encoding tag using BstBI and NotI restriction enzymes to obtain pBKP-Sg1(1-159). Plasmid maps of pRB01-Sg1 and pBKP-Sg1(1-159) are shown indicating unique (single cutter) restriction enzyme sites and ORF regions of interest (Figure 14).

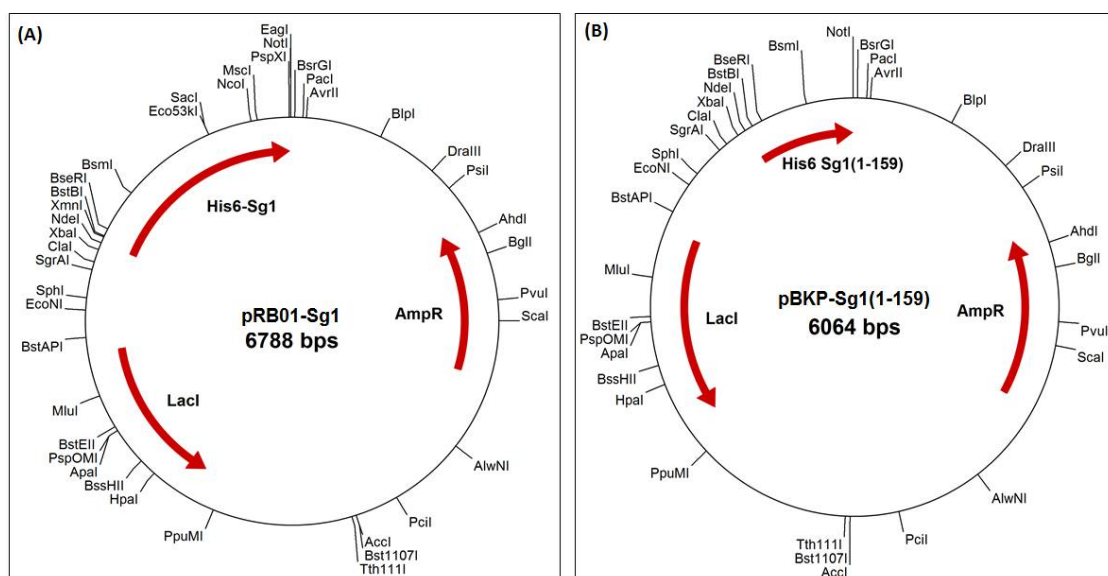


Figure 14. Plasmid maps of pRB01-Sg1 and pBKP-Sg1(1-159)

(A) The plasmid pRB01-Sg1 encodes the following protein sequence from Sg1

```

MKPNIIFVLS LLLILEKQAA VMGQKGGSKG RLPSEFSQFP HGQKGQHYSG QK GKQQTESK
GSFSIQYTYH VDANDHDQSR KSQQYDLNAL HKTTKSQRHL GGSQQLLHNK QEGRDHDKSK
GHFHRVVIHH KGGKAHRGTQ NPSQDQGNP SGKGISSQYS NTEERLWVHG LSKEQTSVSG
AQKGRKQGG SSSYVLQTEE LVANKQQRET KNSHQKNGHY QNVVEVREEH SSKVQSLCPA
HQDKLQHGSK DIFSTQDELL VYNKNQHQT KLNQDQQHGR KANKISYQSS STEERLHYG
ENGVQKDVSQ RSIYSQTEKL VAGKSQIQAP NPKQEPWHGE NAKGESGQST NREQDLLSHE
QKGRHQHGSH GGLDIVIEQ EDDSDRHLAQ HLNNDNRNPLFT

```

(B) The plasmid pBKP-Sg1 (1-159) encodes the following protein sequence from Sg1

```

MKPNIIFVLS LLLILEKQAA VMGQKGGSKG RLPSEFSQFP HGQKGQHYSG QK GKQQTESK
GSFSIQYTYH VDANDHDQSR KSQQYDLNAL HKTTKSQRHL GGSQQLLHNK QEGRDHDKSK
GHFHRVVIHH KGGKAHRGTQ NPSQDQGNP SGKGISSQY

```

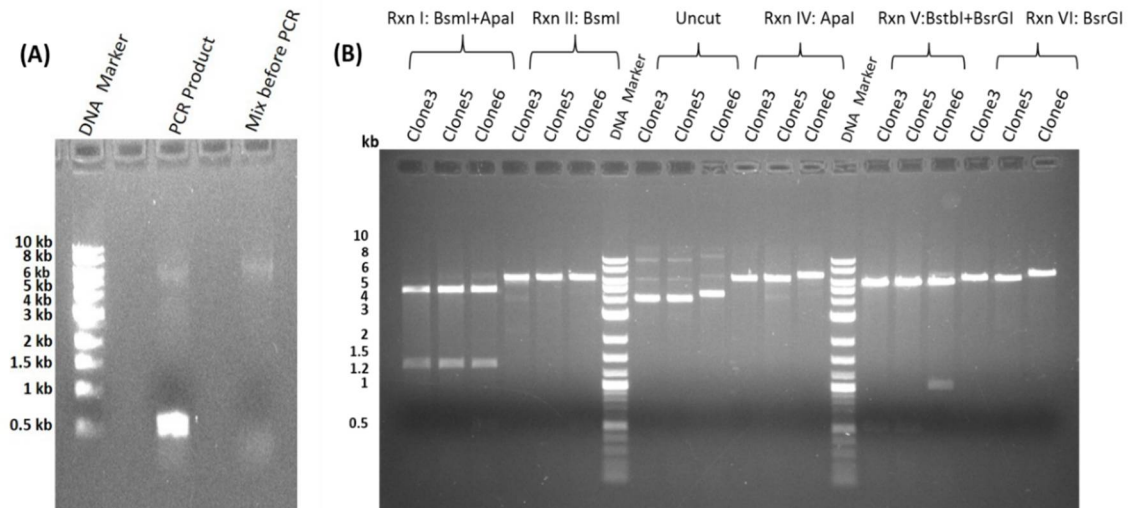


Figure 15. Plasmid construction of pBKP-Sg1(1-159)

(A) PCR product pBKP-Sg1(1-159) obtained using pRB01-Sg1 as template.
(B) pBKP-Sg1(1-159) correct clone confirmation by restriction enzyme digestion. Uncut experimental DNA from all three selected clones (indicated as clone 3, 5, 6) for screening has been used as control. DNA bands visualized under UV light in an ethidium bromide stained agarose gel.

2.3.2 Purification of recombinant Sg1 and Sg1 (1-159) by Ni-NTA affinity chromatography

Recombinant proteins full length Sg1 (Sg1) or Sg1 (1-159) were purified under denaturing conditions to prevent any mis-aggregation by following the protocol as described in methods section (Figure 16).

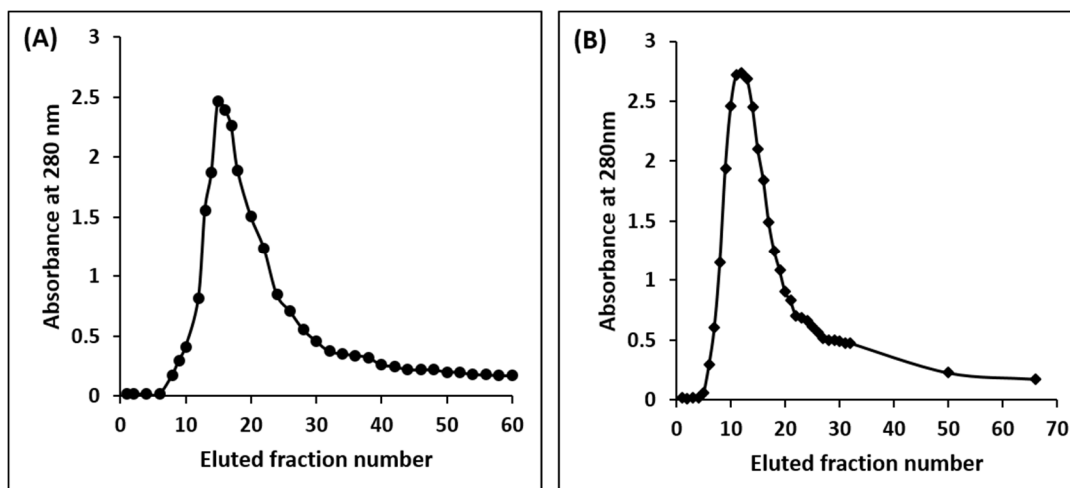


Figure 16. Ni-NTA affinity purification profile of recombinant proteins
(A) Sg1 full length (B) Sg1 (1-159) protein
Purification profile of the eluted proteins (A) Sg1 and (B) Sg1 (1-159) was obtained by measuring absorbance of eluted fractions at 280 nm by using UV-visible spectrophotometer

2.3.3 Assessment of homogeneity and molecular weight of recombinant Sg1 and Sg1 (1-159) proteins

Eluted fractions of Sg1 and Sg1 (1-159) showing high $A_{280\text{nm}}$ were examined for homogeneity and molecular weight respectively by using 10 % or 15 % Sodium dodecyl sulfate polyacrylamide gel electrophoresis (SDS-PAGE) under reducing condition by the method of Laemmli [78]. The eluted proteins were found to be homogenous on SDS-PAGE. As expected based on their amino acid sequence, molecular weights of the purified Sg1 and Sg1 (1-159) were found to be 49 kDa and 18 kDa respectively by SDS-PAGE as estimated using molecular weight standards (Figure 17).

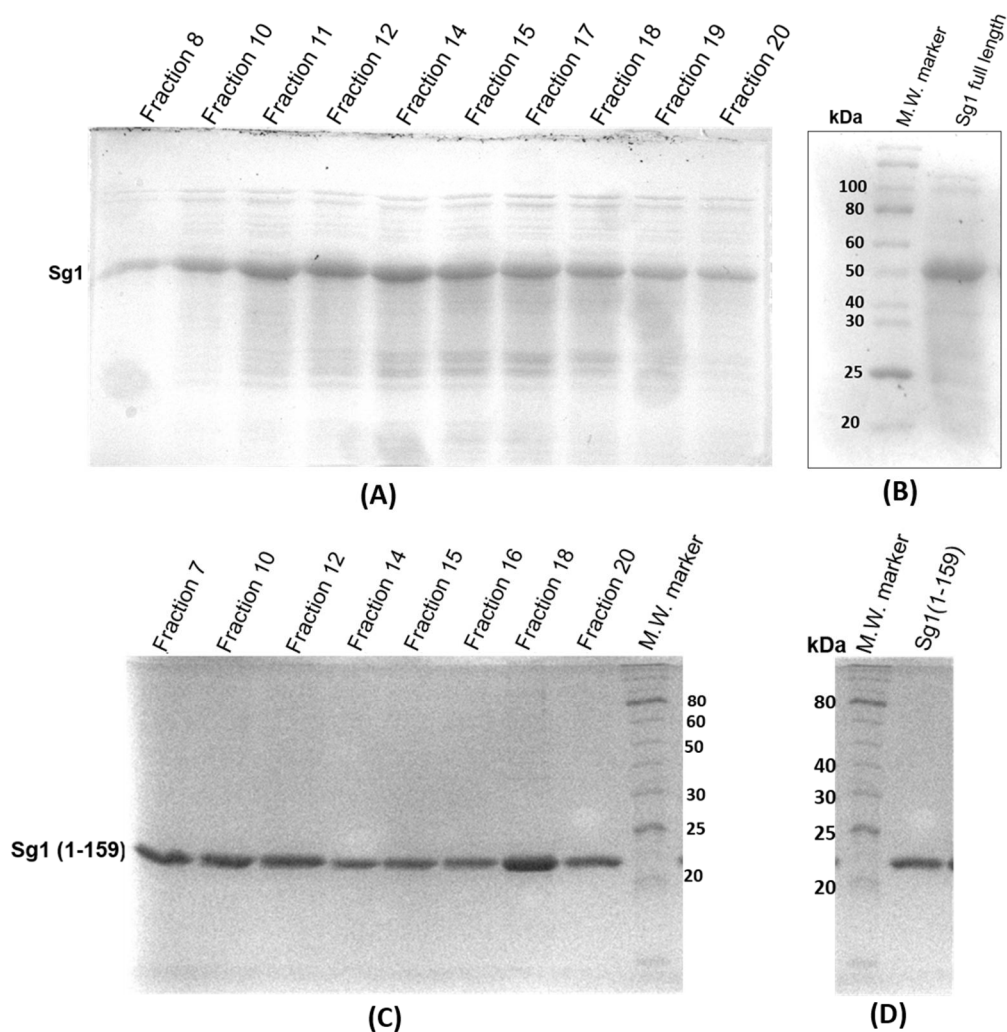


Figure 17. Homogeneities of the recombinant proteins assessed by SDS-PAGE

Fraction from Ni-NTA affinity chromatography purification of (A) Sg1 full length or (C) Sg1 (1-159) fragment were assessed on 10 % and 15 % SDS-PAGE respectively. Pooled homogeneous fractions of (B) Sg1 and (D) Sg1 (1-159) fragment were examined alongside a molecular weight marker on 10 % and 15 % SDS-PAGE respectively. Molecular weights of Sg1 full length and Sg1 (1-159) fragment were respectively estimated to be 49 kDa and 18 kDa.

2.3.3.1 Estimation of molecular weight by relative mobility plot

The homogeneity of recombinant Sg1 and Sg1 (1-159) proteins were assessed by SDS-PAGE. The experimental molecular weight was calculated by plotting relative mobility of different proteins of molecular weight marker (New England Biolabs Inc.; Catalogue

No. P7703S). By substituting the values of relative mobility 0.235 for Sg1 and 0.448 for Sg1 (1-159) in the following equations respectively as obtained from the above plots,

$$y = -0.5686 x + 1.1968$$

$$y = -0.5886 x + 1.1807$$

Where, $x = \log$ (molecular weight, kDa) and y is relative mobility.

The experimental molecular weight of Sg1 was estimated to be 49 kDa and that of Sg1 (1-159) was 17.47 kDa (Figure 18).

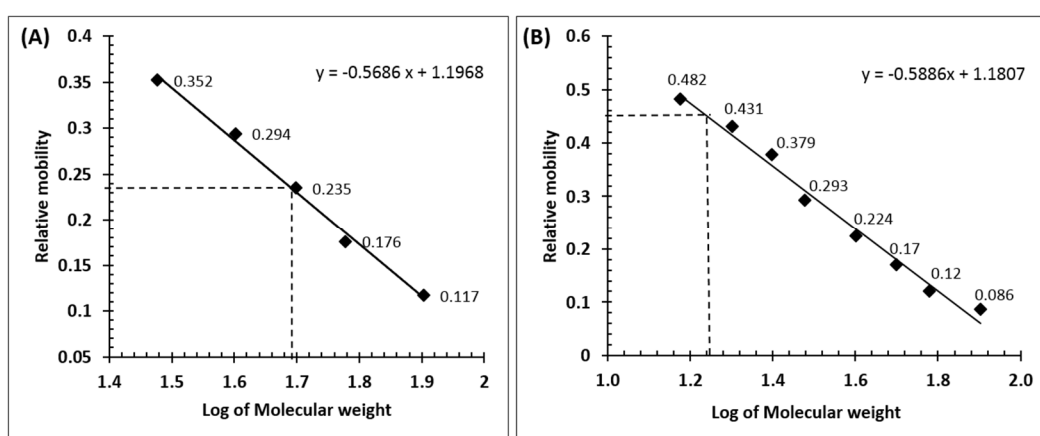


Figure 18. Estimation of mol. wt. of recombinant Sg1 and Sg1 (1-159) using relative mobility plot of mol. wt. standards from figures 17B & 17D

Relative mobility of different proteins in molecular weight standards (from figure 17B & 17D) were plotted against log of their known molecular weights. These standard plots were used for estimation of mol. wt. of (A) Sg1 and (B) Sg1 (1-159) protein.

2.3.4 Identification of His-tag in purified Sg1 by western blotting

As per the fusion design the identity of the purified Sg1 protein was confirmed by probing the presence of N-terminal 6xHis-tag using anti-his antibody by western blotting [79]. The protein band stained by Coomassie was also identified by the anti-his antibody in the western blotting (Figure 19). This confirms presence of his-tag in the recombinant Sg1 protein.

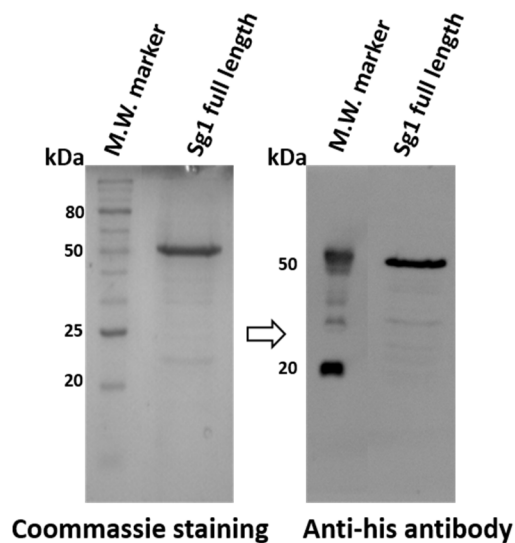


Figure 19. Identification of his₆-tag in the recombinantly purified full length Sg1 protein by anti-his antibody using western blotting

Sg1 protein was electrophoresed on SDS-PAGE gel and transferred to PVDF membrane by electroblotting. Sg1 protein band on the membrane was probed with anti-his antibody.

2.3.5 Characterization of the recombinant Sg1 and Sg1 (1-159) proteins

2.3.5.1 UV-visible absorbance spectroscopy

Protein absorb light in the UV-visible region of the spectrum. Most proteins have high absorbance at ~ 280 nm which can be used for measuring concentration of proteins. Observed absorbance is due to the presence of aromatic amino acid residues such as tryptophan, tyrosine and phenylalanine [80].

When Sg1 and Sg1 (1-159) were examined for absorbance in UV-visible spectrophotometer, protein like absorbance spectra were observed. Sg1 showed peak absorbance at 280 nm and Sg1 (1-159) showed maximum absorbance near 270 nm (Figure 20).

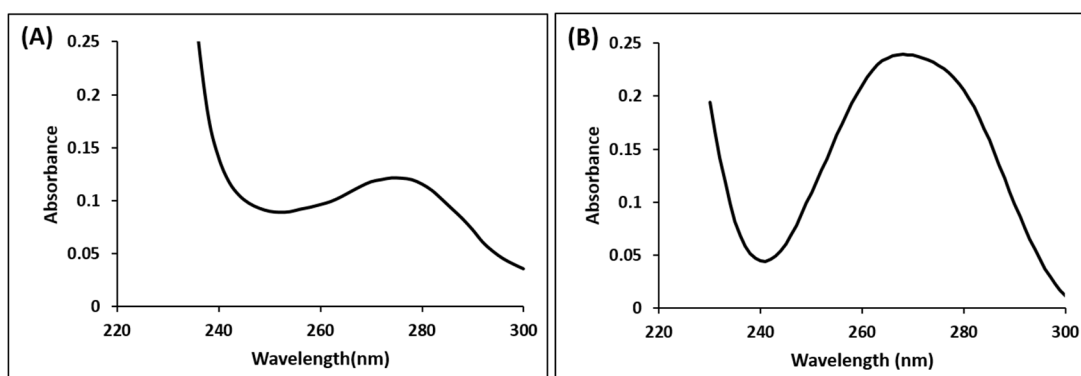


Figure 20. Absorbance spectra of purified recombinant proteins

(A) Sg1 and (B) Sg1 (1-159) by UV-visible spectroscopy

Absorbance spectra of 0.2 mg/ml protein (A) Sg1 or (B) Sg1

(1-159) was recorded using UV-visible spectrophotometer.

Spectra acquired after baseline correction.

As per the amino acid sequence, Sg1 has 2 Trp and 13 Tyr residues whereas Sg1 (1-159) comprises of 0 Trp and 7 Tyr residues. The observed difference in the trend of absorbance spectra of Sg1 and Sg1 (1-159) may be due to difference in composition of aromatic amino acids.

2.3.5.2 Estimation of molar extinction coefficient

(i) Molar extinction coefficient of purified Sg1 full length

The molar absorption coefficient of a peptide or protein is related to its tryptophan (W), tyrosine (Y) and cysteine (C) amino acid composition. This value is approximately equal to the weighted sum of the molar absorption coefficients of these three amino acids at 280 nm. It is calculated by the following equation:

$$\epsilon_{\text{molar}} = (nW \times 5690) + (nY \times 1280) + (nC \times 120)$$

Semenogelin-1 has 2 tryptophan, 13 tyrosine and 1 cysteine residues.

Therefore,

$$\begin{aligned} \epsilon_{\text{molar}} &= (2 \times 5690) + (13 \times 1280) + (1 \times 120) \\ &= 11380 + 16640 + 120 \\ &= 28140 \end{aligned}$$

Also, the relation between ϵ_{molar} and $\epsilon_{\text{percent}}$ is given by the following equation:

$$(\epsilon_{\text{molar}})_{10} = (\epsilon_{\text{percent}}) \times (\text{molecular weight of protein})$$

Therefore,

$$(28140)_{10} = (\epsilon_{\text{percent}}) \times 49000$$

$$\epsilon_{\text{percent}} = 281400/49000$$

$$\epsilon_{\text{percent}} (280 \text{ nm}) = 5.74$$

(ii) Molar extinction coefficient of purified Sg1 (1-159)

Sg1 (1-159) has 0 tryptophan, 7 tyrosine and no cysteine residues.

Therefore,

$$\epsilon_{\text{molar}} = (0 \times 5690) + (7 \times 1280) + (0 \times 120)$$

$$= 8960$$

Also, the relation between ϵ_{molar} and $\epsilon_{\text{percent}}$ is given by the following equation:

$$(\epsilon_{\text{molar}})_{10} = (\epsilon_{\text{percent}}) \times (\text{molecular weight of protein})$$

Therefore,

$$(8960)_{10} = (\epsilon_{\text{percent}}) \times 18000$$

$$\epsilon_{\text{percent}} = 8960/18000$$

$$\epsilon_{\text{percent}} (280 \text{ nm}) = 4.97$$

Concentration of protein can be calculated using the following equation:

$$(A_{280}/\epsilon_{\text{percent}})_{10} = \text{concentration in mg/ml}$$

Protein concentrations were estimated using extinction coefficients of Sg1 full length ($\epsilon_{280}^{1\%} = 6 \text{ (gm/100ml)}^{-1}\text{cm}^{-1}$) and Sg1 (1-159) fragment ($\epsilon_{280}^{1\%} = 4.9 \text{ (gm/100ml)}^{-1}\text{cm}^{-1}$) that were average of values determined spectrophotometrically and from expasy protparam tool using their amino acid sequences [80,81].

2.3.5.3 Intrinsic fluorescence of Sg1 protein

Most of the intrinsic fluorescence emission of a protein is due to excitation of its tryptophan residues. Tryptophan (Trp) fluorescence spectrum of a protein can help to monitor the folded or unfolded state of a protein. In native state Trp are primarily in

hydrophobic environment (buried within the core of the protein) and have high fluorescence intensity and λ_{max} value around 315 nm to 320 nm. In contrast in a hydrophilic environment (exposed to solvent) Trp fluorescence intensity decreases and λ_{max} value is greater than 330 nm [82,83].

As semenogelin-1 contains two Trp residues, we examined Trp fluorescence emission spectra and observed λ_{max} at 350 nm indicating presence of Trp in hydrophilic environment. Comparing the intrinsic fluorescence emission intensity of the protein upon excitation at 292 nm (excites only Trp) vs the excitation at 280 nm (excites both Trp and Tyr), it is apparent that there is significantly large contribution from tyrosine residues. This is consistent with the presence of only 2 tryptophan vs. 13 tyrosine residues in Sg1 protein (Figure 21).

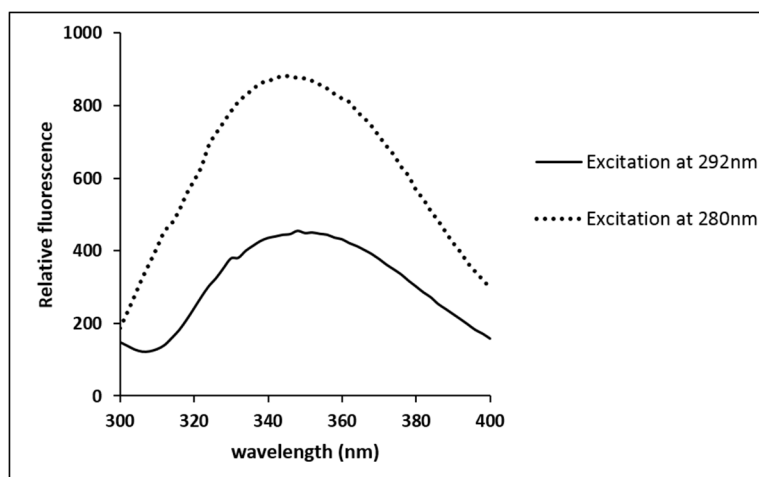


Figure 21. Intrinsic fluorescence emission spectra of Sg1 dialyzed at pH 7.4
Trp fluorescence spectrum of Sg1 (solid line) recorded by excitation at 292 nm and Tyr & Trp fluorescence spectrum of Sg1 (dotted line) acquired by excitation at 280 nm.

2.3.5.4 Refolding of the Sg1 protein purified under denaturing conditions

2.3.5.4.1 Tryptophan fluorescence of Sg1 under different urea concentrations

The recombinant Sg1 protein purified under denaturing conditions in presence of 8 M urea was diluted in 10 mM sodium phosphate buffer, pH 7.4 with decreasing urea

concentration from 8 M to 0.5 M urea, while keeping the protein concentration same (0.2 mg/ml). Tryptophan emission fluorescence spectrum was recorded after excitation at 292 nm by monitoring emission from 300 nm to 400 nm. The spectrum showed blue shift in emission wavelength maximum (λ_{\max}) from ~ 350 nm to ~ 345 nm on decreasing urea concentration from 8 M to 0.5 M urea (Figure 22). Whereas, for the dialyzed protein (0 M urea) further blue shift in λ_{\max} at 336 nm was observed. This suggests presence of tryptophan in relatively hydrophobic environment indicating structure induction after dialysis. However, as tryptophan λ_{\max} is expected to be less than 320 nm if it is in an internalized hydrophobic micro-environment, possibly Sg1 even in absence of any denaturant has very little structure or largely unstructured, as reported earlier [76,82].

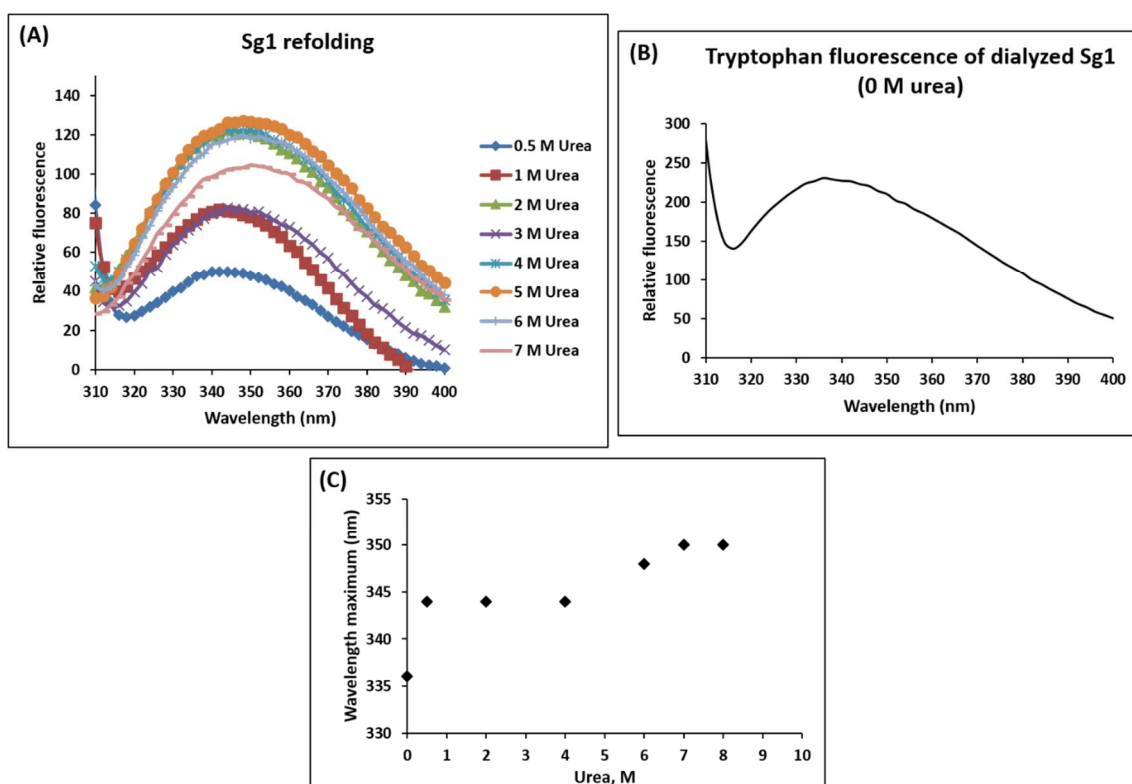


Figure 22. Assessment of refolding of Sg1 by intrinsic tryptophan fluorescence

(A) Trp fluorescence spectrum of Sg1 at different urea concentrations, (B) Trp fluorescence spectrum of dialyzed Sg1 in absence of urea, (C) Trp fluorescence emission λ_{\max} of Sg1 plot against different urea concentrations from 8 M to 0.5 M.

The purified protein showed structural features similar to as reported previously for Sg1 isolated from the human source, as assessed by intrinsic tryptophan fluorescence spectrometry [76].

2.3.5.4.2 Refolding of Sg1 assessed by Far-UV Circular dichroism

Circular dichroism (CD) is a very useful technique for determination of the secondary structure and folding properties of proteins. In proteins, structures such as α -helix and β -sheet are chiral thus absorb circularly polarized light. The absorption of this light acts as a measure of the degree of folding of the protein. CD spectroscopy can be employed for determining the folding state of proteins by measuring the change in far-UV absorption (190 nm to 260 nm) as a function of denaturant concentration [84,85].

CD spectra have earlier reported native Sg1 to be largely unstructured protein [76]. Far-UV spectral features of Sg1 at pH 7.4 in presence of 8 M urea showed mostly random coil (Table 3). At the same pH, on decreasing urea concentration to 2 M, there is relative increase in mean residue ellipticity at 222 nm. Whereas, CD spectra of Sg1 at pH 7.4 in presence of 0.5 M urea comprises of strong negative ellipticities at 208 nm and 215 nm which relatively decreases at 222 nm indicating presence of secondary structure (Figure 23). In 0 M urea, at pH 7.4 the protein comes out of solution so CD spectra could not be recorded. However, in 0 M urea when dialyzed at pH 3.0 the protein did not come of solution. At pH 3.0, far-UV CD spectrum of Sg1 exhibits negative ellipticity at 215 nm indicating presence of β -sheet secondary structure (Figure 23). The refolding studies in presence of decreasing urea concentrations by far-UV circular dichroism of Sg1, showed possibility that the structure contains both α -helix and β -sheet rich domains.

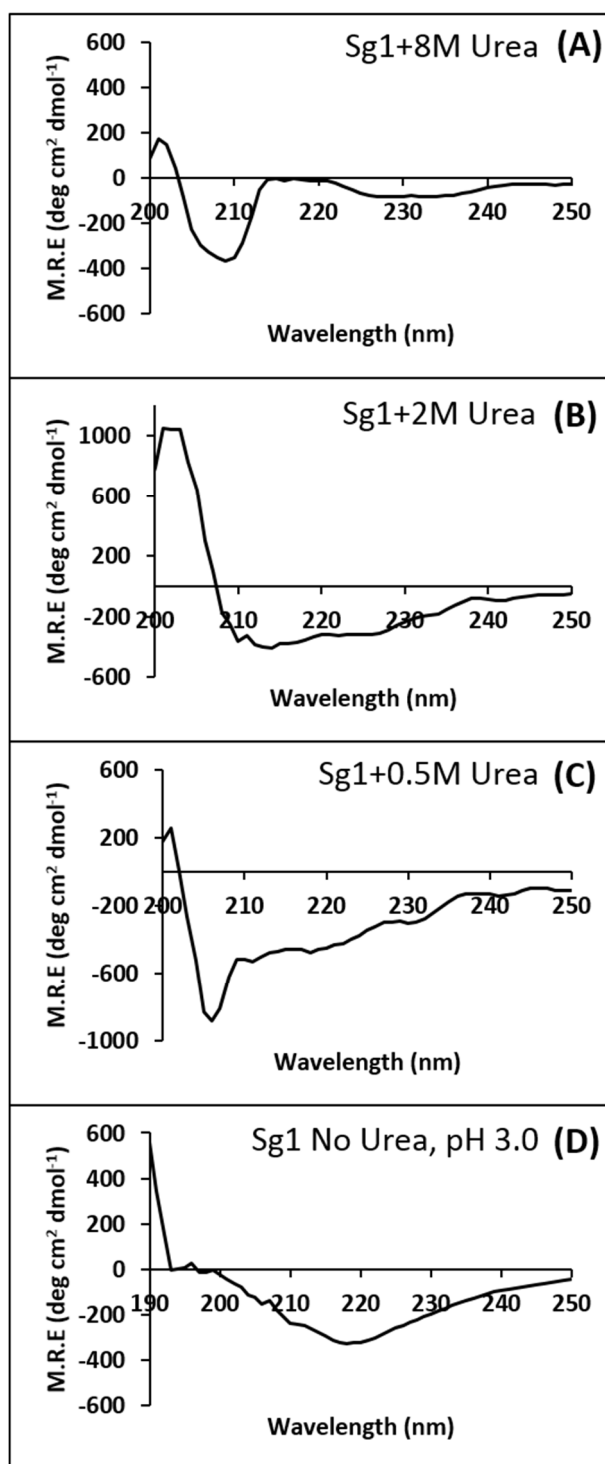


Figure 23. Refolding of Sg1 as assessed by far-UV CD spectra

CD spectra of Sg1 purified under denaturing conditions at pH 7.4 were recorded in presence of decreasing urea concentration (A) 8 M urea, (B) 2 M urea, (C) 0.5 M urea, (D) Sg1 dialysed at pH 3.0 (0 M urea).

Table 3. Secondary structure estimation of Sg1 under different urea concentrations

Panels from Figure 23	Sample	Secondary Structure*			
		Helix (%)	Beta (%)	Turn (%)	Random (%)
A	Sg1+8M Urea, pH 7.4	7.9	0	34.5	57.6
B	Sg1+2M Urea, pH 7.4	41	0	47	12
C	Sg1+0.5M Urea, pH 7.4	20.7	43.4	16	20
D	Sg1 dialyzed No Urea, pH 3.0	33.4	0	14.6	52

* Secondary structures were estimated using Yang's reference [84].

2.3.6 Aggregation of Sg1 and Sg1 (1-159) fractions during dialysis

The proteins Sg1 (49 kDa) and Sg1 (1-159) (18 kDa) purified in 8M urea were subjected to dialysis at 4 °C against 10 mM sodium phosphate buffer, pH 7.4 in presence of 10 mM β -mercaptoethanol, using dialysis membrane having molecular weight cut off 14 kDa and 3.5 kDa respectively. Dialysis helps to remove imidazole, urea and any other small molecule impurities. Also β -mercaptoethanol prevents any unwanted disulphide bond formation.

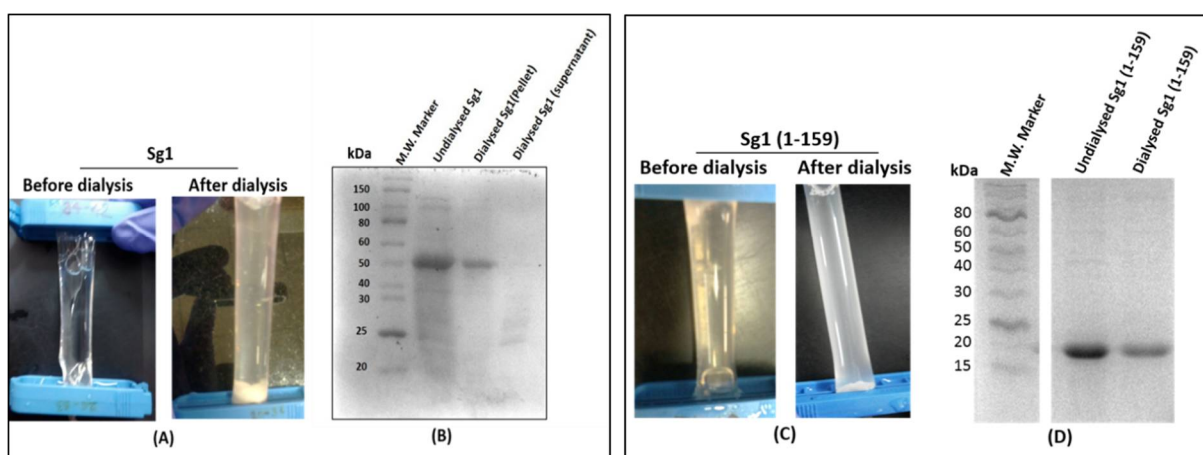


Figure 24. Protein precipitation during dialysis

(A, C) Dialysis of purified Sg1 or Sg1 (1-159) in 10 mM sodium phosphate buffer at pH 7.4. (B, D) SDS-PAGE of undialysed and dialysed Sg1 or Sg1 (1-159) using 10 % and 15 % resolving gel respectively.

Strikingly both the proteins exhibited precipitation during dialysis at pH 7.4 (Figure 24 A and 24 C). To find an appropriate pH at which the dialysis would keep the protein in solution, buffers from pH 3.0 to 10.5 were screened. Only the samples dialyzed at pH 3.0 or pH 4.0 were found to have soluble protein. Whereas, protein was found to precipitate at pH 7.4 and also at pH 9.0. Precipitation was observed even in presence of 150 mM NaCl at alkaline pH. On SDS-PAGE analysis the precipitated protein was found to be homogeneous. The precipitated protein was centrifuged at 10,000 rpm and the pellet fraction was found to be composed of full length Sg1 while the supernatant had very little protein and only minute fragments (Figure 24 B). Knowing that this alkaline pH where recombinant Sg1 precipitates is similar to seminal vesicles where Sg1 is synthesized and secreted [57,86], the precipitates obtained at pH 9.0 were examined for amyloid-like aggregates as discussed in the following chapter.

2.4 Materials and Method

2.4.1 Materials

Ni-NTA agarose was purchased from Qiagen (USA), Ampicillin, Urea, Guanidine hydrochloride, Sodium dodecyl sulfate (SDS), PMSF, Imidazole, Acrylamide, *N, N*-methylene bis-acrylamide, Coomassie brilliant blue R-250, CDP-star chemiluminescent substrate and dialysis membrane were obtained from Sigma (Co. USA). Anti-his antibody, APP-conjugated secondary antibody and Polyvinylidene fluoride (PVDF) membrane were from GE Healthcare. Protease inhibitor cocktail (complete EDTA free) was from Roche Applied Science. Q5 high-fidelity DNA polymerase and restriction enzymes were purchased from New England Biolabs (UK), PCR primers were obtained from Imperial Life Sciences (India). Plasmid isolation miniprep kit was obtained from Qiagen (Germany). Sodium phosphate monobasic, Sodium phosphate dibasic, were of molecular biology grade and procured from HiMedia (India).

2.4.2 Cloning of Sg1 (1-159) and expression of recombinant Sg1 and Sg1 (1-159) proteins

Cloning of Sg1 (1-159) and expression of recombinant Sg1 and Sg1 (1-159) proteins was carried out as follows. A plasmid containing cDNA of SEMG1 ORF for encoding human semenogelin-1 cloned in pReceiver-B01 bacterial expression vector was procured from Gene Copoeia, USA (Cat. No.EX-Z2245-B01). A segment of Sg1 encoding 1-159 amino acid residues was PCR amplified from pReceiver-B01 using primers (Forward: 5'GCCAGCTTCGAATCGAAGGTCGAATGAAGCCCAACATCATC 3' and Reverse: 5'GGTGGCGATGCGGCCGCCTATTAATATTGACTGGATATTCCCTTTC 3') and cloned into the same recombinant expression vector in frame with 6x histidine encoding tag using BstBI and NotI restriction enzymes to obtain pBKP-Sg1(1-159). The identity of pBKP-Sg1(1-159) clone was further verified by DNA Sequencing results. Standard protocol was used for the cloning [87]. The cloned plasmid was transferred into competent DH5 α *E. coli* cells. The transformed DH5 α cells were stored in -86 °C for maintaining the plasmid stock. Recombinant plasmids pReceiver-B01 or pBKP-Sg1 (1-159) respectively encoding full length Sg1 (Sg1) or Sg1 (1-159) fragment were transformed into competent *E. coli* BL21-AI cells (Invitrogen) as per the recommendations of the manufacturer. The bacterial cells were selected on the LB-Amp selection media (LB agar + ampicillin at 50 μ g/ml concentration). When the bacterial cells reached an optical density of 0.25 at 600 nm, 0.15% L-arabinose was added, and cells were further incubated for 45 min at 37 °C until they reach an optical density of 0.4 at 600 nm. Overexpression was induced by 1 mM isopropyl β -D-thiogalactopyranoside (IPTG) for 3 hours at 37 °C with continuous agitation in orbital shaker at 200 rpm. The cells were then harvested by centrifugation at 6000 rpm at 4 °C. The cell pellets were stored at -86 °C for future use.

2.4.2.1 Polymerase chain reaction (PCR)

PCR reaction was set up in a 0.2 ml PCR tube, by mixing the DNA template, corresponding primers, a thermo resistant high-fidelity DNA polymerase (Q5 DNA polymerase), deoxyribonucleoside triphosphates (dNTP's) and a buffer solution

providing an optimum chemical environment for the enzyme activity and stability. Composition of PCR mix is as shown in Table 4.

Table 4. Reagents for PCR amplification of Sg1 (1-159)

Reagents	Volume (µl)
PCR-grade H ₂ O	31
Forward primer (100 µM)	1
Reverse primer (100 µM)	1
DNA Template (70 ng/µl)	5
Q5 Buffer (5X)	10
dNTP (10 mM)	1
Q5 DNA Polymerase	1
Total volume	50

PCR reaction was carried out using PCR Thermal cycler from Applied Biosystems (Thermo Fisher scientific) under following conditions:

Melting temperature (T_m) for the Forward primer is 56 °C and for the Reverse primer is 58 °C

PCR conditions:

- i. Initial activation at 98 °C for 30 sec.
- ii. Denaturation at 98 °C for 10 sec.
- iii. Annealing at 54 °C for 30 sec. Amplification cycles (35x)
- iv. Extension at 72 °C for 30 sec.
- v. Final extension at 72 °C for 2 min.

The PCR products were purified using gel extraction kit (Qiagen). Purification of the PCR product was necessary to eliminate traces of the reagents that can interfere with subsequent applications. Samples were stored at -20 °C.

2.4.2.2 Agarose gel electrophoresis for DNA

0.8 % agarose was boiled in 1x TAE buffer (40 mM Tris, 20 mM Acetic acid, and 1mM EDTA.), then added with ethidium bromide and poured into an electrophoresis gel chamber from Bio-Rad. DNA samples were loaded in wells using final 1x gel loading dye (60 % glycerol, 0.015 % bromophenol blue and 0.06 M EDTA) and run at 80 V for

30 min. Fluorescence from DNA bands were visualized under UV source using G-box from Syngene.

2.4.2.3 Restriction digestion and ligation

Restriction digestion of the vector and PCR product were performed in accordance with the manufacturers specifications for respective restriction enzymes used in a final volume of 50 μ l.

For the preparation of the ligation mix, the volumes of the insert and the vector were calculated according to their concentrations. Ligation was carried out at a molar ratio of 1:3 vector to insert which were mixed with 2 μ l ligation buffer and 1 μ l T4 DNA ligase (NEB) to yield an end volume of 20 μ l. The reaction was incubated at 16 °C for 14 hrs.

Identity of pBKP-Sg1 (1-159) clone was verified by restriction enzyme digestion using following set of restriction enzymes as shown in Figure 15B:

- i. BsmI+ApaI as Rxn I
- ii. BsmI labelled as Rxn II, single cut within the insert
- iii. ApaI as Rxn IV
- iv. BstBI+BsrGI as RxnV, for Insert release.
- v. BsrGI as RxnVI

Insert: 0.5 kb, Vector: 5.5 kb, Ligation product: 6.0 kb (6064bp)

Uncut experimental DNA from all three selected clones (indicated as clone 3, 5, 6) for screening has been used as control in parallel with restriction enzyme digests of the clone. DNA marker was loaded in two different locations.

2.4.2.4 Transformation of *E. coli*

The competent cells used for the transformation procedures were DH5 α and BL21-AI *E.coli* cells. The antibiotic Ampicillin was used at a final concentration of 50 μ g/ml for positive selection of cells acquiring the plasmid of interest. To begin, 50 μ l of the competent cell were thawed on ice, followed by addition of 5 μ l of plasmid DNA. The tubes were then placed on ice for 30 min, then in 42°C water bath for exactly 30 seconds to allow the DNA transfer into cell. Following this heat shock, samples were returned to the ice for 10 min. Next, 750 μ l of Luria-Bertani (LB) media was added to the tubes and

they were then incubated for 90 min at 37 °C. After incubation, cells were centrifuged at 5000 rpm for 2 min. The pellet was then resuspended in 250 µl LB broth. 100 µl of the cell culture was plated on to LB-Amp-agar plates. Simultaneously, one additional plating was carried out following the same procedure but without plasmid DNA as a control and plates were incubated overnight at 37 °C.

2.4.3 Ni-NTA affinity purification of recombinant Sg1 and Sg1 (1-159) proteins

Recombinant proteins full length Sg1 or Sg1 (1-159) were purified under denaturing and reducing conditions to prevent any mis-aggregation by following a protocol previously described for Rnq1 yeast protein [10]. For this, firstly 25 ml Ni-NTA affinity resin (Qiagen) was packed in chromatography column (200 mm x 25 mm). Affinity of Ni-NTA for the histidine residues present in the N term 6x His tag of the target protein helps in its purification. Meanwhile the bacterial cells were lysed under denaturing conditions by sonication at 4°C with 10 ml lysis buffer (50 mM sodium phosphate buffer, pH 7.4, 8 M urea, 5 mM imidazole, 10 mM β-mercaptoethanol) containing protease inhibitor complex. Purification under denaturing conditions helps in preventing mis-aggregation of the amyloidogenic target protein. β-mercaptoethanol was added to all the buffers to prevent scrambled disulfide bond formation. Protease inhibitor was added to prevent proteolytic degradation of samples. Then, cell extract was precleared by centrifugation at 10,000 rpm for 10 mins at 4 °C. The pellet was discarded and the supernatant was used for purification.

Meanwhile, the column was washed and equilibrated with the equilibration buffer (50 mM sodium phosphate buffer, pH 7.4, 8 M Urea, 5 mM imidazole, 10 mM β-mercaptoethanol). The precleared cell extract was loaded onto Ni-NTA agarose affinity column and purification was carried out under denaturing conditions. Unbound and non-specifically bound proteins were washed with 200 ml wash buffer (50 mM sodium phosphate buffer, pH 7.4, 8 M Urea, 10 mM imidazole, 10 mM β-mercaptoethanol). Followed by elution of the his-tagged proteins using elution buffer (50 mM sodium phosphate buffer, pH 7.4, 8 M Urea, 250 mM imidazole, 10 mM β-mercaptoethanol) and

1 ml fractions were collected. The fractions with protein were identified by measuring $A_{280\text{ nm}}$ using the elution buffer as blank.

2.4.4 Western blotting

To confirm the identity of the purified Sg1 full length protein the presence of N-terminal 6x His-tag was probed with anti-his antibody by western blotting [79]. For this Purified Sg1 (10 μg) was electrophoresed on SDS-PAGE and transferred to PVDF (Polyvinylidene fluoride) membrane by electro-blotting. PVDF membrane was blocked with blocking buffer (5 % Casein solution) overnight. Then the membrane was washed using phosphate buffered saline-Tween-20 (PBST) consisting of 137 mM NaCl, 2.7 mM KCl, 8.1 mM Na_2HPO_4 and 1.5 mM KH_2PO_4 , pH 7.4, 0.05 % Tween-20 for 4 times x 30 minutes. The membrane was then incubated with anti-his primary antibody (1:3000 dilution) for 1hr. This allows binding of primary antibody to the 6x His-tag of Sg1. Unbound primary antibody was removed by washing with PBST for 4 times x 30 minutes. Then the membrane was incubated with Alkaline phosphatase (APP)-conjugated secondary antibody (1:8000 dilution) which binds to the primary antibody and again the membrane was washed with PBST for 4 times x 30 minutes to remove any unbound secondary antibody. Finally the blot was detected using CDP-Star as Chemiluminescent substrate for APP and photographed using G-Box (Gel documentation system from Syngene).

2.4.5 Intrinsic fluorescence

Intrinsic fluorescence of proteins arise because of the fluorescent properties of tryptophan and tyrosine residues. Intrinsic fluorescence can be used as a measure for assessment of refolding of purified proteins as fluorescence of these residues depend on their microenvironment and solvent conditions [83].

2.4.6 Refolding of Sg1 assessed by Circular dichroism

Dialyzed Sg1 was incubated with decreasing concentration of urea 8 M, 2 M, 0.5 M in 10 mM sodium phosphate buffer, pH 7.4 while keeping the protein concentration same (1.5 mg/ml). The samples were examined for any change in secondary structure using Far-UV circular dichroism (CD) spectroscopy [85]. CD spectra were recorded using Jasco J-1500

spectropolarimeter in the wavelength range of 190-260 nm using cuvette of 1mm path length. Mean residue ellipticity $[\theta]$ was calculated using the following equation:

$$[\theta] = (\theta_{\text{obs}} * \text{MRW}) / (10 * c * l)$$

Where, θ_{obs} , c , l and MRW represent the observed ellipticity in milli-degrees, protein concentration in mg/ml, path length of cuvette in cm, and mean residue weight taken as 112 Da respectively. The spectra were corrected for baselines.

2.4.7 Dialysis of Sg1 and Sg1 (1-159) purified in 8 M urea

To find a buffer of appropriate pH which would keep the protein in solution, buffers of different pH ranging from 2.0 to 10.5 were screened. The buffers used for different pH were 0.5 M glycine-HCl (pH 2.0, 3.0), 0.5 M sodium acetate (pH 4.0, 5.0), 0.5 M sodium phosphate (pH 6.0, 7.4), 0.5 M tris-HCl (pH 8.4, 9.4), 0.5 M glycine-NaOH (pH 10.5).

Chapter III

Amyloid-like *in vitro* aggregation of Sg1 and Sg1 (1-159) proteins

3.1 Abstract

Senile seminal vesicle amyloidosis (SSVA), that may manifest as hematospermia is associated with deposition of semenogelin-1 (Sg1) protein aggregates in seminal vesicles. Sg1 is the predominant protein that entraps spermatozoa which are freed upon fragmentation of Sg1 by the protease prostate specific antigen (PSA), post semen release. Certain small peptide fragments of Sg1 have been reported to form amyloid aggregates *in vitro* that can enhance HIV infectivity to cell cultures. However, the amyloid deposits in the seminal vesicles are expected to be that of the full length Sg1, as PSA is encountered downstream. So far, amyloid forming ability of full length Sg1 has not been established *in vitro*. Here, we examined the amyloidogenicity of full length Sg1 and a large fragment Sg1 (1-159), using recombinant proteins and tested if Zinc has any effect on their aggregation. Levels of Zinc, which is essential for health of male reproductive system, gradually decline with age. We succeeded in forming aggregates of Sg1 full length and Sg1 (1-159) fragment showing amyloid-like detergent stability, particle sizes as estimated by dynamic light scattering and fibrillar morphologies in TEM. Further we found that presence of Zn^{2+} substantially inhibit their amyloid aggregation *in vitro*. Possibly, high Zn^{2+} found in seminal plasma of young individuals may have preventive role against aggregation of Sg1 in seminal vesicles.

3.2 Introduction

In SSVA disorder, Sg1 amyloid deposits in the sub-epithelium and lumen of seminal vesicles and it would be expected to be of full length Sg1 as it would not have, thus far, encountered PSA. The fragmentation of Sg1 by PSA occurs after it is released out of the vesicles and mixed with prostatic fluid. Thus, amyloidogenicity of full length Sg1 needs to be examined to get a mechanistic insight into the development of SSVA. Also, examination of HIV infectivity in presence of full length Sg1 amyloid aggregates may be physiologically more relevant compared with the thus far obtained amyloid aggregates of Sg1 peptides which are generated only downstream post-ejaculation. In addition, amyloidogenicity of a large Sg1 (1-159) fragment encompassing the reported amyloidogenic peptide regions of Sg1 was also tested.

Some metal ions such as Zn^{2+} and Cu^{2+} have been shown to inhibit amyloid formation of $A\beta_{42}$ peptide which is implicated in development of Alzheimer's disease [61,62]. Also Sg1 has been reported to have high affinity for Zn^{2+} [37]. As the semen of a young male contains high levels of Zn^{2+} , which declines with age and the SSVA cases increase with age, we tested if Zn^{2+} has any effect on the aggregation of Sg1 *in vitro* that could influence the development of SSVA.

We hypothesize that zinc plays a significant role in preventing the Sg1 protein to aggregate into amyloid like confirmation. As we know that seminal zinc concentration decreases with aging and the SSVA disorder occurs at an older age. At an older age zinc is no more available in concentrations that will check the protein from undergoing amyloid like aggregation.

3.3 Results and Discussion

3.3.1 Sg1 aggregation and amyloid formation

3.3.1.1 Aggregation of Sg1 during dialysis

The purified recombinant proteins Sg1 and Sg1 (1-159) were found to precipitate when dialysed at pH 7.4 and pH 9.0. Precipitation was observed even when dialysis was carried out in presence of 150 mM NaCl at alkaline pH. The precipitate was reasonably resistant to dilution as well as denaturation (up to 3.5 M urea), thus presence of amyloid-like

aggregates was suspected [10]. Therefore, the precipitates obtained at pH 9.0 were examined for amyloid-like aggregates.

3.3.1.2 Assessment of amyloid aggregation of Sg1 and Sg1 (1-159)

(i) Thioflavin-T binding assay

We tested binding of amyloid specific dye ThT and examined its fluorescence emission spectrum when added to the precipitates of Sg1 full length (5 mg/ml) and Sg1 (1-159) fragment proteins [7]. The fluorescence emission intensity of ThT exhibited over four-fold increase with concomitant shift in its emission maximum (λ_{max}) to ~490 nm suggesting amyloid-like nature of the precipitates (Figure 25A and 25B).

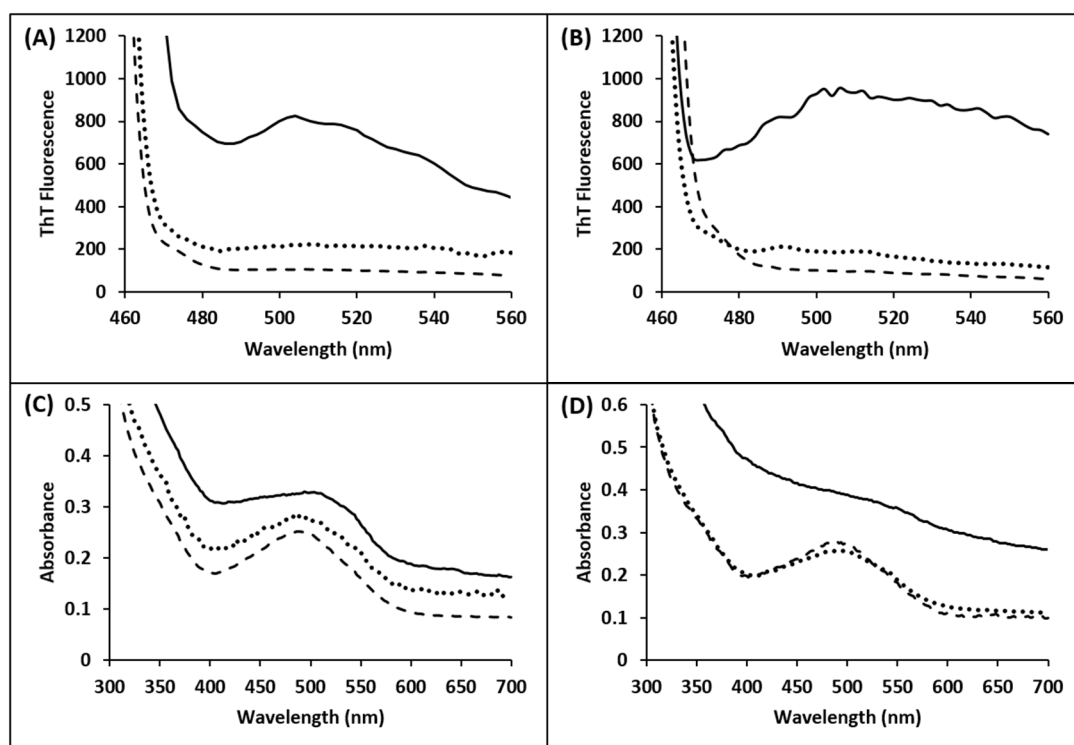


Figure 25. Assessment of amyloid nature of aggregates of Sg1 and Sg1 (1-159)

Amyloid-like nature of aggregates was probed using Thioflavin-T (ThT) and Congo red binding assays [7,88]. ThT fluorescence emission spectra were recorded after mixing ThT (1.6 mM) with 5 mg/ml of full length Sg1 aggregates (A) or Sg1 (1-159) fragment aggregates (B) that were obtained during dialysis of the protein purified in 8 M urea against the dialysis buffer (10 mM tris HCl, pH 9.0, 10 mM β -mercaptoethanol) at 4 °C. Congo red absorption spectra (300 nm-700 nm) were recorded after adding 1.4-fold excess of Congo red dye to Sg1 aggregates (C) or Sg1 (1-159) aggregates (D). Solid lines in spectra represent the aggregated protein

whereas, the dotted lines indicate denatured protein in 8 M urea. Buffer controls are represented by the dashed lines.

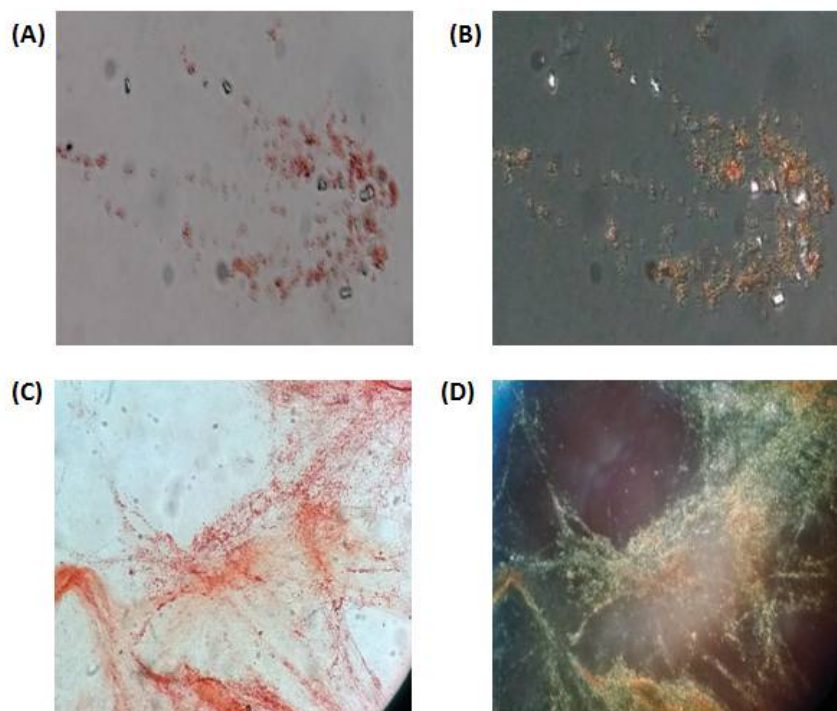


Figure 26. Congo red birefringence of Sg1 and Sg1 (1-159) aggregates

A & C are the bright field images of Sg1 full length and Sg1 (1-159) aggregates respectively and, B & D represent same fields viewed under cross-polarized light for Sg1 full length and Sg1 (1-159) aggregates respectively. 5 μ l of Sg1 full length or Sg1 (1-159) aggregates (12 mg/ml) were mixed with 400 μ M Congo red dye and allowed to bind for 1 hour similar to the protocol described by O'Nuallain et al, 2004. Birefringence was observed using Leica microscope DM2500 under cross-polarized light at 40X magnification.

(ii) Congo red binding assay

- a) *Congo red absorbance spectrum*: To further confirm the amyloid-like nature, when Congo red was incubated with the precipitates, its absorption maximum showed red shift (480 nm to 530 nm) consistent with Congo red binding to amyloid-like aggregates (Figure 25C and 25D). While Congo red binding to

amyloids can also lead to increase in its absorption intensity [88], similar to the observation here for Sg1, the Congo red binding to some amyloids like that of β_2 -microglobulin leads only to red shift in the λ_{max} towards 540 nm but not accompanied by significant absorption intensity increase [89].

b) Congo red birefringence: Polarized light microscopy of Congo red-stained aggregates was carried out by using the protocol as described previously [90]. Sg1 and Sg1 (1-159) aggregates exhibited Congo red birefringence when incubated with Congo red and viewed under polarized light (Figure 26).

3.3.2 Stability assessment of Sg1 aggregates

3.3.2.1 Semi denaturing detergent agarose gel electrophoresis (SDD-AGE)

For amorphous protein aggregates, addition of detergents such as SDS or sarkosyl, even at room temperature, can penetrate and break apart the aggregates into monomers. On the contrary, as amyloid aggregates are formed of several levels of structural organization from monomers to β -sheet-rich oligomers and then into protofibrils and finally into fibrils, addition of detergents at room temperature fail to completely dissociate the monomers unless heated at very high temperatures such as close to boiling [91]. Amyloid aggregates are found to have high stabilities against physical and chemical denaturants and proteolysis [23]. Several amyloid and prion proteins also exhibit modest stability at room temperature to detergents (up to 1-2%) like SDS (e.g. $A\beta_{42}$ amyloid) or Sarkosyl (e.g. HET-s prion amyloid) [92]. Thus, the Sg1 protein precipitated during dialysis was examined for stability against SDS and sarkosyl by SDD-AGE method [91]. Where after pre-incubation with the detergent (1 or 2%) at room temperature, the samples were electrophoresed on 1.5 % agarose gel and visualized by electro-blotting to PVDF membrane and Coomassie staining.

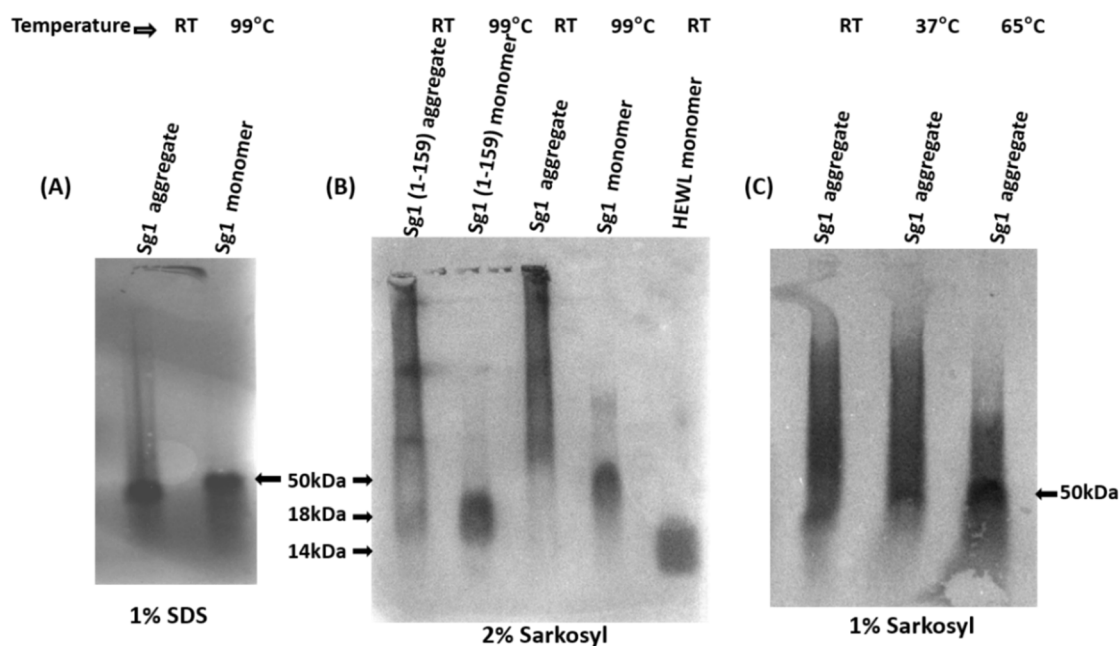


Figure 27. Detergent stability of Sg1 and Sg1 (1-159) amyloid aggregates

Sg1 aggregates (40 μ g) obtained upon dialysis were incubated with 1 % SDS at room temperature (RT) for 10 min and size of aggregates was analyzed using SDD-AGE [91] by electrophoresis on 1.5 % agarose gel followed by electroblotting to PVDF membrane and protein detection by Coomassie staining (A). The aggregates of Sg1 and Sg1 (1-159) were also incubated in presence of 2 % sarkosyl at RT and analyzed similarly by SDD-AGE (B). To obtain monomeric controls, the aggregates (12 μ g) were incubated with 8 M urea and then heated at 99°C for 10 min in presence of 1 % SDS (A) or 2 % sarkosyl (B) before electrophoresis. In panel (B) the HEWL monomer was used to mark 14 kDa position. (C) A combinatorial effect of 1 % sarkosyl and heat on the size of aggregates was also examined by SDD-AGE after incubation at RT, 37°C or 65°C for 10 min.

When treated with 1 % SDS most of the precipitated protein was found to convert to monomers, suggesting a partial resistance of Sg1 full length aggregates to 1 % SDS (Figure 27A). As the resistance to SDS mediated disaggregation was minimal, we tested stability of aggregates against 2 % sarkosyl and found that both Sg1 full length and Sg1 (1-159) aggregates exhibited high molecular weight species suggesting stability against 2 % sarkosyl (Figure 27B). The observed high molecular weight smear on SDD-AGE in presence of detergents is expected if the aggregates had amyloid-like property. As

expected, when the aggregates pre-incubated in presence of 1 % sarkosyl were heated to 65°C higher molecular weight aggregates were seen to break down to smaller aggregates although they resisted disaggregation up to 37°C when tested (Figure 27C). Previous studies on stabilities of [PIN⁺] aggregates have shown disaggregation when heated to 60°C with SDS [93].

3.3.2.2 Proteinase-K resistance

Several amyloid and prion proteins have also been reported to exhibit resistance to proteinase-K digestion albeit to different extents, possibly due to their compact structure causing inaccessibility of the core [6]. When we examined the proteinase-K resistance of Sg1 aggregates and analyzed by tricine SDS-PAGE the aggregates exhibited full resistance to proteinase-K digestion even after 15 min as seen by the residual protein intensity of the monomer (Figure 28). The non-aggregated protein, when treated similarly was found amenable to proteinase-K digestion and the residual protein monomer was found to significantly decrease (Figure 28). The observed stability of the Sg1 aggregates to proteinase-K digestion is consistent with as expected of amyloid-like aggregates.

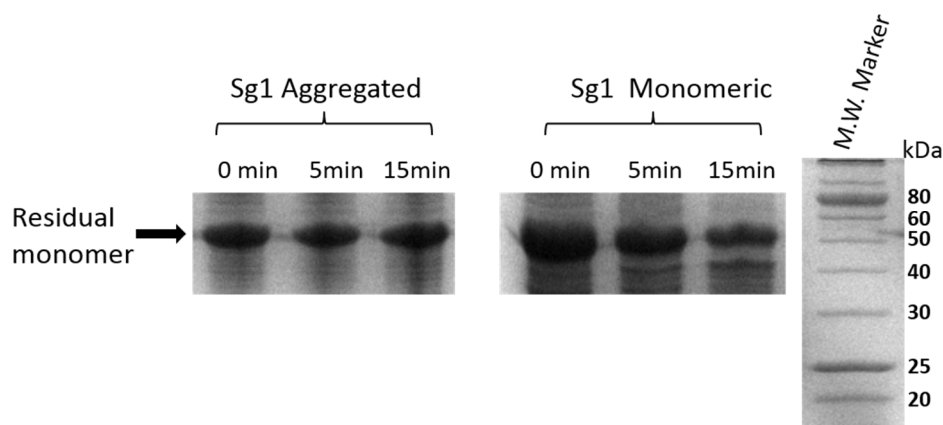


Figure 28. Partial resistance of Sg1 amyloid aggregates to Proteinase-K digestion

Sg1 aggregates or monomers (0.7 $\mu\text{g}/\mu\text{l}$) were incubated at 37°C with Proteinase-K (PK) at PK/aggregate ratio of 1:2000. The aliquots were removed at 0, 5 and 15 min and proteolysis was stopped by addition of 5 mM PMSF. Samples were electrophoresed on Tricine SDS-PAGE (16%) gel and protein was visualized using Coomassie [94]. The monomeric protein used for comparison was pre-obtained by dialysis of the purified protein at pH 3.0 with 2 M urea. The presence of urea (2 M) did not inhibit PK activity as reported previously [10].

3.3.3 Kinetics of *in vitro* amyloid aggregation of Sg1

3.3.3.1 Effect of pH on aggregation trend of Sg1

For many amyloid proteins the *in vitro* aggregation into amyloid conformation follows a signature lag-dependent sigmoidal kinetics [5]. When re-solubilized Sg1 full length protein was incubated at different pH with intermittent agitation and monitored for aggregation by ThT binding, the aggregation was observed at basic pH but not under acidic pH conditions (Figure 29). A lag dependent sigmoidal kinetics of aggregation for Sg1 protein was observed at pH 9.4 suggesting it to be the optimal pH (Figure 29). This bears a parallel to the *in vivo* alkaline pH of the seminal vesicles where Sg1 aggregates and deposits [57].

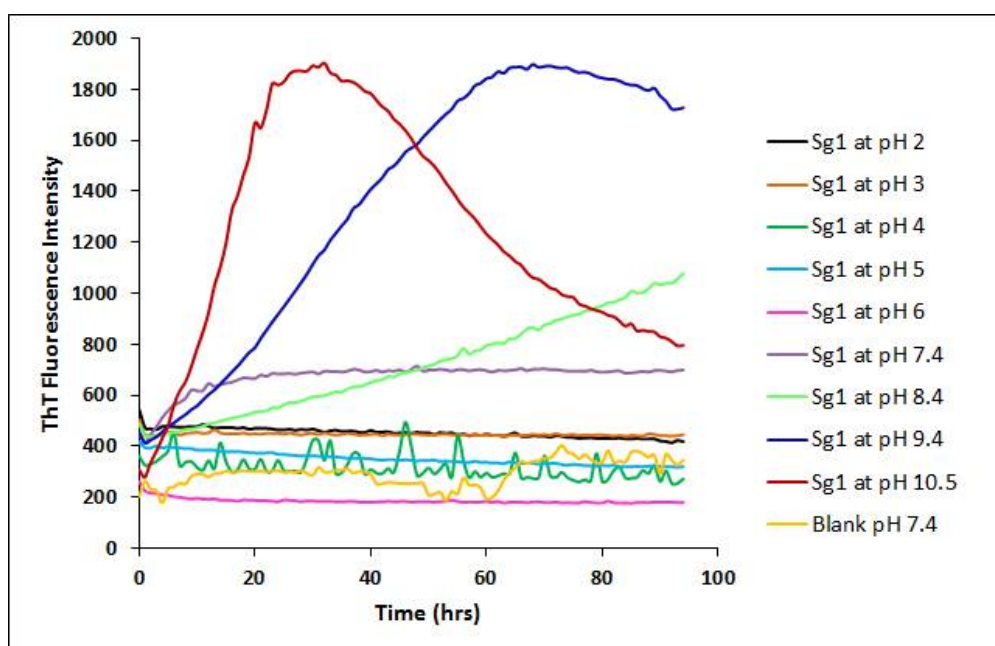


Figure 29. Sg1 aggregation at different pH

Full length Sg1 (12 mg/ml) was incubated with ThT at 30°C at different pH (2.0 to 10.5) along with 1 M urea and agitated intermittently. ThT fluorescence emission intensity at 485 nm was recorded every 5 min using Spectramax- M5[°] microplate reader.

3.3.3.2 Comparative aggregation kinetics

When Sg1 and Sg1 (1-159) proteins were examined for aggregation under similar conditions, the kinetic trends obtained for the two proteins were amyloid-like, however, non-overlapping (Figure 30A). The aggregation of Sg1 (1-159) seemed to reach saturation by ~ 60 hrs of incubation whereas, Sg1 aggregation required ~80 hrs to peak.

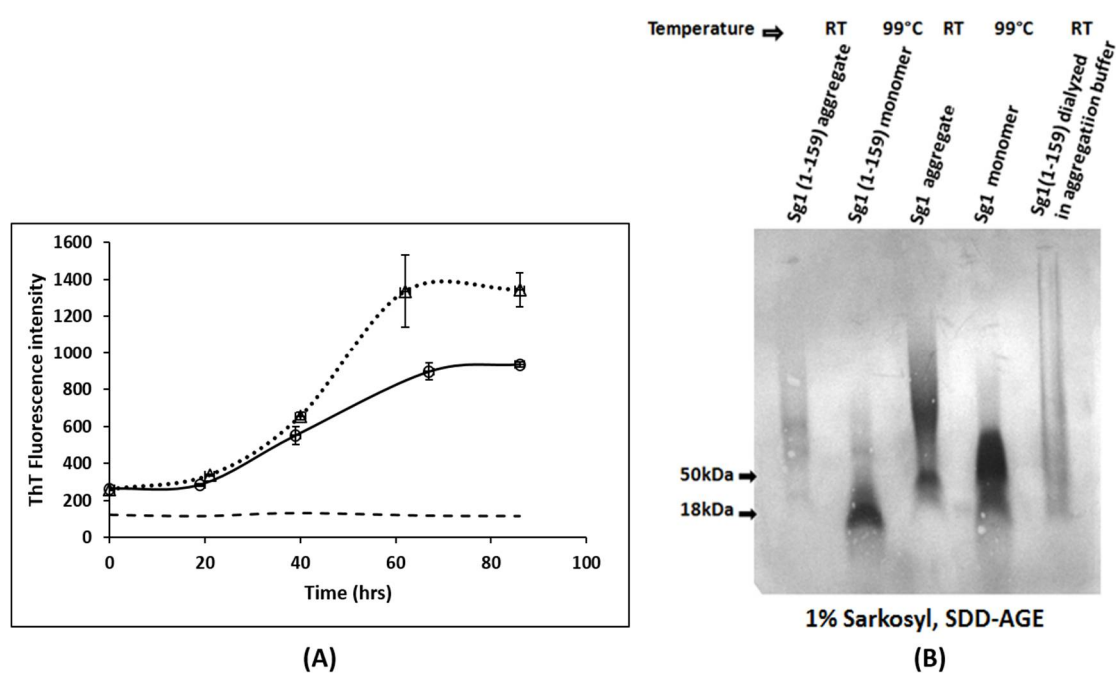


Figure 30. Aggregation of Sg1 (1-159) compared with Sg1

(A) 12 mg/ml of Sg1 (solid line) or Sg1 (1-159) fragment (dotted line) were incubated in presence of 0.5 M GuHCl and 1.5M urea, 100 mM β -mercaptoethanol with ThT at 30°C, pH 9.0 and agitated (200 rpm) in shaking incubator. ThT fluorescence emission was recorded at 485 nm after withdrawing aliquots at intervals of 20 hrs. Using triplicate samples, error bars representing standard deviation were obtained. A blank containing all the constituents except the protein was used for comparison (dashed line). (B) The aggregates of Sg1 and Sg1 (1-159) were incubated in presence of 1 % sarkosyl at RT and analyzed by SDD-AGE. Lane 1 and 3 represent sarkosyl stability of Sg1 (1-159) and Sg1 full length aggregates formed after 86 hrs of incubation in aggregation buffer; lane 2 and 4 have monomeric Sg1 (1-159) and Sg1 respectively; lane 5 represents higher molecular weight aggregates of Sg1 (1-159) obtained upon dialysis in aggregation buffer containing 0.25 M GuHCl and 1 M urea, pH 9.0 at 30°C with shaking.

The observed rapid aggregation of Sg1 (1-159) is analogous to reports of faster aggregation of some other amyloid and prion domains compared to their full-length proteins [95]. Prolonged incubation after the ThT fluorescence had reached saturation lead to decline in ThT fluorescence intensity, similar to previously reported trend for other amyloids like that of the Rnq1 prion protein [10]. Further suggestive of amyloid-like aggregation, detergent stability was also observed for the samples which displayed amyloid-like sigmoidal kinetics monitored by ThT fluorescence increase (Figure 30B, Lane 1 and 3).

3.3.4 Secondary structure estimation by Circular dichroism

Circular dichroism (CD) spectroscopy technique makes use of the fact that chiral molecules will interact differently with right and left circularly polarized light. Peptides and proteins have chiral properties with the amide group in the peptide bond being main chromophore in far-UV region (190-260 nm) of CD spectrum [85].

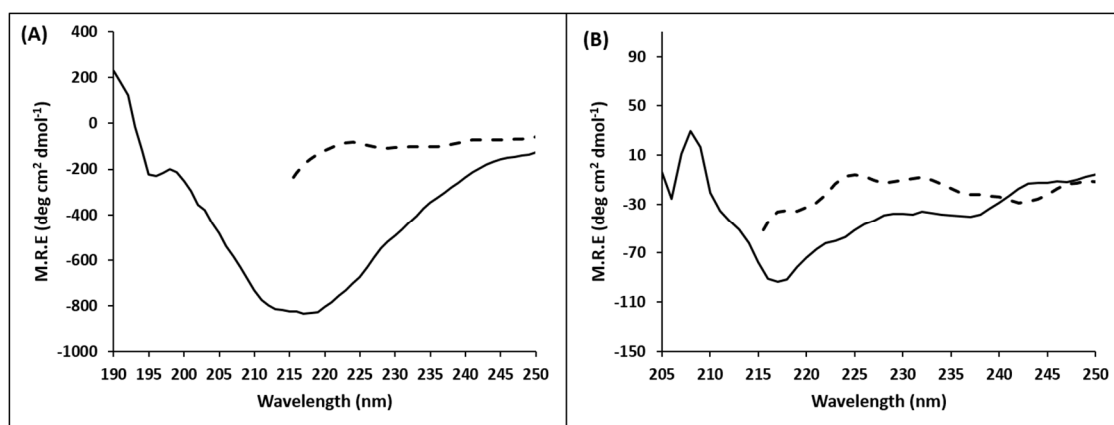


Figure 31. Far-UV Circular dichroism spectra of Sg1 and Sg1 (1-159) aggregates

CD spectra of Sg1 (A) and Sg1 (1-159) (B) aggregates formed upon dialysis against aggregation buffer (pH 9.0) were recorded after diluting the aggregates (final: 2 mg/ml) in the same buffer, using Jasco J-1500 spectropolarimeter and 1 mm path length quartz cuvette. Data is represented as mean residue ellipticity (MRE). CD spectra of denatured Sg1 (A) and Sg1 (1-159) (B) in 6 M GuHCl (dashed line) was recorded for comparison.

CD spectra have earlier reported native Sg1 to be largely unstructured while a small peptide that converted into hydrogel with amyloid-like characteristics, has displayed β -sheet rich conformation [52,76]. Change in secondary structure of Sg1 and Sg1 (1-159) upon aggregate formation was analyzed by Far-UV CD spectroscopy in the wavelength range 190-260 nm. Increase in β sheet content was hinted by the negative ellipticity around 215 nm (Figure 31A and 31B). The denatured proteins in 6 M GuHCl showed largely unstructured conformation.

3.3.5 Transmission electron microscopy of Sg1 and Sg1 (1-159) aggregates

Transmission electron micrographs of Sg1 and Sg1 (1-159) aggregates were obtained after diluting the aggregates in aggregation buffer, pH 9.0. For improving contrast samples were negatively stained with 0.2 % phosphotungstic acid. TEM of Sg1 peptides have previously been reported to exhibit fibrillar structures >500 nm in size [48]. Here Sg1 and Sg1 (1-159) aggregates showed fibrillar structures of varying sizes and morphologies suggesting their amyloid nature. In the TEM images straight, twisted, short and very well grown fibres were also observed (Figure 32).

3.3.6 Estimation of Sg1 aggregate sizes by Dynamic light scattering (DLS)

After confirming that the formed aggregates are amyloid-like ordered aggregates and not amorphous aggregates. Dynamic light scattering was performed to examine the particle size of the aggregates. DLS measures time-dependent fluctuations in the scattering intensity arising from particles undergoing random Brownian motion. Analysis of these fluctuations can be used to obtain information about Diffusion coefficient and particle size. Decay in correlation function is related to the motion of the particle specifically to the diffusion coefficient. The method provides ability to measure size characteristics of proteins in a liquid medium [96]. Previously reported DLS data for fragments of Sg1 showed amyloid aggregates of varying sizes some of them were nearly 500 nm in size [52,53]. Full length Sg1 and Sg1 (1-159) aggregates obtained upon dialysis at pH 9.0 were diluted into aggregation buffer such that final concentration is 2 mg/ml.

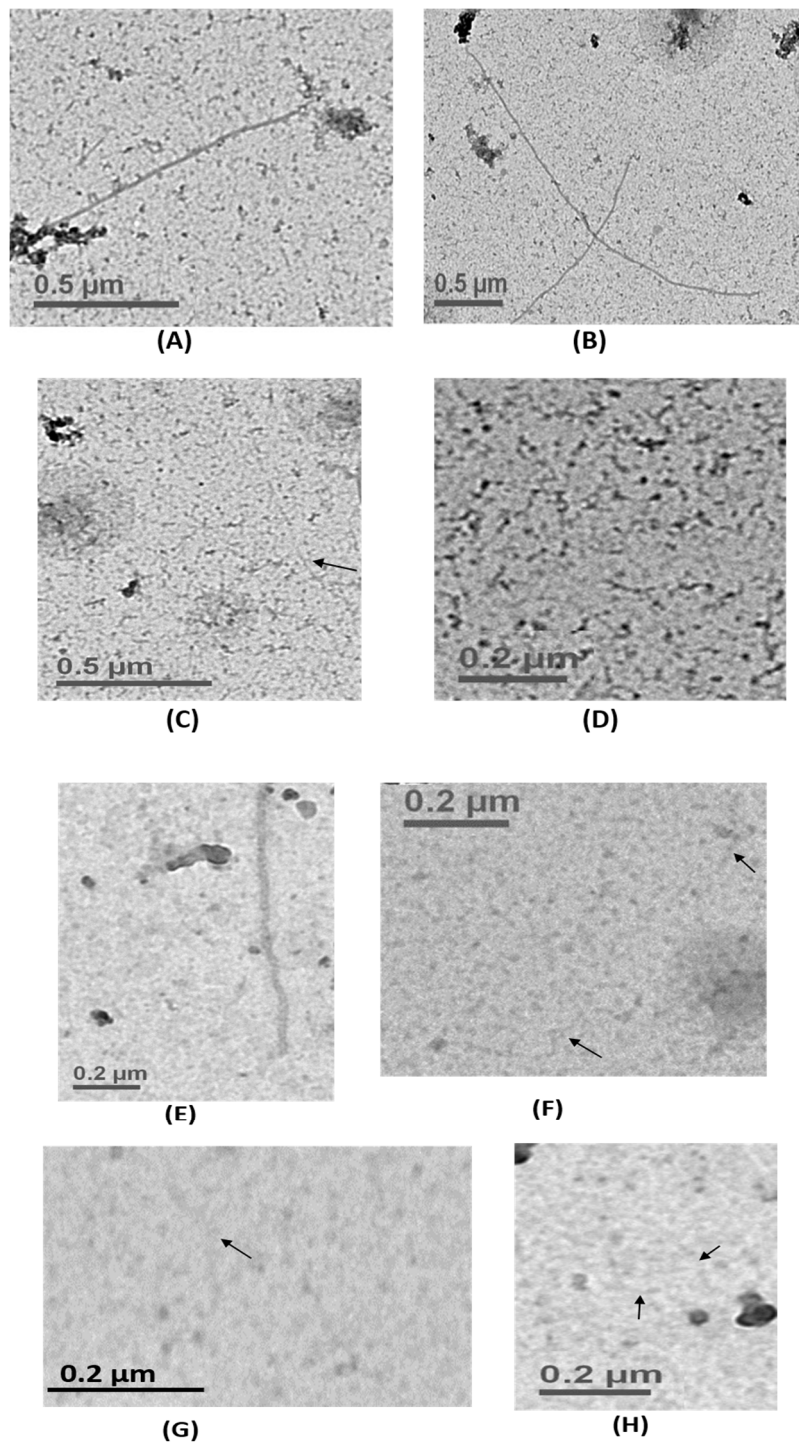


Figure 32. Transmission electron micrographs of Sg1 and Sg1 (1-159) aggregates Sg1 aggregates (A-D) and Sg1 (1-159) aggregates (E-H) formed after dialysis in 10 mM Tris-HCl, pH 9.0 buffer in presence of 10 mM β -mercaptoethanol were analysed by high resolution TEM (T20G2), operated at 200 kV . Scale bars are indicated on each image. Arrows indicate towards fibrillary aggregates.

Dynamic light scattering measurements were carried out at room temperature using Delsa Nano C Particle Analyzer (Beckman Coulter) and data were processed using Delsa Nano 3.7 software. Measurements were carried out using 1 ml quartz cuvette with the sample chamber pre-maintained at 25 °C.

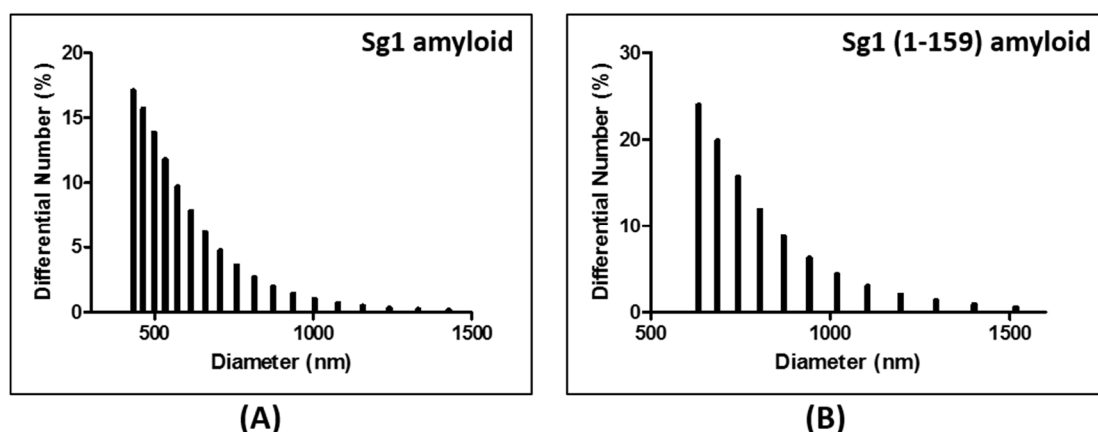


Figure 33. Estimation of Sg1 and Sg1 (1-159) aggregate sizes by DLS

Scattering measurements were carried out on (A) Sg1 and (B) Sg1 (1-159) aggregates formed at pH 9.0. Samples were diluted in aggregation buffer to final concentration of 2 mg/ml at room temperature before recording the spectrum.

DLS measurements of Sg1 aggregates showed large size aggregates of ~ 500-700 nm thereby indicating the formation of higher size entity which is consistent with amyloid-like aggregation (Figure 33). From the number distribution of the molecular species from DLS data, the mean hydrodynamic radii obtained for the samples were: Sg1 aggregates: 576 ± 167 nm (polydispersity: 30.6 %); Sg1 (1-159) aggregates: 799 ± 212 nm (polydispersity: 71 %).

3.3.7 Inhibition of Sg1 aggregation by Zn^{2+}

Significant reduction in seminal levels of Zn^{2+} has been observed with male aging and it correlates with increased infertility [54]. The Sg1 protein has previously been reported to have remarkable affinity for Zn^{2+} [37]. We examined whether a correlation exists between decline in Zn^{2+} levels and increased aggregation of Sg1 leading to SSVA which is a late-onset disorder affecting male reproductive system. When the effect of Zn^{2+} was investigated on the amyloid aggregation of Sg1 and Sg1 (1-159) proteins Zn^{2+} was found

to inhibit the aggregation when present at 15-fold molar excess (Figure 34A). For both the proteins equimolar Zn^{2+} was found to be nearly non-inhibitory whereas, the 15 fold excess Zn^{2+} was highly inhibitory causing ~ 70-90 % reductions in their aggregation as monitored by ThT fluorescence. Unlike the inhibition by Zn^{2+} , there was no reduction in Sg1 aggregation in presence of an organic compound 3AP (Figure 34B) belonging to the class of aminophenols which were previously found to prevent aggregation of $A\beta_{42}$ and HEWL *in vitro* [97,98]. Although, Zn^{2+} has been previously found to inhibit Alzheimer's disease $A\beta_{42}$ peptide's aggregation [62], the finding here that it indeed also inhibits Sg1 aggregation could influence the understanding of SSVA in the view of the importance of Zn^{2+} to the male reproductive system. Although, many promiscuous inhibitors have been shown for amyloids, the observed inhibition here by Zn^{2+} of Sg1 amyloid aggregation *in vitro*, may be specific due to the relevance of Zn^{2+} to male reproductive system and the previously reported presence of Zn^{2+} binding sites on the Sg1 protein [54, 55].

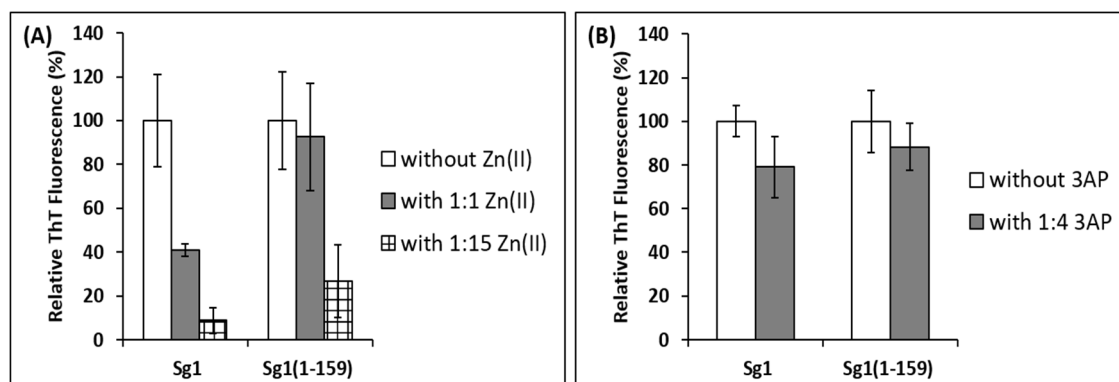


Figure 34. Aggregation of Sg1 and Sg1 (1-159) fragment in presence of Zn^{2+} or 3-aminophenol

(A) Aggregation of Sg1 full length and Sg1 (1-159) fragment (12 mg/ml) were examined in presence of equimolar Zn^{2+} or in 15-fold molar excess of Zn^{2+} by ThT fluorescence assay. After 88 hrs of incubation ThT fluorescence of the samples was compared with a positive control lacking Zn^{2+} , the ThT fluorescence of which was considered as 100%. Error bars represent standard deviation. (B) Effect of 3-aminophenol on Sg1 amyloid aggregation was assessed by incubating the protein samples (12 mg/ml) Sg1 full length or Sg1 (1-159) fragment with 4 molar excess of 3AP under similar aggregation conditions and recording ThT fluorescence intensity after 88 hrs of incubation as above. Data presented here after appropriate baseline corrections, where Zn^{2+} or 3AP were found to have no interference to ThT fluorescence assay.

The findings here of amyloid-like aggregation of Sg1 and Sg1 (1-159) proteins and the inhibition of the aggregation by Zn^{2+} may have implications towards therapeutic strategies for SSVA which may be imminent especially as Sg1 amyloid is reported to enhance HIV infectivity in cell cultures.

3.4 Materials and Methods

3.4.1 Materials

Thioflavin-T, N-Lauroylsarcosine sodium salt (Sarkosyl), Sodium dodecyl sulfate (SDS), β -mercaptoethanol, Proteinase-K, Polyvinylidene fluoride (PVDF) membrane were from GE Healthcare. 96 microwell plate from Thermo scientific (US). Sodium phosphate monobasic, Sodium phosphate dibasic, Zinc chloride were of molecular biology grade and procured from HiMedia (India). 3-Amino phenol (catalog no. A11943) was obtained from Alfa Aesar (India). All other chemicals were of high purity.

3.4.2 Sg1 aggregation and amyloid formation

3.4.2.1 Assessment of amyloid aggregation of Sg1 and Sg1 (1-159)

(i) Thioflavin-T binding assay

Thioflavin-T is a planar organic dye reported to bind specifically to amyloid aggregates upon which its fluorescence properties significantly change [7]. Extrinsic fluorescence spectrum of ThT upon amyloid binding was measured by exciting at 442 nm and recording emission from 460 nm to 560 nm. An enhanced ThT fluorescence emission intensity at 485 nm- 490 nm usually indicates binding to amyloid-like conformation [7]. ThT fluorescence was either monitored upon incubating samples with intermittent shaking in Spectramax- M5^e microplate reader (Molecular Devices) or aliquots were examined at intervals (20 hrs) from samples incubated in constant shaking incubator. Agitation has been shown previously to accelerate amyloid aggregation for several amyloids which is attributed to be due to role of air-water interface or faster fragmentation of large size agglomerates of amyloid aggregates [10,13,83,99].

(ii) Congo red binding assay

- a) **Congo red absorbance spectrum:** Congo red dye is known to bind to amyloid aggregates, which results in a red shift in its absorbance maximum (λ_{\max}) from 480 nm to 540 nm [88]. To assess the amyloid nature of Sg1 and Sg1 (1-159) aggregates, a 400 μ M Congo red stock solution was prepared in PBS buffer, pH 7.4 (0.137 M NaCl, 2.7 mM KCl, 1.5 mM KH_2PO_4 , 8.1 mM Na_2HPO_4) with 0.4 % ethanol to avoid micelle formation [88]. Congo red (122 μ M) was mixed with 87 μ M of the sonicated protein precipitate of full length Sg1 and Sg1 (1-159). The samples were allowed to incubate for 15 minutes at room temperature. Congo red binding assay was performed by recording absorbance from 300 nm-700 nm to examine the shift in λ_{\max} . [88]. The sample showed red shift from 480 nm to 530 nm, supporting the amyloid nature of the precipitate obtained during dialysis of full length Sg1 as well as for Sg1 (1-159) fragment.
- b) **Congo red birefringence:** 5 μ l of Sg1 full length or Sg1 (1-159) aggregates (12 mg/ml) were mixed with 400 μ M Congo red dye and allowed to bind for 1 hour similar to the protocol described by O'Nuallain et al, 2004 [90]. Birefringence was observed using Leica microscope DM2500 under cross-polarized light at 40X magnification.

3.4.3 Kinetics of *in vitro* amyloid aggregation of Sg1

3.4.3.1 Effect of pH on aggregation trend of Sg1

To screen the conditions required for amyloid like aggregate formation and determine the buffer conditions optimum for Sg1 aggregation, aggregation kinetics of Sg1 was assessed at different pH (pH 2.0 - 10.5). For the aggregation assay, the protein precipitate of Sg1 obtained during dialysis at pH 7.4 (10 mM sodium phosphate buffer, 10 mM β -mercaptoethanol) was first re-solubilized in 5 M urea and then diluted in different pH buffers ranging from pH 2.0 to 10.5 to obtain 12 mg/ml protein and 1M urea concentrations. Samples were incubated at a constant temperature of 30 °C, along with agitation for 30 seconds every 5 minutes using auto-mix function which permits linear

shaking in Spectramax- M5^e microplate reader to promote aggregate formation. Samples were monitored for amyloid formation by ThT fluorescence measurement.

3.4.3.2 Comparative aggregation kinetics

In order to examine the comparative aggregation kinetics of Sg1 and Sg1 (1-159), the protein precipitates obtained from dialysis at pH 9.0, were first re-solubilized in 6 M GuHCl and then diluted to final 0.5 M GuHCl in aggregation buffer (0.25 M Tris HCl pH 9.0 with 1.5 M urea and 100 mM β -mercaptoethanol). Samples were added with ThT (1.6 mM) and agitated (200 rpm) in orbital shaking incubator at 30°C and monitored for amyloid aggregation at intervals of 20 hrs.

3.4.4 Stability assay of Sg1 aggregates

3.4.4.1 Semi denaturing detergent agarose gel electrophoresis (SDD-AGE)

Unlike amorphous protein aggregates, many amyloid and prion aggregates exhibit modest stability to detergents like SDS or sarkosyl (~1-2 %) at room temperature [23,92]. Stability against detergents is one of the key features of amyloid where the bulky aggregates only partially disassemble on treatment with ionic detergents. For assessing the detergent stability of Sg1 and Sg1 (1-159) amyloid aggregates at room temperature a method called Semi Denaturing Detergent Agarose Gel Electrophoresis (SDD-AGE) was used. This method was described by Bagriantsev, S.N. et al. in the year 2006 [91]. Since the aggregates are bigger in size they cannot be analysed in polyacrylamide gel which has small pores. The pore size is not sufficient for the passage and resolution of amyloid like aggregates thus agarose gel was used for running large protein polymers. This method enables the characterization of large protein polymers which are stable in SDS or Sarkosyl at room temperature. The Sg1 and Sg1 (1-159) aggregates were incubated with 1 % SDS or 2 % sarkosyl at room temperature for 10 min with non-reducing Laemmli sample buffer and examined on 1.5 % agarose gel by electrophoresis followed by electroblotting to PVDF membrane using SDD-AGE method as described previously [78,91]. The proteins on the PVDF membrane were visualized by staining with Coomassie brilliant blue R-250 [78,91].

Amyloid aggregates can be resolved based on their size and detergent insolubility using the method SDD-AGE. The process involves the following five steps:

1. Preparation of agarose gel
2. Preparation of protein samples
3. Agarose gel electrophoresis
4. Transfer to Polyvinylidene difluoride (PVDF) membrane
5. Detection of protein on PVDF membrane

Buffers and reagents:

Buffer for making agarose gel (1.5%): Tris 20 mM, Glycine 200 mM, Agarose 1.5 %, SDS 0.1%; Sample buffer (4x) without SDS and DTT: Tris 240mM, Bromophenol blue 0.2%, Glycerol 20%; Electrophoresis running buffer: Tris 20 mM, Glycine 200 mM, SDS 0.1%; Transfer buffer: Tris 20 mM, Glycine 200 mM, SDS 0.1 %, Methanol 15%; Staining solution: 0.4 g Coomassie brilliant blue R-250, methanol 30%, acetic acid 10% and water 60%; Destaining solution: Methanol 40%, acetic acid 10%, water 50%.

Step 1: Preparation of agarose gel

- a) 1.5% agarose gel was prepared in tris-glycine buffer. The weighed amount of agarose was completely dissolved using microwave.
- b) After agarose melted 0.1% SDS was added drop wise from 10% stock with gentle swirling to avoid bubble formation.
- c) Agarose solution was then poured into the casting tray enough for submerging the comb teeth.
- d) After the gel was set, comb was removed and the gel was placed in the gel tank containing the electrophoresis buffer with 0.1% SDS.

Step 2: Preparation of protein samples

- a) To an aliquot of protein sample, SDS or sarkosyl solution was added from 10% stock such that the final concentration of the ionic detergent becomes 2 %.
- b) The mixture was incubated for 10 min at room temperature to check for the stability of amyloid aggregates against the used ionic detergent.

Step 3: Agarose gel electrophoresis

- a) From the 4X stock of sample buffer, aliquots were added to the samples to get a mixture containing 1X sample buffer.
- b) Samples containing 1X sample buffer were incubated at room temperature for 10 minutes and were then loaded on gel.
- c) The gel was allowed to run at 125 volts for half an hour.

Step 4: Transfer to PVDF membrane

- a) A piece of PVDF membrane was cut to the same dimensions as the agarose gel.
- b) To activate the PVDF membrane it was submerged in methanol for 1 minute and then rinsed with distilled water followed by soaking it in transfer buffer.
- c) Two pieces of blotting paper were also cut in same dimensions as gel.
- d) In a tray, both the blotting paper and the activated PVDF membrane were then soaked in transfer buffer.
- e) The agarose gel was trimmed and oriented by making a cut in the lower right corner.
- f) Then each module was assembled in the following order starting from the bottom electrode plate (the cathode): First a black foam mesh was placed at the bottom of electrode plate, then a thick absorbent/blotting paper, thoroughly soaked in transfer buffer, the agarose gel, the wet PVDF membrane, a thick absorbent paper, a single foam mesh and then the upper electrode (the anode).
- g) While assembling the stack, care must be taken to avoid any bubble entrapping between the gel and the membrane which may hinder the transfer of protein.
- h) The electrodes were then connected and transfer was allowed to proceed for a minimum of 2.0 hours at 100 volts, at 4°C.

Step 5: Detection of protein on PVDF membrane

After transfer, the membrane was stained with Coomassie R-250 for 10 minutes. Followed by destaining using destaining solution and the image was captured using gel doc (G-box, syngene).

3.4.4.2 Proteinase-K resistance

Several amyloid aggregates have been reported to exhibit moderate resistance to digestion by proteinase-K [10,23]. The aggregated Sg1 full length protein (14 μ M) was incubated with proteinase-K (0.3 μ g/ml) at 37 °C for 0, 5 or 15 min in protease assay buffer (10 mM Tris HCl, 5 mM CaCl₂, pH 7.8). The proteolysis reaction was terminated by adding 5 mM PMSF and samples were mixed with reducing SDS-sample buffer and boiled for 6 min at 96°C before electrophoresis on 16% Tricine SDS-PAGE [94], which can give better resolution of small peptides and protein fragments [94]. Protein was visualized by prior fixing of the gel in fixing solution (50 % methanol, 10 % acetic acid, 100 mM ammonium acetate) for 30 mins followed by staining with Coomassie brilliant blue R-250.

3.4.5 Secondary structure estimation by CD

Sg1 and Sg1 (1-159) aggregates formed upon dialysis at pH 9.0 in presence of 10 mM β -mercaptoethanol were examined for any change in secondary structure using Far-UV circular dichroism (CD) spectroscopy. Sg1 and Sg1 (1-159) aggregates were diluted (~ thirty fold) in 10 mM tris HCl, pH 9.0 buffer, before acquiring the CD spectra [100]. CD spectra were recorded using Jasco J-1500 spectropolarimeter in the wavelength range of 190-260 nm using cuvette of 1mm path length and 2 mg/ml protein. Mean residue ellipticity $[\theta]$ was calculated using the following equation:

$$[\theta] = (\theta_{\text{obs}} * \text{MRW}) / (10 * c * l)$$

Where, θ_{obs} , c, l and MRW represent the observed ellipticity in milli-degrees, protein concentration in mg/mL, path length of cuvette in cm, and mean residue weight taken as 112 Da respectively. The spectra were corrected for baselines.

3.4.6 Transmission electron microscopy (TEM) of Sg1 and Sg1 (1-159) aggregates

The transmission electron micrographs of Sg1 and Sg1 (1-159) aggregates were acquired using a high-resolution transmission electron microscope (FEI Tecnai, T20G2), operated at 200 kV. A drop of the suspension was placed on a carbon-coated copper grid, dried in desiccator and negatively stained with 0.2 % Phosphotungstic acid (PTA) for 2 minutes, before imaging.

3.4.7 Estimation of Sg1 aggregate sizes by DLS

Full length Sg1 and Sg1 (1-159) aggregates obtained upon dialysis at pH 9.0 were diluted into aggregation buffer such that final concentration is 2 mg/ml. Dynamic light scattering measurements were carried out at room temperature using Delsa Nano C Particle Analyzer (Beckman Coulter) and data were processed using Delsa Nano 3.7 software. Measurements were carried out using 1 ml quartz cuvette with the sample chamber pre-maintained at 25 °C. The samples were illuminated with a 658 nm laser light and scattering intensity were measured at 165° angle.

3.4.8 Inhibition of Sg1 aggregation by Zn²⁺

Reduction in seminal levels of zinc has also been reported with aging [54]. Therefore, it was investigated whether Zn²⁺ can exert any effect on the *in vitro* aggregation of Sg1. Any *in vitro* effect of Zn²⁺ if further corroborated by *in vivo* investigations, could show role of Zn²⁺ concentration on Sg1 aggregation and the development of SSVA. For this, a stock solution of ZnCl₂ (30 mM) was prepared in 10 mM tris HCl pH 9.0 buffer and used for the studies. 12 mg/ml Sg1 and Sg1 (1-159) fragment were incubated with Zn²⁺ solution to obtain molar ratios of 1:1 or 1:15 and aggregation was examined by ThT binding assay in presence of 100 mM β-mercaptoethanol. Certain aminophenols such as p-aminophenol, have been reported to disaggregate amyloid aggregates of Aβ₄₂ peptide and hen egg white lysozyme protein (HEWL) when incubated at equimolar ratios [97,98]. Here, we tested whether 3-aminophenol (3AP) at four-fold molar excess would have any effect on the aggregation of Sg1 or Sg1 (1-159) fragment.

Chapter IV

New insights into amyloid-like *in vitro* aggregation of human serum albumin protein

4.1 Abstract

Amyloid aggregates display striking features of detergent stability and self-seeding. Human Serum Albumin (HSA), a preferred drug-carrier molecule, can also aggregate *in vitro*. So far, key amyloid properties of stability against ionic detergents and self-seeding, are unclear for HSA aggregates. Precautions against amyloid contamination would be required if HSA aggregates were self-seeding. Here, we show that HSA aggregates display detergent sarkosyl stability and have self-seeding potential. HSA dimer is preferable for clinical applications such as a plasma expander, due to its longer retention in circulation and lesser oedema owing to its larger molecular size. Here, HSA was homo-dimerized *via* free cysteine-34, without the use of any potentially immunogenic cross-linkers that are usually pre-requisite for HSA homo-dimerization. Alike the monomer, HSA dimers also aggregated as amyloid, necessitating considerations for precautions while using for therapeutics.

4.2 Introduction

Human serum albumin (HSA) which is the most abundant protein in blood plasma, can form amyloid-like aggregates *in vitro* [71,72]. HSA is an all- α helix, globular protein made of a single peptide chain of 585 amino acids with one free sulfhydryl group at cysteine-34 [63]. It has multiple physiological roles like: as a nutrients transporter & carrier protein in blood for several compounds (e.g.: fatty acids, amino acids, bile salts, metals and hormones etc.) and as a regulator for blood pH & osmotic pressure [65-67]. It has also found applications as a safe and non-immunogenic drug carrier and as a versatile plasma expander, as its administration is considered to be helpful in the treatment of severe hypoalbuminemia during burns, nephritic syndrome, chronic liver cirrhosis and haemorrhagic shocks [68]. Notably, HSA dimers are preferable as a plasma expander as well as a drug carrier due to their increased circulatory life and alleviating effect on the oedema associated with unwanted extravasation of the monomeric HSA [68,69].

HSA has been used as a model amyloid protein and is found to form amyloid-like aggregates *in vitro* at physiological pH 7.4 and also at acidic pH but only at elevated temperatures, when present in aqueous solvents [71]. HSA aggregation has been reported at physiological pH at lower temperatures also (25°C, 37°C, 65°C) however in presence of organic solvent ethanol [72-74]. HSA aggregates display varying morphologies under different aggregation conditions, possibly due to formation of different structural intermediates during the aggregation pathway [71,72]. Unlike a typical amyloid aggregation trend, which follows a lag dependent sigmoidal kinetics, there is absence of any apparent lag period in HSA aggregation [5,72]. Although HSA aggregates conform to several amyloid aggregate-associated properties such as thioflavin-T (ThT) dye binding and Congo red binding, certain important properties such as the self-seeding ability and detergent stability have not been established yet. Amyloid self-seeding is usually assayed *in vitro* and monitored as decrease in lag period of aggregation, suggesting acceleration of conversion of monomers to aggregates [10]. If HSA aggregates exhibited self-seeding at physiological conditions, any unwanted HSA amyloid contamination in samples used for therapeutics, could potentially seed the *in vivo* circulating HSA monomers into amyloid form, which would be hazardous.

Here we first converted HSA into aggregates exhibiting amyloid-like ThT dye binding and then we examined if the aggregates display amyloid-like detergent stability. Furthermore, we examined self-seeding behaviour of HSA aggregates at sub-optimal aggregation temperature, in the view that few previous attempts at optimal aggregation conditions were inconclusive, possibly due to lack of a discernible lag period in aggregation [72,75]. Due to buried nature of the free cysteine-34 in HSA structure, HSA dimers employed for clinical applications have often been obtained using chemical cross-linkers of cysteine, which may potentially be immunogenic [68]. Here we succeeded in homodimerizing HSA *via* disulfide linkage using denaturation in urea and hydrogen peroxide (H₂O₂) induced oxidation. We then examined if HSA homodimers retain the amyloidogenic properties similar to the HSA monomers.

4.3 Results and Discussion

4.3.1 *In vitro* formation of HSA aggregates

Temperature is important factor in HSA protein aggregate formation. Elevated temperature favoured aggregation as it might promote partial unfolding. HSA protein was diluted in aggregation buffer (10 mM sodium phosphate buffer pH 7.4 containing 50 mM NaCl) to a final concentration of 20 mg/ml and incubated without agitation at 65°C for 52 hrs in a water bath to induce aggregation as reported previously [71,72]. Amyloid aggregate formation was assessed by ThT and Congo red binding assays as described below.

(i) Thioflavin-T binding assay for HSA aggregates

ThT dye has been reported to bind specifically to amyloid aggregates which changes its fluorescence properties significantly [7]. HSA aggregates (20 mg/ml) were mixed with ThT solution (2 mM final) and extrinsic fluorescence emission spectrum of ThT was monitored by excitation at 442 nm and recording emission from 460 nm to 560 nm. HSA aggregates showed an enhanced ThT fluorescence emission intensity around 485 nm indicating amyloid-like ThT binding (Figure 35A) as also reported previously [72]. Excitation spectra of ThT, after addition to HSA aggregates, was also recorded between 250-455 nm after fixing the emission

to 495 nm [7]. HSA aggregates showed ThT fluorescence excitation maxima near 450 nm (Figure 35B).

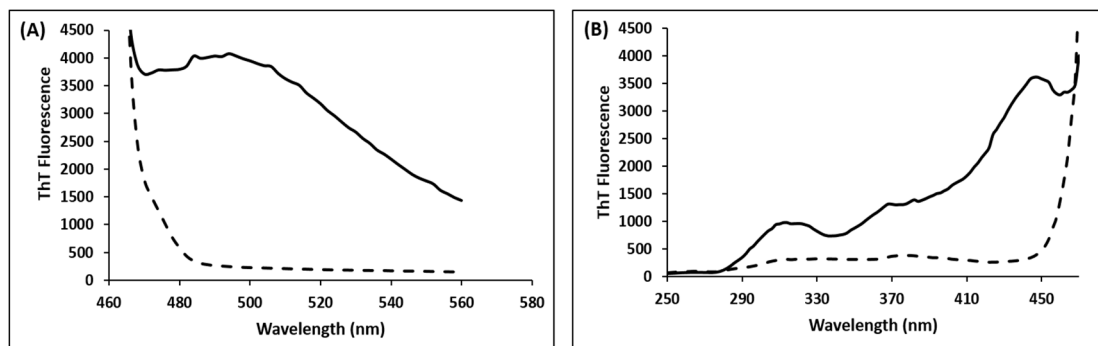


Figure 35. Assessment of amyloid nature of HSA aggregates by ThT fluorescence

HSA aggregates formed by incubation at 65°C for 52 hrs were added with ThT and fluorescence emission spectrum (A) and ThT excitation spectrum (B) of these aggregates were recorded. Solid lines in both panels A and B represent ThT spectra with HSA aggregates and dashed lines indicate buffer control spectra.

(ii) Congo red binding assay for HSA aggregates

The dye Congo red can bind to amyloid aggregates with high specificity, which can manifest as a red shift in its absorption maximum (λ_{\max}) from 480 nm to 540 nm or increase in absorption intensity in 480-540 nm range [88].

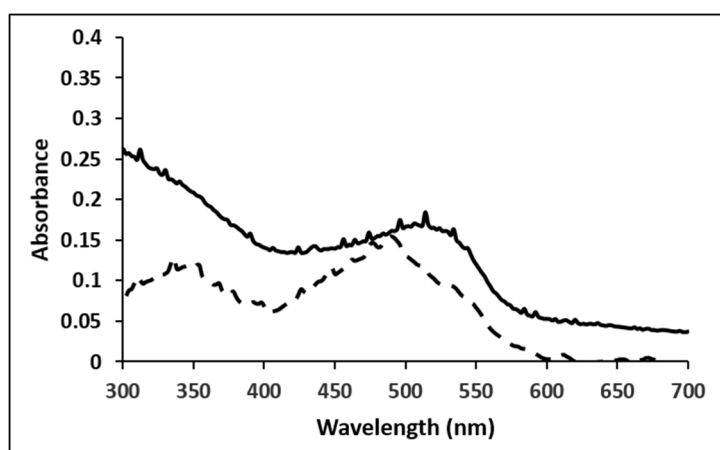


Figure 36. Congo red absorbance spectrum in presence of HSA aggregates

Congo red absorption spectrum of HSA aggregates (solid line) formed upon incubation of HSA at 65°C for 52 hrs. Dashed line represent Congo red spectrum of free dye in buffer, pH 7.4.

Congo red absorption spectrum was recorded from 300 nm to 400 nm after mixing it with HSA aggregates in 1:1 molar ratio. Congo red absorption maximum of free dye at 480 nm shifted to 540 upon binding to HSA aggregates indicative of amyloid-like aggregation (Figure 36).

4.3.2 Intrinsic tryptophan fluorescence of HSA aggregates

Intrinsic fluorescence of Tryptophan residues is a good parameter to study folding and unfolding of a protein [101]. When amyloid formation occurs, Trp residues present on the surface (hence in hydrophilic micro-environment) of the native protein may be expected to get internalized (hence in hydrophobic micro-environment) leading to change in the Trp fluorescence emission pattern. Thus, Trp fluorescence emission spectra was recorded (excitation wavelength at 292 nm; emission scan 300-400 nm) to study HSA amyloid formation as it contains surface Trp residues in its native conformation [102]. In native state monomeric HSA protein gives Trp fluorescence emission λ_{max} at 340 nm which undergoes blue shift to 332 nm upon HSA aggregation (Figure 37).

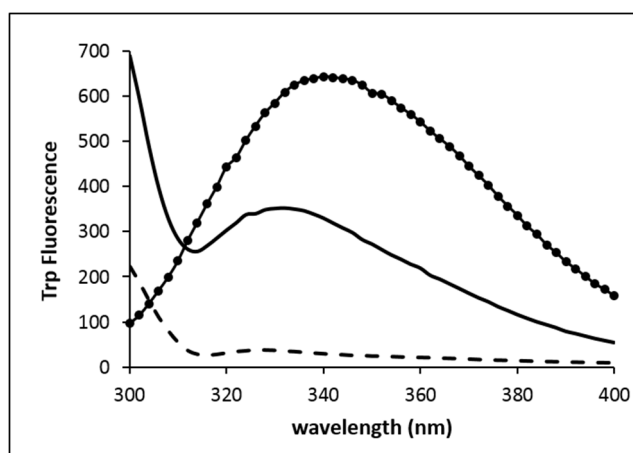


Figure 37. Tryptophan fluorescence emission spectra of HSA aggregates

Tryptophan fluorescence emission spectra was recorded (excitation at 292 nm; emission scan 300-400 nm) to examine HSA amyloid formation. HSA aggregates (solid line) showed a blue shift in Trp emission maximum from 340 nm to 332 nm as compared to monomeric HSA protein (solid dots). Spectra shown with dashed line represent buffer control.

4.3.3 Estimation of molecular sizes of HSA aggregates by DLS

Furthermore, the HSA aggregates formed at 65 °C, when analyzed by dynamic light scattering, as expected, showed polydispersity with hydrodynamic radii of $\sim 156 \pm 21$ nm, thereby supporting an amyloid, rather than just oligomeric, nature of the aggregates (Figure 38B). Measurements were carried out using 1 ml quartz cuvette with the sample chamber pre-maintained at 25 °C. The samples were illuminated with a 658 nm laser light and scattering intensity were measured at 165° angle. From the number distribution of the molecular species from DLS data, the mean hydrodynamic radii obtained for the samples were: HSA monomer: 3.2 ± 0.9 nm (polydispersity: 18 %); HSA amyloid aggregates: 156 ± 21 nm (polydispersity: 30 %). The buffers used for these samples were: HSA monomer: 50 mM glycine-HCl+50 mM NaCl, pH 3.0, 8 M urea; HSA amyloid aggregates: 10 mM sodium phosphate + 50 mM NaCl, pH 7.4 (Figure 38A and 38B).

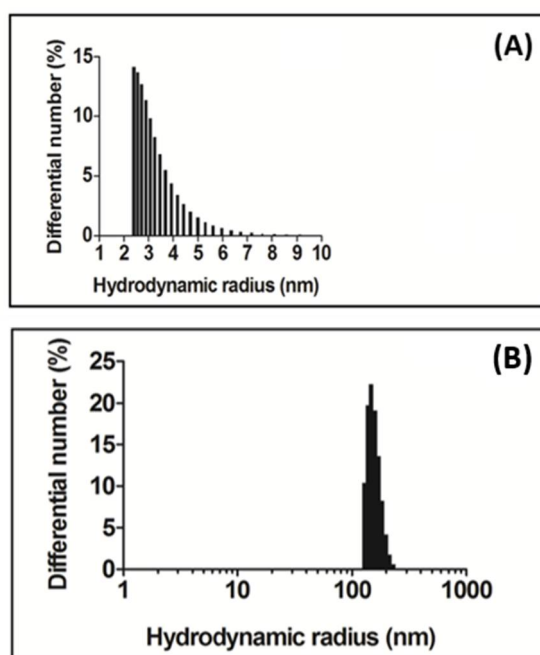


Figure 38. Estimation of molecular sizes of HSA aggregates by DLS
Dynamic light scattering measurements were carried out on HSA monomer (A) and HSA amyloid aggregates which are formed by incubation at 65 °C for 52 hrs (B).

4.3.4 Transmission electron microscopy of HSA aggregates

When analyzed by TEM, the HSA aggregates formed at 65 °C showed elongated fibrillar morphologies as reported previously thereby confirming their amyloid nature [71] (Figure 39A-D).

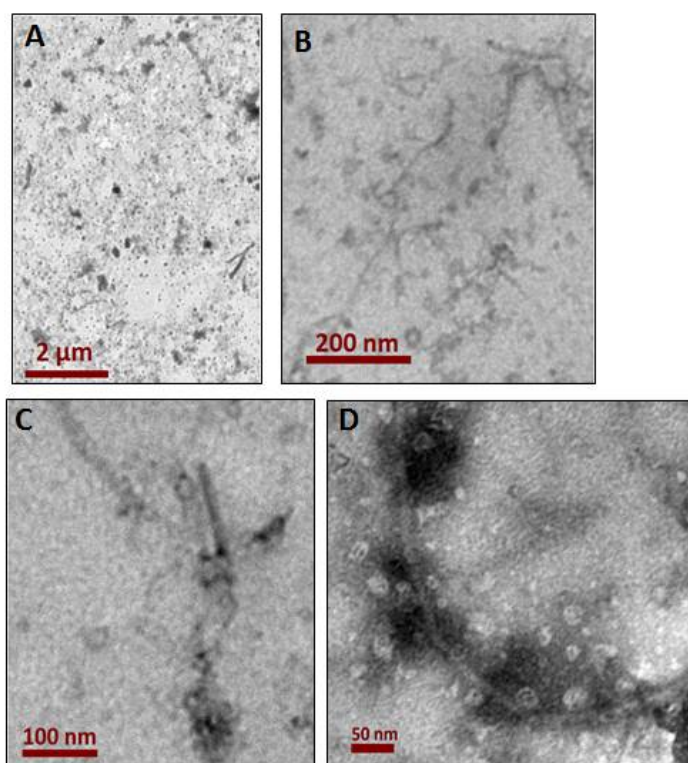


Figure 39. Morphologies of HSA amyloid aggregates viewed in TEM
(A-D) TEM images of negatively stained HSA amyloid aggregates, obtained by incubation at 65°C for 52 hrs at pH 7.4, that were used for sarkosyl stability assay and as pre-formed seed in subsequent experiments.

4.3.5 Evaluation of HSA aggregates as true amyloid

4.3.5.1 Semi denaturing detergent agarose gel electrophoresis (SDD-AGE)

Protein amyloid aggregates show increased stability against denaturants (e.g. urea) and ionic detergents (e.g. SDS and sarkosyl) when compared with amorphous aggregates [23]. Assay was performed to examine the stability of HSA aggregates against ionic detergent sarkosyl (2 %) using SDD-AGE (Figure 40), HSA aggregates exhibited higher molecular

weight species upon incubation with 2 % sarkosyl at room temperature, indicating their resistance against dis-aggregation. Using calibration curve generated by relative mobility of proteins of known molecular weight, it was estimated that the sarkosyl-stable species of HSA amyloid aggregates were over 6084 kDa in size and thus composed of over 90 monomers. The observed sarkosyl stability strongly supports amyloid nature of HSA aggregates.

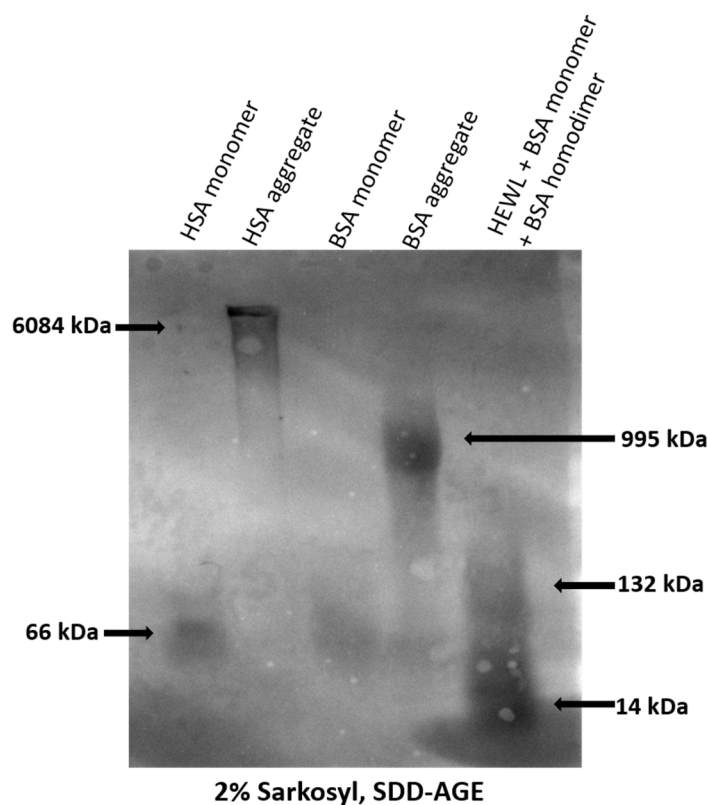


Figure 40. Amyloid-like detergent stability of HSA aggregates

Stability of HSA aggregates against 2 % sarkosyl was assessed by using SDD-AGE. Samples were incubated with 2% sarkosyl at room temperature for 10 minutes and electrophoresed on 1.5 % agarose gel followed by electroblotting to PVDF membrane and visualized by Coomassie staining. High molecular weight smear of HSA aggregates (Lane 2) is shown relative to the stained HSA and BSA monomers. A mixture of HEWL, BSA monomer and BSA homodimer were used as markers. Lane 1: HSA monomer; Lane 2: HSA aggregates; Lane 3: BSA monomer; Lane 4: BSA amyloid aggregates, Lane 5: mixture of HEWL, BSA monomer & BSA homodimer.

4.3.5.2 Assay of seeding capability of HSA aggregates

In addition to detergent stability, ability to self-seed aggregation of their monomers distinguishes amyloid aggregates from amorphous protein aggregates [5]. In order to visualize kinetics of seeding, a lag dependent growth of the amyloid is a pre-requisite. For many amyloidogenic proteins, addition of pre-formed seed completely eliminates the lag phase whereas, for others such as the human TDP-43 protein implicated in Amyotrophic Lateral Sclerosis, seeding manifests as reduction in the lag period [103]. Previously, it has been shown that HSA amyloid aggregation proceeds without any lag phase at 65 °C [72]. Therefore, self-seeding ability of pre-formed HSA aggregates could not be monitored at the optimal 65°C temperature. Thus, we examined a suboptimal aggregation temperature (50°C) where spontaneous aggregation of HSA would be expectedly negative due to lack of successful oligomeric nuclei formation, that normally precedes amyloid aggregation [2]. However, the added pre-formed seeds which contain pre-formed nuclei may initiate the conversion of monomers to aggregates and show the seeding kinetics even at suboptimal aggregation temperatures.

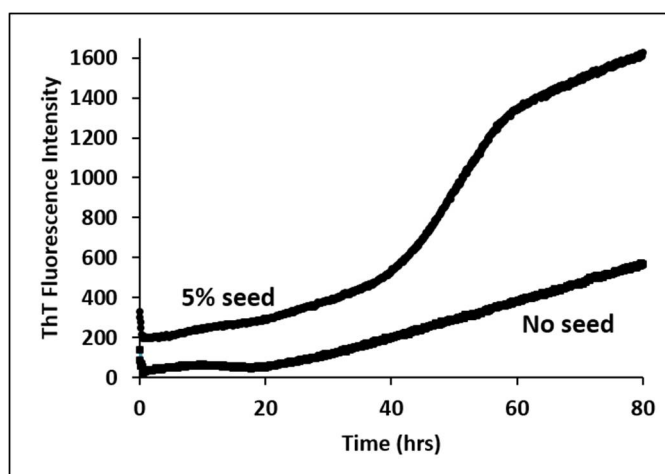


Figure 41. Amyloid-like self-seeding of HSA aggregates

Pre-formed HSA aggregates (as 5% seed) were added to monomeric HSA (20 mg/ml) dissolved in aggregation buffer of pH 7.4 containing 2 mM ThT. Mixture was incubated at 50°C for 96 hrs without agitation in Spectramax- M5^o microplate reader. ThT fluorescence emission intensities were recorded every 5 min. Aggregation kinetics of HSA monomer without pre-formed seed was used as a control.

Similar strategy has been used to demonstrate self-seeding of TDP-43 amyloid at suboptimal aggregation conditions, where the sample were kept at static, in the view that shaking causes aggregation of TDP-43 without a lag phase [103]. Indeed, as per our hypothesis, the HSA amyloid aggregates showed self-seeding at 50°C as observed by amyloid-like increase in ThT fluorescence intensity (Figure 41) [7]. Notably, the self-seeding of the HSA aggregation was observed to reduce the lag phase but not completely abrogate it.

4.3.5.3 TEM of self-seeded HSA aggregates

HSA aggregates obtained at 50 °C by seeding with pre-formed aggregates also showed fibrillar amyloid-like structures as observed by TEM, thereby supporting the process of HSA amyloid self-seeding (Figure 42 A-D).

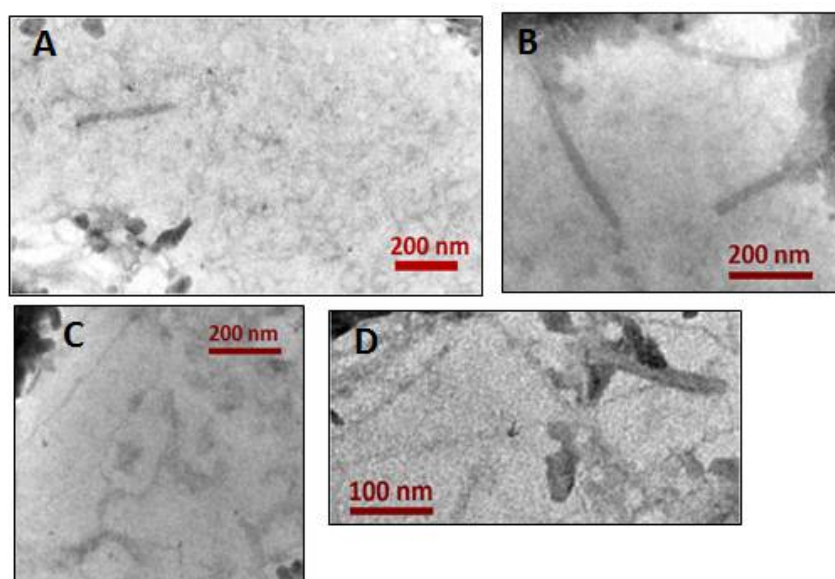


Figure 42. Morphologies of HSA amyloid aggregates obtained upon seeded aggregation

(A-D) TEM images of HSA amyloid aggregates which were previously obtained by incubation at 50 °C by seeded aggregation were acquired by TEM (T20G2) operated at 200 kV. A drop of the aggregates suspension was placed on a carbon-coated copper grid, dried in desiccator and negatively stained with 0.2 % Phosphotungstic acid (PTA) for 2 minutes, before imaging.

4.3.5.4 Cross-seeding of HSA and BSA aggregates

Amyloid cross-seeding between prion form of bovine PrP^{Sc} protein and the human soluble PrP^C protein, is proposed as the basis of species-barrier crossing of prion transmission, which is yet to be proven beyond doubt [24,95,104]. Bovine and human prion proteins causing Bovine spongiform encephalopathy and Creutzfeldt-Jakob disease have been known to have biochemical and pathological similarities [24]. In this line, we examined whether bovine serum albumin (BSA) and HSA amyloid can show cross-seeding in the view that HSA and BSA proteins share over 76 % sequence similarity [105].

Monomeric HSA (10 mg/ml) was incubated with sonicated, pre-formed BSA aggregates (as 5 % seed) at 50 °C in 10 mM sodium phosphate buffer, pH 7.4 containing 50 mM NaCl in presence of ThT. Gradual, sigmoidal increase in ThT fluorescence intensity was observed with time suggesting possibility of amyloid-like cross-seeding of HSA aggregates (Figure 43A). Similar trend was also found when monomeric BSA was incubated with pre-formed HSA aggregates (5 % seed) (Figure 43B). If pre-formed HSA and BSA aggregates are successfully able to cross-seed each other's aggregation, they may act as good candidates for amyloid cross-seeding mechanism investigations. Study of their cross-seeding ability may serve as a possible model for species barrier cross-seeding of amyloid aggregates.

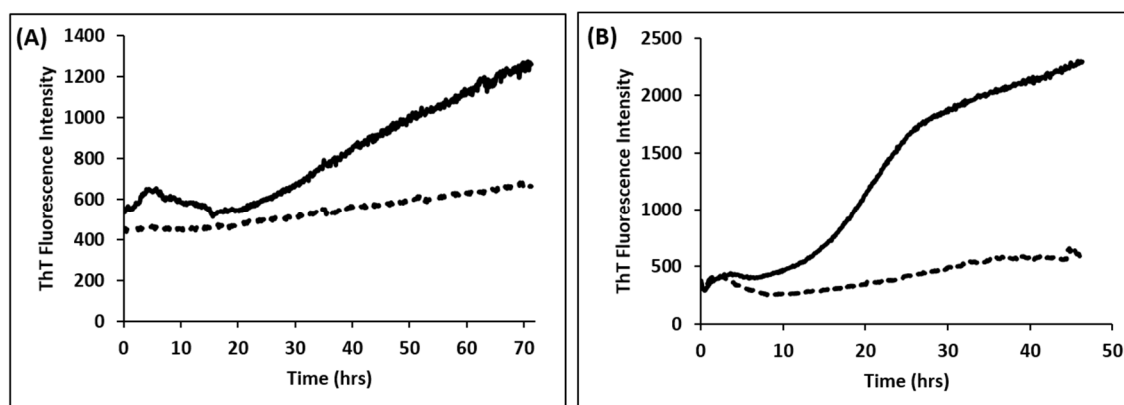


Figure 43. Cross-seeding kinetics of HSA and BSA aggregation

(A) Solid line represents HSA cross-seeded by pre-formed BSA aggregates (5% seed) and dashed line represent unseeded HSA. (B) BSA cross-seeded by pre-formed HSA aggregates (solid line). Dashed line indicate unseeded BSA.

4.3.6 HSA homo-dimerization and purification

4.3.6.1 Estimation of free sulfhydryl group in HSA by Ellman's method

5,5'-dithiobis-(2-nitrobenzoic acid) (DTNB) also known as Ellman's reagent was used to determine the number of free sulfhydryl group in HSA [106]. Sulfhydryl groups may be quantitated by using the extinction coefficient of TNB released upon reaction with DTNB. Protein samples of BSA, HSA or lysozyme at 0.15 mM concentration were mixed with DTNB (4 mg/ml) in the reaction buffer (sodium phosphate buffer pH 8.0) and incubated for 15 minutes at room temperature and absorption was measured at 412 nm. Subsequently, free -SH group content was calculated using the following equation. The reported molar absorptivity of TNB in this buffer system at 412 nm is 14,150. Molar absorptivity, E , is defined as follows:

$$E=A/bc$$

(where, A = absorbance, b = path length in cm, c = concentration in moles/liter)

Solving for concentration gives the following formula: $c=A/bE$.

Table 5. Estimation of free cysteine in HSA by Ellman's reagent assay

Concentration of the sample	Estimated no. of free - SH group/molecule	Reported no. of free - SH group/molecule
HSA (0.10 mM) ^[Ref. 61]	1.0	1.0
β- mercaptoethanol (0.25 mM)	1.1	1.0
BSA (0.15 mM) ^[Ref.105]	0.5	0.5
Lysozyme (0.07 mM) ^[Ref.106]	0.1	0.0

In order to dimerize HSA molecules *via* disulfide linkage, the availability of one free cysteine residue needed to be confirmed. This estimation of the free cysteine was carried out using Ellman's reagent assay (Table 5) [106]. Free cysteine estimation was also carried

out for BSA, β -mercaptoethanol and Hen Egg White Lysozyme for comparison and validation of the estimation [63,107,108].

4.3.6.2 H₂O₂ induced disulfide-linked homo-dimerization of HSA

With the goal of examining whether homodimer of HSA which finds several clinical applications retains amyloidogenicity, we first tried to dimerize HSA *via* its cysteine-34 residues. Conjugation of two HSA monomers *via* their free cysteine-34 was carried out in presence of 8 M urea and 25 mM/100 mM H₂O₂. Urea (8 M) was used for exposing out the one free cysteine-34, which is present in a 10 Å deep crevice in the native molecule [109]. Unfolding of HSA in 8 M urea, has already been shown to be reversible [110]. Optimal H₂O₂ concentration required for dimerization was found to be 25 mM and any further increase, even to 100 mM, did not elevate the levels of dimer formation. As shown in Figure 44 (lane 4 and 6) the ratio of dimer to monomer molecules in presence of 25 mM H₂O₂ was ~ 2 : 3 as estimated by *Image J* densitometry software [111]. Formation of very little dimer population as seen in lanes 2 & 8 of Figure 43 support that presence of both urea and H₂O₂ together, are necessary for efficient dimerization.

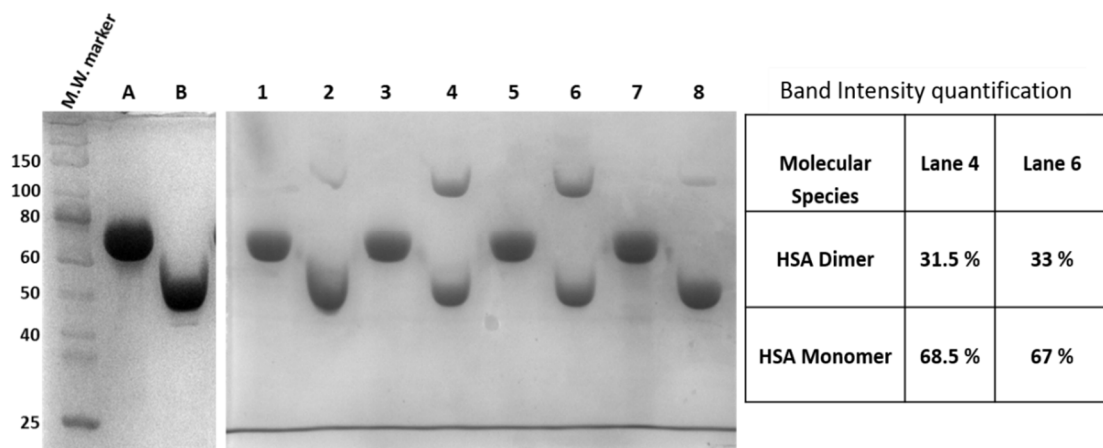


Figure 44. Hydrogen peroxide induced dimerization of HSA.

HSA homodimer formation was monitored on 10% SDS-PAGE under reducing (R) and non-reducing (NR) conditions. HSA+ 8 M urea (R): Lane A & Lane 1; HSA+ 8 M urea (NR): Lane B & Lane 2; HSA+8 M Urea+25 mM H₂O₂: Lane 3 (R) and Lane 4 (NR); HSA+8 M Urea+100mM H₂O₂: Lane 5 (R) and Lane 6 (NR); HSA+ 100 mM H₂O₂: Lane 7 (R) and Lane 8 (NR). Comparison of lane 4 and 6 shows that presence of H₂O₂ and urea together is essential for efficient dimerization of HSA. Relative intensity of HSA dimer and HSA monomer bands were estimated by using *Image J* software [111].

4.3.6.3 Size exclusion chromatography

4.3.6.3.1 Separation of HSA monomers and dimers by gel filtration using FPLC

As the dimerization of HSA was not a 100% efficient process, thus the dimers needed to be separated out from monomers. The HSA dimers were purified from the mixture of monomers based on the differences in their molecular weights, by SEC using Superose 6 column on FPLC (Figure 44A). As expected, two peaks were obtained in the elution profile, the first peak fractions contained predominantly dimer molecules while the second peak fractions showed mostly monomers (Figure 45A and 45B). The fractions containing predominantly HSA dimers were pooled and further analyzed for amyloid forming ability under conditions as described for HSA monomer.

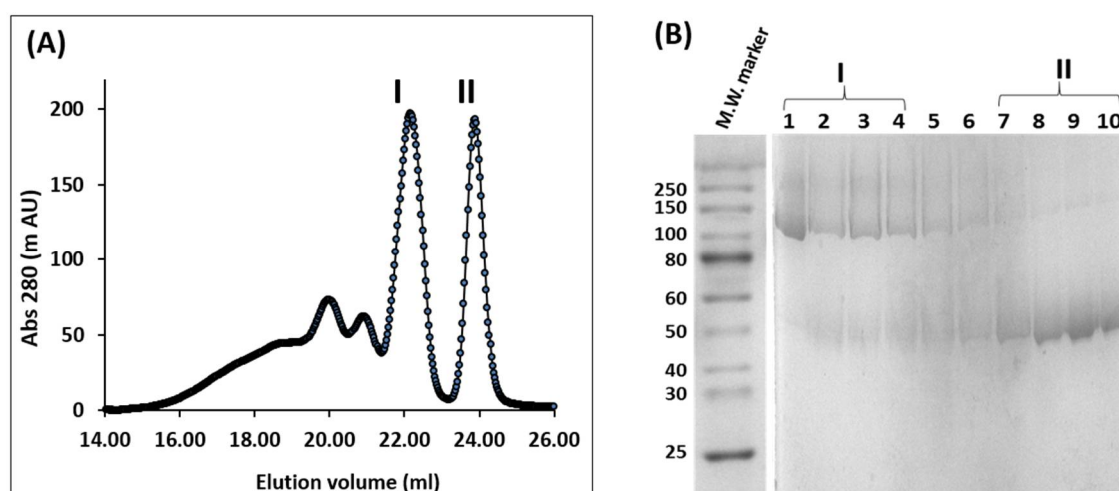


Figure 45. Purification of HSA dimer by size exclusion chromatography

(A) Elution profile showing separation of HSA dimer (peak-I) and HSA monomer (peak-II) by size exclusion chromatography on Superose 6, 10/300 GL column using ÄKTA™ FPLC system. (B) Homogeneity of the purified fractions from FPLC was assessed by 10% SDS-PAGE. Lanes 1, 2, 3 & 4 from peak-I in (A) were pooled as dimer fractions and lanes 7, 8, 9 & 10 from peak-II in (A) were pooled as monomer fractions.

4.3.6.3.2 Estimation of hydrodynamic radius of purified HSA dimer by DLS

From the number distribution of the molecular species from DLS data, the mean hydrodynamic radii obtained for the samples were: HSA monomer: 3.2 ± 0.9 nm (polydispersity: 18 %); Purified HSA dimer: 6.7 ± 1.3 nm (polydispersity: 20 %) (Figure

46). The buffers used for these samples were: HSA monomer: 50 mM glycine-HCl+50 mM NaCl, pH 3.0, 8 M urea; HSA dimer: 10 mM sodium phosphate + 50 mM NaCl, pH 7.4, 8 M urea.

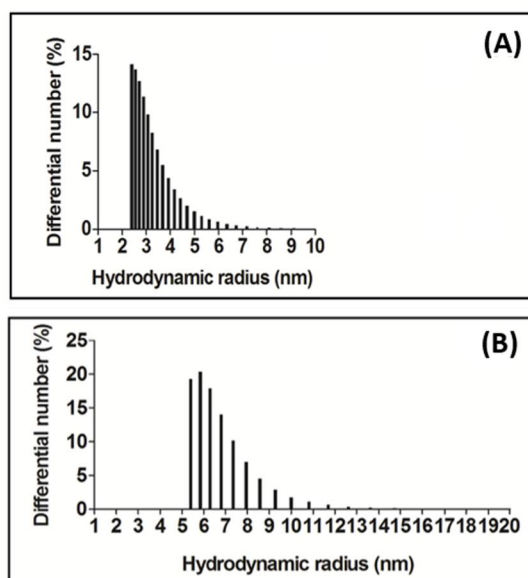


Figure 46. Comparison of hydrodynamic radius of HSA monomer (A) and purified HSA dimer (B) using DLS.

Scattering measurements were carried out on HSA monomer (A) which was compared with the DLS data for purified HSA homo-dimer (B). Samples were at final concentration of 5 mg/ml. Measurements were carried out at room temperature using Delsa Nano C Particle Analyzer (Beckman Coulter) and data were processed using Delsa Nano 3.7 software. The samples were illuminated with a 658 nm laser light and scattering intensity were measured at 165° angle.

4.3.6.3.3 Stability of HSA homodimer to mild reducing agent

The formed HSA homodimer was examined for its stability to mild reducing agent DTT (2.5 mM). Assessment of stability of HSA homodimer to reducing condition is important for better applicability, in the view that HSA drug formulations could be administered through injection in blood which may carry mild reducing agents. Also, if applied for drug delivery to tumors where microenvironment may be reducing, it may lead to breakdown of dimer to monomer. HSA homo-dimerization mixture is incubated with sample buffer containing 2.5 mM DTT and examined for stability by SDS-PAGE. Same

sample was also loaded in presence of reducing sample buffer and completely non-reducing sample buffer for comparison. We observed that the presence of mild reducing agent does not have any effect on HSA homodimer as the sample is quite comparable to the sample in presence of non-reducing sample buffer (Figure 47).

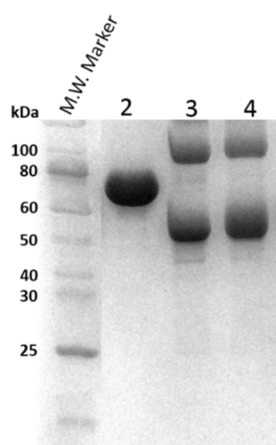


Figure 47. Assessment of stability of HSA homodimer to reducing agent by SDS-PAGE.

Lane 2: HSA homo-dimerization mixture (reducing condition, 100 mM DTT); Lane 3: HSA homo dimerization mixture (non-reducing condition); Lane 4: HSA homo-dimerization mixture (reducing condition with 2.5 mM DTT).

4.3.7 *In vitro* amyloid-like aggregation of HSA homodimer

4.3.7.1 ThT and Congo red binding assays

The HSA dimers were found to aggregate and exhibit amyloid-like ThT fluorescence emission and excitation similar to HSA monomer aggregates (Figure 48A and 48B) [7]. Also, when added with Congo red, the dimer aggregates caused red shift in Congo red absorption maximum from 480 nm to 540 nm accompanied by increase in absorption intensity near 540 nm suggesting amyloid-like nature of the aggregates (Figure 49) [88].

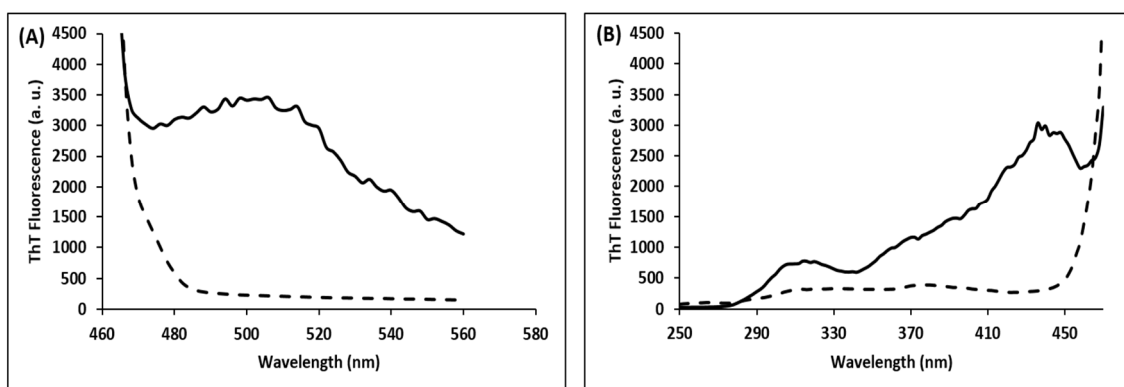


Figure 48. Assessment of amyloid nature of HSA dimer aggregates

(A) HSA dimers (20 mg/ml) were incubated in aggregation buffer 10 mM sodium phosphate, pH 7.4, with 50 mM NaCl at 65°C for 52 hrs. ThT fluorescence emission spectrum of HSA dimer aggregates (solid line) added with 2 mM ThT, was recorded by excitation at 442 nm. (B) ThT fluorescence excitation spectra of aggregates of HSA dimers (solid line), were recorded from 250-455 nm using emission at 495 nm. In both cases (A & B) the dashed line represents buffer control spectrum.

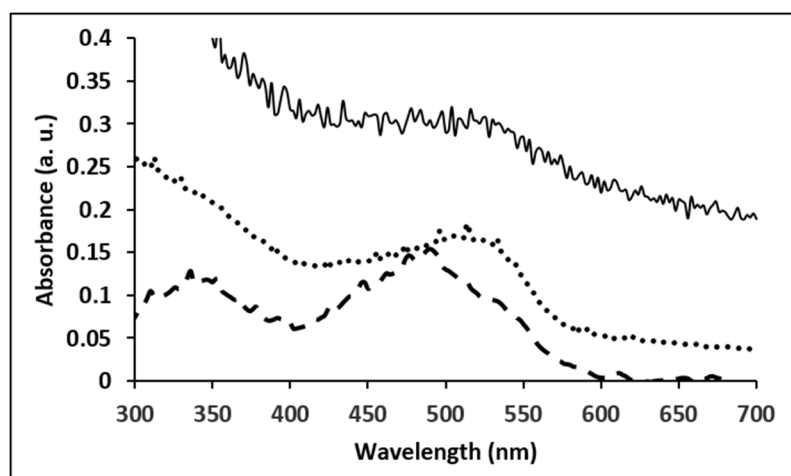


Figure 49. Assessment of Congo red binding of HSA dimer aggregates

HSA dimer aggregates (solid line) or HSA monomer aggregates (dotted line) (10 mg/ml) were mixed with Congo red in 1:1 molar ratio and Congo red binding was assessed by recording absorption spectra from 300-700 nm and compared with that of HSA monomer aggregates (dotted line). Absorption wavelength maximum shift from 480 nm to 540 nm, indicates presence of amyloid. The dashed line represents buffer control spectrum.

4.3.7.2 Atomic Force Microscopy (AFM) of HSA dimer aggregates

Amyloid fibrils are highly ordered fibrillar structures. Atomic force microscopy (AFM) is one of the most widely used techniques to study the structural properties of amyloid fibrils. Some of the advantages of AFM for amyloid observation includes relatively easier sample preparation and avoidance of any unwanted structural changes to amyloid aggregate samples [112]. Amyloid-like fibrillar morphology of the HSA dimer aggregates was ascertained by AFM imaging which showed presence of elongated curly fibers of height ranging from ~ 15 to 20 nm (Figure 50). Similar morphologies of HSA amyloid aggregates have also been reported elsewhere [113].

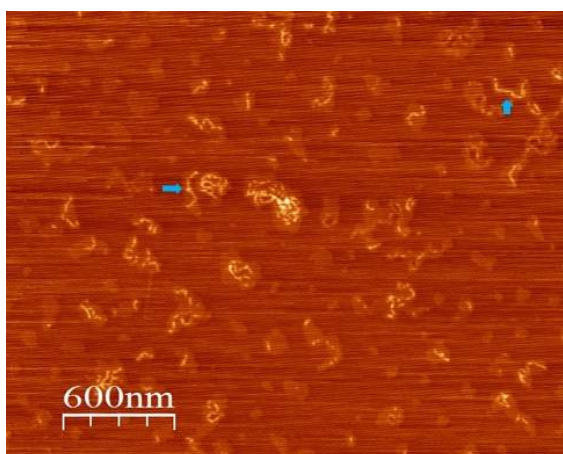


Figure 50. AFM imaging of HSA dimer aggregates.

HSA dimer aggregates formed after 52 hrs of incubation at 65 °C. Before imaging, the sample was diluted 30 folds in aggregation buffer and drop casted on freshly cleaved mica sheet and dried. Typical fibrillar amyloid aggregates have been arrow-marked.

4.4 Materials and Methods

4.4.1 Materials

Recombinant HSA expressed in *Saccharomyces cerevisiae*, Congo red, Thioflavin-T, N-Lauroylsarcosine sodium salt (Sarkosyl), Sodium dodecyl sulphate (SDS), Hydrogen peroxide, 5, 5'-Dithio-bis (2-Nitrobenzoic acid) (DTNB, Ellman's reagent) and dialysis membrane were purchased from Sigma-Aldrich, USA. Polyvinylidene fluoride

membrane (PVDF) and Superose 6, 10/300 GL high performance gel filtration column was obtained from GE Healthcare, USA. Urea, Sodium chloride, Sodium phosphate dibasic and monobasic were purchased from Himedia, India. All other chemicals were also of high purity.

4.4.2 Amyloid aggregation and detection

HSA protein was diluted in aggregation buffer (10 mM sodium phosphate buffer pH 7.4 containing 50 mM NaCl) to a final concentration of 20 mg/ml and incubated without agitation at 65°C for 52 hrs in a water bath to induce aggregation as reported previously [71,72]. Amyloid aggregate formation was assessed by ThT and Congo red binding assays as described below.

4.4.2.1 Thioflavin-T binding assay

HSA aggregates (20 mg/ml) were mixed with ThT solution (2 mM final) and ThT fluorescence emission spectrum was monitored by excitation at 442 nm and recording emission from 460 nm to 560 nm. Excitation spectra of ThT, after addition to aggregates, was also recorded between 250-455 nm after fixing the emission to 495 nm [7].

4.4.2.2 Congo red binding assay

The dye Congo red can bind to amyloid aggregates with high specificity, which can manifest as a red shift in its absorption maximum (λ_{max}) from 480 nm to 540 nm or increase in absorption intensity in 480-540 nm range [88]. To examine amyloid nature of HSA aggregates, Congo red dye was solubilized in phosphate buffered saline, pH 7.4 and then mixed with ~150 μM HSA aggregates in 1:1 molar ratio. The mixture was incubated for 30 min at room temperature and Congo red absorption was recorded from 300 nm to 700 nm [88].

4.4.3 Semi-denaturing detergent agarose gel electrophoresis (SDD-AGE)

Several amyloid and prion aggregates have been shown to exhibit stability against disaggregation by ionic detergents like SDS or sarkosyl (~1-2 %), when tested at room temperature [10,23,92]. Amyloid-like detergent stability of the HSA aggregates was

examined by SDD-AGE [91]. Briefly, the HSA aggregates were first incubated with 2 % sarkosyl at room temperature for 10 min and then mixed with non-reducing Laemmli sample buffer lacking detergent and electrophoresed on 1.5 % agarose gel. Protein from the gel was electro-blotted to PVDF membrane and visualized by Coomassie staining [78,91].

4.4.4 Amyloid seeding assay

Many amyloid aggregates exhibit lag depended sigmoidal kinetics of formation [5]. Upon addition of pre-formed aggregates (seed), the lag in aggregation can either shorten or completely disappear due to a process termed ‘self-seeding’, where the monomers are induced to aggregate with rapidity by the seed [103,114]. To confirm ordered amyloid structure and distinguish it from randomly misfolded amorphous aggregates which cannot show seeding ability. The formed amyloid aggregates of HSA were subjected to self-seeding analysis (Figure 51). HSA aggregates (5%) pre-formed at 65°C were briefly sonicated to break the clumps and added to monomeric HSA (20 mg/ml) dissolved in aggregation buffer of pH 7.4 containing 2 mM ThT. Sonication breaks the large amyloid aggregates into smaller seeds with suitable ends for amyloid growth. This mixture was then incubated with intermittent shaking at 50°C for 96 hrs in Spectramax- M5^e multimode microplate reader (Molecular Devices) and amyloid conversion of the monomer was monitored by recording ThT fluorescence. Aggregation kinetics of an HSA sample incubated without any pre-formed seed was used for comparison. A sample containing only the 5 % sonicated seed and lacking any HSA monomer was used as a control.

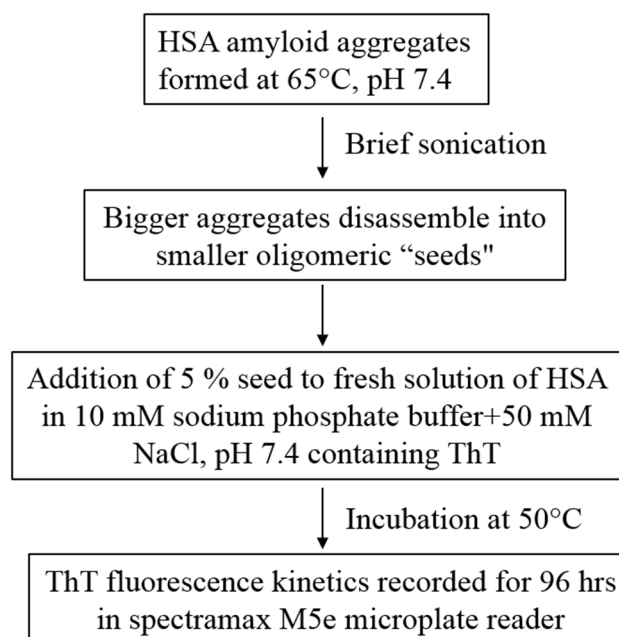


Figure 51. Steps for self-seeding aggregation assay of HSA

4.4.5 Transmission Electron Microscopy

The electron micrographs of HSA aggregates were acquired using a high-resolution transmission electron microscope (FEI Tecnai, T20G2), operated at 200 kV. TEM imaging was carried out by following same method as described in before in materials and methods section of chapter III.

4.4.6 Atomic Force Microscopy

Atomic force microscopy (AFM) of HSA aggregates obtained from cysteine-linked homo dimers was performed by drop-casting 30-fold diluted aggregates on a freshly cleaved mica sheet. Multimode scanning probe microscope from Veeco Instrument Inc., USA equipped with a Nanoscope IV controller and AFM probe model - Tap190Al (tip radius: ~ 10 nm, & tip height: 17 μm) purchased from Budget Sensors, were used in tapping-mode at ambient conditions to scan the sample. The cantilever had a resonant frequency of ca. 162 kHz and nominal spring constant of ca. 48 N/m with a 30 nm thick aluminium reflex coating on the back side of the cantilever of the length 225 μm . Imaging was carried out at a rate of 1 Hz and at a resolution of 512 \times 512 pixels.

4.4.7 Dynamic Light Scattering

Dynamic Light Scattering was recorded using Delsa Nano C Particle Analyzer (Beckman Coulter) and data were processed using Delsa Nano 3.7 software. DLS measurements were carried out similar to as described before in chapter III.

4.4.8 HSA homo-dimerization and purification

4.4.8.1 H₂O₂ induced disulfide-linked homo-dimerization of HSA

HSA molecule has one free cysteine-34, which is reported to be buried in a cleft of ~10 Å [109]. We first confirmed the presence and accessibility of free cysteine by Ellman's method using DTNB reagent (Table 5) [106]. H₂O₂ was used as an oxidizing agent for converting two free sulfhydryl groups (-SH) into a disulfide bond. HSA (150 μM) was pre-incubated in 8 M urea to increase accessibility of the -SH groups and then mixed with 10 mM, 25 mM or 100 mM H₂O₂ in reaction buffer (50 mM glycine-HCl pH 3.0 containing 50 mM NaCl) and incubated at room temperature for 30 minutes. Formation of homodimer was assessed by SDS-PAGE under non-reducing conditions. Samples electrophoresed with reducing sample buffer were used to examine whether the dimers were indeed disulfide linked.

4.4.8.2 Size-exclusion chromatography

As the efficacy of H₂O₂ induced dimerization of HSA was not 100%, the dimers needed to be purified from the monomers. As the dimers and monomers differ by 66 kDa, thus we attempted separation using size-exclusion chromatography (SEC) on Superose 6, 10/300 GL column with exclusion limit of 4×10^7 using FPLC (ÄKTA™ FPLC™, GE) system. Briefly, 400 μl of HSA dimerization mixture was dialyzed using membrane of 25 kDa mol. wt. cut-off to remove the urea and H₂O₂. Dialyzed sample containing the mixture of monomer and dimer (10 mg/ml) was loaded on to the SEC column pre-equilibrated with loading buffer (50 mM Glycine-HCl pH 3.0 with 150 mM NaCl) and the protein was eluted using the same buffer. Fractions of 0.25 ml volume were collected and elution of the protein was profiled using the UV detector of the FPLC by absorbance at 280 nm. Purity of fractions was assessed by SDS-PAGE using non-reducing sample buffer. Fractions containing HSA dimers, were pooled and ammonium sulfate precipitated to

concentrate the protein. The pelleted protein was dissolved in aggregation buffer and examined for amyloid aggregation using the method described above for HSA monomers.

Chapter V

Conclusions

Protein misfolding has been shown to lead to several devastating diseases such as Alzheimer's, Parkinson's, Creutzfeldt–Jakob disease and Prion diseases etc. Several non-disease causing proteins like Human serum albumin can also form amyloid.

Aggregation of human Seminogelin-1 protein is implicated in development of SSVA disorder. The first part of this thesis describes were the cloning, expression and purification of recombinant human Sg1 and Sg1 (1-159) using *E. coli* and also their characterization. These purified proteins were further utilized for study of their amyloid forming capability.

The thesis explores new insights into amyloid-like aggregation of human proteins Sg1 and HSA, the most abundant proteins in seminal plasma and blood plasma respectively. This is the first study to investigate the amyloid forming ability of Sg1 full length protein *in vitro*. So far, only small peptides of Sg1 have been demonstrated to be amyloidogenic *in vitro*. We succeeded in obtaining aggregates of Sg1 and Sg1 (1-159) which manifested amyloid-like binding to Thioflavin-T and Congo red dyes and also followed lag-dependent sigmoidal growth pattern and beta-sheet rich conformation, as observed previously for several amyloids. Furthermore, these aggregates also exhibited amyloid-like stabilities to ionic detergents: SDS & Sarkosyl. Also showed partial resistance to Proteinase-K digestion. In addition, dynamic light scattering results estimated presence of > 400 nm size particles in both Sg1 and Sg1(1-159) aggregates, as expected of

amyloid-like aggregates. The data showed that Sg1 and its fragment Sg1 (1-159) form amyloid-like aggregates *in vitro*. It is known that, seminal levels of Zinc, which is known to bind to Sg1 *in vivo* and is essential for health of male reproductive system, gradually decline with age [54,55]. Notably, presence of Zn^{2+} substantially inhibited the *in vitro* aggregations of Sg1 and Sg1 (1-159) proteins, a finding that may have relevance to understanding of the development of SSVA. The results might help to develop amyloid inhibitors.

The later part of the study demonstrates new features of amyloid-like aggregation of HSA. Here, it is observed that HSA aggregates display true amyloid characteristics of self-seeding and detergent stability. The findings here that HSA aggregates are stable to sarkosyl at room temperature, strongly advocate their amyloid-like nature. A signature of amyloid aggregates is self-seeding ability wherein they coax the monomers to misfold and join the aggregates, thus if HSA aggregates were true amyloid displaying self-seeding would be imperative. Furthermore, if found to be self-seeding precautions to prevent any amyloid contamination in drug formulations containing HSA would become essential. Especially in the view that encapsulation of drugs by HSA as well as amyloid formation by HSA are frequently obtained at elevated temperatures [71,115]. By assessing the seeding kinetics at suboptimal conditions, we found that HSA aggregates can indeed show self-seeding feature. Although, HSA has not been shown to aggregate *in vivo*, seeding by amyloid contamination from drugs may become an inducing risk factor for initiating *in vivo* HSA aggregation. It is known that amyloid aggregate contamination of prion protein PrP^{Sc} from surgery or infected food sources can start *in vivo* conversion of monomeric PrP^C into aggregated PrP^{Sc} causing Creutzfeldt Jacob disease [6,24]. We also succeeded, in obtaining disulfide linked dimers of HSA, without employing any cross-linking agent. These dimers being free of any immunogenic cross-linking agent may be preferable for therapeutic applications over conventional HSA dimers obtained *via* chemical cross-linking. As HSA dimers are widely considered as better drug carriers than monomers, we examined whether dimers are also capable of amyloid aggregation. Indeed, we found that HSA dimers also possess amyloid forming capabilities alike the monomers. This further necessitates precautionary considerations.

The results presented in this thesis can have some possible future implications and can potentiate future research directions. For example, Sg1 full length and Sg1 (1-159) amyloids can in future be used to examine whether they can also enhance HIV infectivity similar to the amyloid of small Sg1 peptides. Observed Sg1 amyloid Inhibition by Zn^{2+} could be examined to develop preventive or therapeutic strategies for SSVA. Self-seeding ability of HSA aggregates suggests need for precautions. Protein misfolding cyclic amplification (PMCA) like techniques can be considered for possible screening for presence of any amyloid in HSA drug formulations. Observed cross-seeding between HSA and BSA could be explored in detail and can serve as a possible model for examining species barrier crossing of amyloid and prion propagation or infection. Obtained HSA homodimer without chemical cross-linker, being non-immunogenic, may be preferable over conventional HSA dimers containing chemical cross-linker for therapeutic applications such as a plasma expander or a drug carrier.

Chapter VI

Bibliography

- [1] Dobson, C.M. (2003). Protein folding and misfolding. *Nature* 426, 884-90.
- [2] Chiti, F. and Dobson, C.M. (2006). Protein misfolding, functional amyloid, and human disease. *Annu Rev Biochem* 75, 333-66.
- [3] Nelson, R., Sawaya, M.R., Balbirnie, M., Madsen, A.O., Riek, C., Grothe, R. and Eisenberg, D. (2005). Structure of the cross-beta spine of amyloid-like fibrils. *Nature* 435, 773-8.
- [4] Greenwald, J. and Riek, R. (2010). Biology of amyloid: structure, function, and regulation. *Structure* 18, 1244-60.
- [5] Collins, S.R., Douglass, A., Vale, R.D. and Weissman, J.S. (2004). Mechanism of prion propagation: amyloid growth occurs by monomer addition. *PLoS Biol* 2, e321.
- [6] Prusiner, S.B. (1998). Prions. *Proc Natl Acad Sci U S A* 95, 13363-83.
- [7] LeVine, H., 3rd. (1993). Thioflavine T interaction with synthetic Alzheimer's disease beta-amyloid peptides: detection of amyloid aggregation in solution. *Protein Sci* 2, 404-10.
- [8] Khurana, R., Coleman, C., Ionescu-Zanetti, C., Carter, S.A., Krishna, V., Grover, R.K., Roy, R. and Singh, S. (2005). Mechanism of thioflavin T binding to amyloid fibrils. *J Struct Biol* 151, 229-38.

- [9] Khurana, R., Uversky, V.N., Nielsen, L. and Fink, A.L. (2001). Is Congo red an amyloid-specific dye? *J Biol Chem* 276, 22715-21.
- [10] Patel, B.K. and Liebman, S.W. (2007). "Prion-proof" for [PIN+]: infection with in vitro-made amyloid aggregates of Rnq1p-(132-405) induces [PIN+]. *J Mol Biol* 365, 773-82.
- [11] Pepys, M.B. (2006). Amyloidosis. *Annu Rev Med* 57, 223-41.
- [12] Sipe, J.D., Benson, M.D., Buxbaum, J.N., Ikeda, S., Merlini, G., Saraiva, M.J. and Westermark, P. (2010). Amyloid fibril protein nomenclature: 2010 recommendations from the nomenclature committee of the International Society of Amyloidosis. *Amyloid* 17, 101-4.
- [13] Soto, C. (2003). Unfolding the role of protein misfolding in neurodegenerative diseases. *Nat Rev Neurosci* 4, 49-60.
- [14] Linke, R.P. et al. (2005). Senile seminal vesicle amyloid is derived from semenogelin I. *J Lab Clin Med* 145, 187-93.
- [15] Fowler, D.M., Koulov, A.V., Balch, W.E. and Kelly, J.W. (2007). Functional amyloid--from bacteria to humans. *Trends Biochem Sci* 32, 217-24.
- [16] Patel, B.K., Gavin-Smyth, J. and Liebman, S.W. (2009). The yeast global transcriptional co-repressor protein Cyc8 can propagate as a prion. *Nat Cell Biol* 11, 344-9.
- [17] Maji, S.K. et al. (2009). Functional amyloids as natural storage of peptide hormones in pituitary secretory granules. *Science* 325, 328-32.
- [18] Bhattacharya, M., Jain, N. and Mukhopadhyay, S. (2011). Insights into the mechanism of aggregation and fibril formation from bovine serum albumin. *J Phys Chem B* 115, 4195-205.
- [19] Vishveshwara, N. and Liebman, S.W. (2009). Heterologous cross-seeding mimics cross-species prion conversion in a yeast model. *BMC Biol* 7, 26.
- [20] Cherny, I. and Gazit, E. (2008). Amyloids: not only pathological agents but also ordered nanomaterials. *Angew Chem Int Ed Engl* 47, 4062-9.
- [21] Tanaka, M., Chien, P., Yonekura, K. and Weissman, J.S. (2005). Mechanism of cross-species prion transmission: an infectious conformation compatible with two highly divergent yeast prion proteins. *Cell* 121, 49-62.

- [22] Gupta, S., Chattopadhyay, T., Pal Singh, M. and Surolia, A. (2010). Supramolecular insulin assembly II for a sustained treatment of type 1 diabetes mellitus. *Proc Natl Acad Sci U S A* 107, 13246-51.
- [23] Prusiner, S.B. (1982). Novel proteinaceous infectious particles cause scrapie. *Science* 216, 136-44.
- [24] Aguzzi, A., Sigurdson, C. and Heikenwaelder, M. (2008). Molecular mechanisms of prion pathogenesis. *Annu Rev Pathol* 3, 11-40.
- [25] Wickner, R.B. (1994). [URE3] as an altered URE2 protein: evidence for a prion analog in *Saccharomyces cerevisiae*. *Science* 264, 566-9.
- [26] Derkatch, I.L., Bradley, M.E., Zhou, P., Chernoff, Y.O. and Liebman, S.W. (1997). Genetic and environmental factors affecting the de novo appearance of the [PSI⁺] prion in *Saccharomyces cerevisiae*. *Genetics* 147, 507-19.
- [27] Wasmer, C., Lange, A., Van Melckebeke, H., Siemer, A.B., Riek, R. and Meier, B.H. (2008). Amyloid fibrils of the HET-s(218-289) prion form a beta solenoid with a triangular hydrophobic core. *Science* 319, 1523-6.
- [28] Tanaka, M., Chien, P., Naber, N., Cooke, R. and Weissman, J.S. (2004). Conformational variations in an infectious protein determine prion strain differences. *Nature* 428, 323-8.
- [29] Argon, A., Simsir, A., Sarsik, B., Tuna, B., Yorukoglu, K., Niflioglu, G.G. and Sen, S. (2012). Amyloidosis of seminal vesicles; incidence and pathologic characteristics. *Turk Patoloji Derg* 28, 44-8.
- [30] Herranz Fernandez, L.M., Arellano Ganan, R., Nam Cha, S., Jimenez Galvez, M. and Pereira Sanz, I. (2003). [Localized amyloidosis of the seminal vesicles]. *Actas Urol Esp* 27, 825-8.
- [31] Pitkanen, P., Westermarck, P., Cornwell, G.G., 3rd and Murdoch, W. (1983). Amyloid of the seminal vesicles. A distinctive and common localized form of senile amyloidosis. *Am J Pathol* 110, 64-9.
- [32] Lilja, H., Abrahamsson, P.A. and Lundwall, A. (1989). Semenogelin, the predominant protein in human semen. Primary structure and identification of closely related proteins in the male accessory sex glands and on the spermatozoa. *J Biol Chem* 264, 1894-900.

- [33] Robert, M. and Gagnon, C. (1999). Semenogelin I: a coagulum forming, multifunctional seminal vesicle protein. *Cell Mol Life Sci* 55, 944-60.
- [34] Lilja, H. and Lundwall, A. (1992). Molecular cloning of epididymal and seminal vesicular transcripts encoding a semenogelin-related protein. *Proc Natl Acad Sci U S A* 89, 4559-63.
- [35] Robert, M. and Gagnon, C. (1996). Purification and characterization of the active precursor of a human sperm motility inhibitor secreted by the seminal vesicles: identity with semenogelin. *Biol Reprod* 55, 813-21.
- [36] Robert, M., Gibbs, B.F., Jacobson, E. and Gagnon, C. (1997). Characterization of prostate-specific antigen proteolytic activity on its major physiological substrate, the sperm motility inhibitor precursor/semenogelin I. *Biochemistry* 36, 3811-9.
- [37] Jonsson, M., Linse, S., Frohm, B., Lundwall, A. and Malm, J. (2005). Semenogelins I and II bind zinc and regulate the activity of prostate-specific antigen. *Biochem J* 387, 447-53.
- [38] Jonsson, M., Lundwall, A. and Malm, J. (2006). The semenogelins: proteins with functions beyond reproduction? *Cell Mol Life Sci* 63, 2886-8.
- [39] Edstrom, A.M., Malm, J., Frohm, B., Martellini, J.A., Giwercman, A., Morgelin, M., Cole, A.M. and Sorensen, O.E. (2008). The major bactericidal activity of human seminal plasma is zinc-dependent and derived from fragmentation of the semenogelins. *J Immunol* 181, 3413-21.
- [40] Wang, Z., Widgren, E.E., Sivashanmugam, P., O'Rand, M.G. and Richardson, R.T. (2005). Association of eppin with semenogelin on human spermatozoa. *Biol Reprod* 72, 1064-70.
- [41] Lundwall, A., Bjartell, A., Olsson, A.Y. and Malm, J. (2002). Semenogelin I and II, the predominant human seminal plasma proteins, are also expressed in non-genital tissues. *Mol Hum Reprod* 8, 805-10.
- [42] Bonilha, V.L., Rayborn, M.E., Shadrach, K., Lundwall, A., Malm, J., Bhattacharya, S.K., Crabb, J.W. and Hollyfield, J.G. (2006). Characterization of semenogelin proteins in the human retina. *Exp Eye Res* 83, 120-7.

- [43] Zhang, S. et al. (2014). Seminal plasma protein in renal cell carcinoma: expression of semenogelin I is a predictor for cancer progression and prognosis. *Tumour Biol* 35, 9095-100.
- [44] Rodrigues, R.G., Panizo-Santos, A., Cashel, J.A., Krutzsch, H.C., Merino, M.J. and Roberts, D.D. (2001). Semenogelins are ectopically expressed in small cell lung carcinoma. *Clin Cancer Res* 7, 854-60.
- [45] Zhang, Y., Wang, Z., Liu, H., Giles, F.J. and Lim, S.H. (2003). Pattern of gene expression and immune responses to Semenogelin 1 in chronic hematologic malignancies. *J Immunother* 26, 461-7.
- [46] Lim, S.H., Zhang, Y. and Zhang, J. (2012). Cancer-testis antigens: the current status on antigen regulation and potential clinical use. *Am J Blood Res* 2, 29-35.
- [47] Munch, J. et al. (2007). Semen-derived amyloid fibrils drastically enhance HIV infection. *Cell* 131, 1059-71.
- [48] Roan, N.R. et al. (2011). Peptides released by physiological cleavage of semen coagulum proteins form amyloids that enhance HIV infection. *Cell Host Microbe* 10, 541-50.
- [49] French, K.C., Roan, N.R. and Makhatadze, G.I. (2014). Structural characterization of semen coagulum-derived SEM1(86-107) amyloid fibrils that enhance HIV-1 infection. *Biochemistry* 53, 3267-77.
- [50] Roan, N.R. et al. (2014). Liquefaction of semen generates and later degrades a conserved semenogelin peptide that enhances HIV infection. *J Virol* 88, 7221-34.
- [51] Roan, N.R., Chu, S., Liu, H., Neidleman, J., Witkowska, H.E. and Greene, W.C. (2014). Interaction of fibronectin with semen amyloids synergistically enhances HIV infection. *J Infect Dis* 210, 1062-6.
- [52] Frohm, B., DeNizio, J.E., Lee, D.S., Gentile, L., Olsson, U., Malm, J., Akerfeldt, K.S. and Linse, S. (2015). A peptide from human semenogelin I self-assembles into a pH-responsive hydrogel. *Soft Matter* 11, 414-21.
- [53] Castellano, L.M., Bart, S.M., Holmes, V.M., Weissman, D. and Shorter, J. (2015). Repurposing Hsp104 to Antagonize Seminal Amyloid and Counter HIV Infection. *Chem Biol* 22, 1074-86.

- [54] Elzanaty, S. (2007). Association between age and epididymal and accessory sex gland function and their relation to sperm motility. *Arch Androl* 53, 149-56.
- [55] Molina, R.I., Martini, A.C., Tissera, A., Olmedo, J., Senestrari, D., de Cuneo, M.F. and Ruiz, R.D. (2010). Semen quality and aging: analysis of 9.168 samples in Cordoba. Argentina. *Arch Esp Urol* 63, 214-22.
- [56] Mankad, M., Sathawara, N.G., Doshi, H., Saiyed, H.N. and Kumar, S. (2006). Seminal plasma zinc concentration and alpha-glucosidase activity with respect to semen quality. *Biol Trace Elem Res* 110, 97-106.
- [57] Owen, D.H. and Katz, D.F. (2005). A review of the physical and chemical properties of human semen and the formulation of a semen simulant. *J Androl* 26, 459-69.
- [58] Elzanaty, S., Richthoff, J., Malm, J. and Giwercman, A. (2002). The impact of epididymal and accessory sex gland function on sperm motility. *Hum Reprod* 17, 2904-11.
- [59] Yoshida, K., Kawano, N., Yoshiike, M., Yoshida, M., Iwamoto, T. and Morisawa, M. (2008). Physiological roles of semenogelin I and zinc in sperm motility and semen coagulation on ejaculation in humans. *Mol Hum Reprod* 14, 151-6.
- [60] Kelleher, S.L., McCormick, N.H., Velasquez, V. and Lopez, V. (2011). Zinc in specialized secretory tissues: roles in the pancreas, prostate, and mammary gland. *Adv Nutr* 2, 101-11.
- [61] House, E., Mold, M., Collingwood, J., Baldwin, A., Goodwin, S. and Exley, C. (2009). Copper abolishes the beta-sheet secondary structure of preformed amyloid fibrils of amyloid-beta(42). *J Alzheimers Dis* 18, 811-7.
- [62] Tougu, V., Karafin, A., Zovo, K., Chung, R.S., Howells, C., West, A.K. and Palumaa, P. (2009). Zn(II)- and Cu(II)-induced non-fibrillar aggregates of amyloid-beta (1-42) peptide are transformed to amyloid fibrils, both spontaneously and under the influence of metal chelators. *J Neurochem* 110, 1784-95.
- [63] Sugio, S., Kashima, A., Mochizuki, S., Noda, M. and Kobayashi, K. (1999). Crystal structure of human serum albumin at 2.5 Å resolution. *Protein Eng* 12, 439-46.

- [64] Biswas, S. and Chowdhury, P.K. (2015). Unusual domain movement in a multidomain protein in the presence of macromolecular crowders. *Phys Chem Chem Phys* 17, 19820-33.
- [65] Fanali, G., di Masi, A., Trezza, V., Marino, M., Fasano, M. and Ascenzi, P. (2012). Human serum albumin: from bench to bedside. *Mol Aspects Med* 33, 209-90.
- [66] Yang, F., Zhang, Y. and Liang, H. (2014). Interactive association of drugs binding to human serum albumin. *Int J Mol Sci* 15, 3580-95.
- [67] Quinlan, G.J., Martin, G.S. and Evans, T.W. (2005). Albumin: biochemical properties and therapeutic potential. *Hepatology* 41, 1211-9.
- [68] Taguchi, K., Chuang, V.T., Maruyama, T. and Otagiri, M. (2012). Pharmaceutical aspects of the recombinant human serum albumin dimer: structural characteristics, biological properties, and medical applications. *J Pharm Sci* 101, 3033-46.
- [69] Matsushita, S., Chuang, V.T., Kanazawa, M., Tanase, S., Kawai, K., Maruyama, T., Suenaga, A. and Otagiri, M. (2006). Recombinant human serum albumin dimer has high blood circulation activity and low vascular permeability in comparison with native human serum albumin. *Pharm Res* 23, 882-91.
- [70] Yasuda, H. (2008). Solid tumor physiology and hypoxia-induced chemo/radio-resistance: novel strategy for cancer therapy: nitric oxide donor as a therapeutic enhancer. *Nitric Oxide* 19, 205-16.
- [71] Taboada, P., Barbosa, S., Castro, E. and Mosquera, V. (2006). Amyloid fibril formation and other aggregate species formed by human serum albumin association. *J Phys Chem B* 110, 20733-6.
- [72] Juarez, J., Taboada, P. and Mosquera, V. (2009). Existence of different structural intermediates on the fibrillation pathway of human serum albumin. *Biophys J* 96, 2353-70.
- [73] Pandey, N.K., Ghosh, S., Tripathy, D.R. and Dasgupta, S. (2015). Effect of temperature and solvent on fibrillation of human serum albumin. *Protein Pept Lett* 22, 112-8.

- [74] Juarez, J., Alatorre-Meda, M., Cambon, A., Topete, A., Barbosa, S., Taboada, P. and Mosquera, V. (2012). Hydration effects on the fibrillation process of a globular protein: the case of human serum albumin. *Soft Matter* 8, 3608-3619.
- [75] Juarez, J., Lopez, S.G., Cambon, A., Taboada, P. and Mosquera, V. (2009). Influence of electrostatic interactions on the fibrillation process of human serum albumin. *J Phys Chem B* 113, 10521-9.
- [76] Malm, J., Jonsson, M., Frohm, B. and Linse, S. (2007). Structural properties of semenogelin I. *FEBS J* 274, 4503-10.
- [77] Malm, J., Hellman, J., Magnusson, H., Laurell, C.B. and Lilja, H. (1996). Isolation and characterization of the major gel proteins in human semen, semenogelin I and semenogelin II. *Eur J Biochem* 238, 48-53.
- [78] Laemmli, U.K. (1970). Cleavage of structural proteins during the assembly of the head of bacteriophage T4. *Nature* 227, 680-5.
- [79] Dickinson, J. and Fowler, S. (2002) Quantification of Proteins on Western Blots Using ECL. In *The Protein Protocols Handbook* (Walker, J., ed.), pp. 429-437. Humana Press
- [80] Aitken, A. and Learmonth, M. (1996) Protein Determination by UV Absorption. In *The Protein Protocols Handbook* (Walker, J., ed.), pp. 3-6. Humana Press
- [81] Wilkins, M.R., Gasteiger, E., Bairoch, A., Sanchez, J.C., Williams, K.L., Appel, R.D. and Hochstrasser, D.F. (1999). Protein identification and analysis tools in the ExPASy server. *Methods Mol Biol* 112, 531-52.
- [82] Chen, Y. and Barkley, M.D. (1998). Toward understanding tryptophan fluorescence in proteins. *Biochemistry* 37, 9976-82.
- [83] Lakowicz, J.R. (2006) *Principles of Fluorescence Spectroscopy*, Springer US
- [84] Venyaminov, S., Baikalov, I.A., Shen, Z.M., Wu, C.S. and Yang, J.T. (1993). Circular dichroic analysis of denatured proteins: inclusion of denatured proteins in the reference set. *Anal Biochem* 214, 17-24.
- [85] Greenfield, N.J. (2006). Using circular dichroism spectra to estimate protein secondary structure. *Nature protocols* 1, 2876-2890.

- [86] Harnisch, B. and Oates, R. (2012) Pre-IVF Evaluation of the Infertile Man. In *In Vitro Fertilization* (Ginsburg, E.S. and Racowsky, C., eds), pp. 17-29. Springer New York
- [87] Sambrook, J. and Russell, D. (2001) *Molecular Cloning: A Laboratory Manual*, Cold Spring Harbor Laboratory Press
- [88] Klunk, W.E., Jacob, R.F. and Mason, R.P. (1999). Quantifying amyloid beta-peptide (A β) aggregation using the Congo red-A β (CR-A β) spectrophotometric assay. *Anal Biochem* 266, 66-76.
- [89] Borysik, A.J., Morten, I.J., Radford, S.E. and Hewitt, E.W. (2007). Specific glycosaminoglycans promote unseeded amyloid formation from [A β]₂-microglobulin under physiological conditions. *Kidney Int* 72, 174-181.
- [90] O'Nuallain, B., Williams, A.D., Westermarck, P. and Wetzel, R. (2004). Seeding specificity in amyloid growth induced by heterologous fibrils. *J Biol Chem* 279, 17490-9.
- [91] Bagriantsev, S.N., Kushnirov, V.V. and Liebman, S.W. (2006). Analysis of amyloid aggregates using agarose gel electrophoresis. *Methods Enzymol* 412, 33-48.
- [92] Taneja, V., Maddelein, M.L., Talarek, N., Saupe, S.J. and Liebman, S.W. (2007). A non-Q/N-rich prion domain of a foreign prion, [Het-s], can propagate as a prion in yeast. *Mol Cell* 27, 67-77.
- [93] Bagriantsev, S. and Liebman, S.W. (2004). Specificity of prion assembly in vivo. [PSI⁺] and [PIN⁺] form separate structures in yeast. *J Biol Chem* 279, 51042-8.
- [94] Schagger, H. (2006). Tricine-SDS-PAGE. *Nat Protoc* 1, 16-22.
- [95] Vitrenko, Y.A., Gracheva, E.O., Richmond, J.E. and Liebman, S.W. (2007). Visualization of aggregation of the Rnq1 prion domain and cross-seeding interactions with Sup35^{NM}. *J Biol Chem* 282, 1779-87.
- [96] Berne, B.J. and Pecora, R. (2000) *Dynamic light scattering: with applications to chemistry, biology, and physics*, Courier Corporation
- [97] De Felice, F.G. et al. (2004). Targeting the neurotoxic species in Alzheimer's disease: inhibitors of A β oligomerization. *FASEB J* 18, 1366-72.

- [98] Vieira, M.N., Figueroa-Villar, J.D., Meirelles, M.N., Ferreira, S.T. and De Felice, F.G. (2006). Small molecule inhibitors of lysozyme amyloid aggregation. *Cell Biochem Biophys* 44, 549-53.
- [99] Sarkar, N. and Dubey, V.K. (2013). Exploring critical determinants of protein amyloidogenesis: a review. *J Pept Sci* 19, 529-36.
- [100] Norlin, N., Hellberg, M., Filippov, A., Sousa, A.A., Grobner, G., Leapman, R.D., Almqvist, N. and Antzutkin, O.N. (2012). Aggregation and fibril morphology of the Arctic mutation of Alzheimer's Aβ peptide by CD, TEM, STEM and in situ AFM. *J Struct Biol* 180, 174-89.
- [101] Vivian, J.T. and Callis, P.R. (2001). Mechanisms of tryptophan fluorescence shifts in proteins. *Biophys J* 80, 2093-109.
- [102] Wang, Y., Petty, S., Trojanowski, A., Knee, K., Goulet, D., Mukerji, I. and King, J. (2010). Formation of amyloid fibrils in vitro from partially unfolded intermediates of human gammaC-crystallin. *Invest Ophthalmol Vis Sci* 51, 672-8.
- [103] Furukawa, Y., Kaneko, K., Watanabe, S., Yamanaka, K. and Nukina, N. (2011). A seeding reaction recapitulates intracellular formation of Sarkosyl-insoluble transactivation response element (TAR) DNA-binding protein-43 inclusions. *J Biol Chem* 286, 18664-72.
- [104] Foo, C.K., Ohhashi, Y., Kelly, M.J., Tanaka, M. and Weissman, J.S. (2011). Radically different amyloid conformations dictate the seeding specificity of a chimeric Sup35 prion. *J Mol Biol* 408, 1-8.
- [105] Huang, B.X., Kim, H.Y. and Dass, C. (2004). Probing three-dimensional structure of bovine serum albumin by chemical cross-linking and mass spectrometry. *J Am Soc Mass Spectrom* 15, 1237-47.
- [106] Ellman, G.L. (1959). Tissue sulfhydryl groups. *Arch Biochem Biophys* 82, 70-7.
- [107] Riener, C.K., Kada, G. and Gruber, H.J. (2002). Quick measurement of protein sulfhydryls with Ellman's reagent and with 4,4'-dithiodipyridine. *Anal Bioanal Chem* 373, 266-76.

- [108] Phillips, D.C. (1967). THE HEN EGG-WHITE LYSOZYME MOLECULE. Proceedings of the National Academy of Sciences of the United States of America 57, 483-495.
- [109] Francis, G.L. (2010). Albumin and mammalian cell culture: implications for biotechnology applications. Cytotechnology 62, 1-16.
- [110] Burton, S.J., Quirk, A.V. and Wood, P.C. (1989). Refolding human serum albumin at relatively high protein concentration. Eur J Biochem 179, 379-87.
- [111] Schneider, C.A., Rasband, W.S. and Eliceiri, K.W. (2012). NIH Image to ImageJ: 25 years of image analysis. Nat Methods 9, 671-5.
- [112] Gosal, W.S., Myers, S.L., Radford, S.E. and Thomson, N.H. (2006). Amyloid under the atomic force microscope. Protein Pept Lett 13, 261-70.
- [113] Arya, S., Kumari, A., Dalal, V., Bhattacharya, M. and Mukhopadhyay, S. (2015). Appearance of annular ring-like intermediates during amyloid fibril formation from human serum albumin. Phys Chem Chem Phys 17, 22862-71.
- [114] Harper, J.D. and Lansbury, P.T., Jr. (1997). Models of amyloid seeding in Alzheimer's disease and scrapie: mechanistic truths and physiological consequences of the time-dependent solubility of amyloid proteins. Annu Rev Biochem 66, 385-407.
- [115] Chen, C.Q., Lin, W., Coombes, A.G., Davis, S.S. and Illum, L. (1994). Preparation of human serum albumin microspheres by a novel acetone-heat denaturation method. J Microencapsul 11, 395-407.

Publications

1. Neetu Sharma, Vishwanath S., and Basant K Patel (2016) Recombinant human Semenogelin-1 (Sg1) and Sg1 (1-159) form detergent stable amyloid like aggregates *in vitro*. Protein & Peptide letters, 23, 87-96.
2. Neetu Sharma^{*}, Vishwanath S.^{*}, Sonalika Maurya^{*}, Archana Prasad, Puneet Khandelwal, Subhash Chandra Yadav and Basant K Patel (2015) New insights into *in vitro* amyloidogenic properties of Human serum albumin suggest considerations for therapeutic precautions. ^{*} Equal contribution. FEBS Letters 589, 4033-4038.
3. Vishwanath S., Nalla Lakshmi Prasanna, Neetu Sharma, Archana Prasad, and Basant K Patel. Wild-type Hen Egg White Lysozyme amyloid aggregation can form prion-like conformational variants. (Under communication).